ENHANCEMENT OF TRANSITION METAL-BASED SUPERCAPACITOR MATERIALS FOR IMPROVED PERFORMANCE

by

ISMAILA TAIWO BELLO

A Thesis

submitted in accordance with the requirements for
the degree of

DOCTOR OF PHILOSOPHY

in

Physics

at the

UNIVERSITY OF SOUTH AFRICA

SUPERVISOR: Prof. M.S. Dhlamini
CO-SUPERVISOR: Dr. E.L. Mathevula
Prof. B.M. Mothudi

November, 2022.

DECLARATION

Name: ISMAILA TAIWO BELLO

Student number: 67137601

Degree: Doctor of Philosophy (PhD) in PHYSICS

Exact wording of the title of the thesis as appearing on the electronic copy submitted for examination:

ENHANCEMENT OF TRANSITION METAL-BASED SUPERCAPACITOR MATERIALS FOR IMPROVED PERFORMANCE

I declare that the above thesis is my own work and that all the sources that I have used or quoted have been indicated and acknowledged by means of complete references.

I further declare that I submitted the thesis to originality checking software and that it falls within the accepted requirements for originality.

I further declare that I have not previously submitted this work, or part of it, for examination at Unisa for another qualification or at any other higher education institution.

(The thesis will not be examined unless this statement has been submitted.)

9th November, 2022

SIGNATURE DATE

UNIVERSITY OF SOUTH AFRICA

Title of thesis:

ENHANCEMENT OF TRANSITION METAL-BASED SUPERCAPACITOR MATERIALS FOR IMPROVED PERFORMANCE

KEY TERMS:

Molybdenum Sulfide; supercapacitors; electrode materials; specific capacitance; Mn-dope MoS_2 nanoflowers; Co-doped MoS_2; energy storage; transition metals; electrochemical; bibliometric analysis;

DEDICATION

This work is dedicated to Almighty Allah, the giver of knowledge and wisdom, to all those whose knowledge and work served as the foundation of this work, my parents and the two martyrs of love, (FAA and Hydroxyle), may Allah grant you both Aljanah fridaus.

ACKNOWLEDGEMENTS

All praises, adorations, and glorifications are due to Almighty Allah, who made this quest a successful one. “So, which of the favors of my Lord would I deny”?

Special thanks to my inestimable mentor and supervisor Prof. M.S. Dhlamini for believing in me and for his guidance throughout my stay at UNISA. No doubt, the Academic Community is indeed blessed with such a rare gem. I also appreciate my co-supervisors Prof. B.M. Mothudi (CoD) and Dr. E.L. Mathevula for their support and encouragement.

Great thanks to The World Academy of Sciences (TWAS) and National Research Foundation (NRF) for awarding me the African Renaissance Doctoral Fellowship (GUID: 116080 & 1391799) from 2019 to 2022. I am also grateful to the University of South Africa (UNISA) for providing an enabling environment to carry out my research work and the Department for unhampering access to the usage of the equipment throughout my stay in UNISA.

I will never forget the expertise and support I got from Dr. G.L Kabongo, Prof. L.L. Noto, Prof. P. Mbule, and other members of the academic and technical staff of the department. Also, the motherly love and support from Ms. Hlela Rosemary Bongi (Administrator) throughout my stay in the department, is well appreciated.

I am also grateful for the support I received from; Dr. K.O. Otun who guided me on the nitty-gritty of the synthesis techniques, Dr. D.O. Idisi, who took his precious time to read the first draft of my thesis, and Dr. A.O. Oladipo and Dr. S.A. Adio, who respectively guided me on the arts of publications and the bibliometric analysis of this research. To my colleagues Dr. J.A. Oke, J. Bodunrin, S.O. Amusat, Gayi Nyongombe, Oliver Mnisi, Mpho William, and William Moloto, I am very grateful.

I am greatly indebted to my parents for guiding me on the right path from cradle till this moment. All the Bello family; Alhaja Kudirat A. Lawal, Dr. M.A. Bello, Hajia Amirat Yussuf-Bello, Alhaja Ruqoyah Lawal and other members are duly appreciated. You are the best.

To Prof. and Mrs. Giwa, your moral and financial support are well recognized, only God can reward you abundantly. Prof. R.O. ROM Kalilu, Prof. A.O. Awodugba, Prof. L.A. Sunmonu, Prof. Y.K. Sanusi, Prof. L.A. Jimoda, Prof. O.S. Bello, Prof (Dr.) Adedokun, Dr. (Mrs.) D.O.

Aderibigbe, Dr. K.O. Suleman, Dr. MBA Babarinde, Dr. A.A. Akanbi and Sayyidah Ummuhani Abduroheem, I am grateful for the unwavering and unrelenting support you gave me throughout my study.

My profound appreciation goes to Sheikh Usman Giwa, Sheikh Abdurofiu Inaolaji Kede, Sheikh Munirudeen Raji, Ustaz Jamiu Aminullah, Khalifa Isaq Bello, and Mukadam Kafeel Bello for their elderly support.

To my partners in progress; Sayyidys Adnan Adeyemi, AbdulWahab Olukade, Abdulwasiu Ogoro, Girigisu Alabidun, Najeemdeen Arayemi, Abdulateef Tijani, Saheed Taiwo, Abeeblah Shuaib, Abdurahman Olusokun, Ibrahim Giwa, Hassan Shittu, Abdulquadr Akindeere, and Toyyiba Yussuf, I am very grateful for your support and encouragement. To the two martyrs of love, (FAA and Hydroxyle), I say thank you and I seek that Allah grants you both Aljanah fridaus. Mariam Adekola, your unquantifiable moral support, and encouragement mean a lot to me, thank you.

Finally, my undiluted gratitude goes to my adorable wife Mrs. Khafeelat Romoke Bello for her care, understanding, encouragement, and the sacrifices made during my sojourn to the Republic of South Africa to acquire knowledge. KAY you are more than a wife to me, thank you very much. To my charming children Muhammad Bello (BMB) and Rizqiyyah Abidemi (RMB), Daddy loves you More.

PUBLICATIONS

[1] **I.T. Bello**, E.L. Mathevula, B.M. Mothudi, and M.S. Dhlamini, In-situ Crystallites Size-and-Lattice strain dependent of electrochemical Performances of Co-doped MoS_2 using Williamson-Hall Methods (Manuscript-in-preparation)

[2] **I.T. Bello**, A.O. Oladipo, O. Adedokun, and M.S. Dhlamini, (2020). Recent advances on the preparation and electrochemical analysis of MoS_2-based materials for supercapacitor applications: A mini-review. *Materials Today Communications*, Volume 25, 101664. Page 1-9. https://doi.org/10.1016/j.mtcomm.2020.101664

[3] **I.T. Bello,** S.A. Adio, A.O. Oladipo, O. Adedokun, E.L. Mathevula, and M.S. Dhlamini, (2021). Molybdenum sulfide-based supercapacitors: from synthetic, bibliometric, and qualitative perspectives. *International Journal of Energy Research*, Volume 45, No. 9, Page 12665-12692. https://doi.org/10.1002/er.6690

[4] **I.T. Bello,** K.O. Otun, Gayi Nyongombe, O. Adedokun, G.L. Kabongo, and M.S. Dhlamini, (2022), Synthesis, Characterization, and Supercapacitor Performance of a mixed-phase Mn-doped MoS_2 Nanoflower. *Nanomaterials*, Volume 12, Page 1-12. https://doi.org/10.3390/nano12030490

[5] **I.T. Bello,** K.O. Otun, Gayi Nyongombe, O. Adedokun, G.L. Kabongo, and M.S. Dhlamini, (2022), Non-Modulated Synthesis of Cobalt-Doped MoS_2 for Improved Supercapacitor Performance. *International Journal of Energy Research*, Volume 46, No. 7, Page 8908-8918. https://doi.org/10.1002/er.7765

[6] **I.T. Bello,** D.O. Idisi, K.O. Suleman, Y. Ajayeoba, O. Adedokun, A.O. Awodugba, and M.S. Dhlamini, (2022). Thickness variation effects on the efficiency of simulated hybrid Cu_2ZnSn_4-based solar cells using SCAPS-1D. *Biointerface Research in Applied Chemistry*, Volume 12, No. 6, Page 7478-7487, https://doi.org/10.33263/BRIAC126.74787487

[7] Nyongombe, Gayi, **I.T. Bello,** K.O. Otun, G.L. Kabongo, B.M. Mothudi, L.L. Noto, and M.S. Dhlamini, (2022). Unveiling the benefits of Dimethyl Sulfoxide as a binder solvent on the electrochemical performance of Layered Double Hydroxides. *Electrochimica Acta*, Volume 419, 140386, Page 1-12 https://doi.org/10.1016/j.electacta.2022.140386

[8] Nyongombe, Gayi, G.L. Kabongo, **I.T. Bello**, L.L. Noto, and M.S. Dhlamini, (2022). The impact of drying temperature on the crystalline domain and the electrochemical performance of NiCoAl-LDH. *Energy Reports*, Volume 8, Page 1151-1158, https://doi.org/10.1016/j.egyr.2021.12.042

[9] K.O. Otun, S.O. Amusat, **I.T. Bello,** J. Abdulsalam, A.T. Ajiboye, A.A. Adeleke, S.O. Azeez, (2022), Recent advances in the synthesis of various analogues of MOF-based nanomaterials: A mini-review, *Inorganica Chimica Acta*, Volume 536, 120890, Page 1-15 https://doi.org/10.1016/j.ica.2022.120890

[10] D.O. Idisi, J.A. Oke, and **I.T. Bello,** (2021). Graphene Oxide/Au nanoparticles: Synthesis, properties, and applications: A mini-review. *International Journal of Energy Research*, Volume 45, No. 14, Page 19772-19788, https://doi.org/10.1002/er.7073

[11] O. Adedokun, **I.T. Bello**, Y.K. Sanusi, and A.O. Awodugba, (2020) Effect of precipitating agents on the performance of ZnO nanoparticles-based photo-anodes in dye-sensitized solar cells. *Surfaces and Interfaces.* Volume 21, 100656, Page 1-7. https://doi.org/10.1016/j.surfin.2020.100656

[12] G.A. Alamu, O. Adedokun, **I.T. Bello,** and Y.K. Yekinni, (2021). Plasmonic Enhancement of Visible Light Absorption in Ag-TiO_2 based Dye-Sensitized Solar Cells. *Chemical Physics Impact*, Volume 3, 100037, Page 1-11, https://doi.org/10.1016/j.chphi.2021.100037

[13] O. Adedokun, O.L. Adedeji, **I.T. Bello,** M.K. Awodele, and A.O. Awodugba, (2021). Fruit peels pigment extracts as a photosensitizer in ZnO-based Dye-Sensitized Solar Cells. *Chemical Physics Impact*, Volume 3, 100039, Page 1-8, https://doi.org/10.1016/j.chphi.2021.100039

[14] M.A. Kareem, **I.T. Bello,** H.A. Shittu, P. Sivaprakash, O. Adedokun, and S. Arumugam, (2022). Synthesis, Characterization and Photocatalytic Application of Silver doped Zinc Oxide nanoparticles. *Cleaner Materials*, Volume 3, 100041, Page 1-7, https://doi.org/10.1016/j.clema.2022.100041

[15] H.A. Shittu, M.A. Kareem, P. Sivaprakash, O. Adedokun, **I.T. Bello,** and S. Arumugam, (2022**).** Effects of low-doping concentration on silver-doped SnO_2 and its photocatalytic application. *Biointerface Research in Applied Chemistry*, Volume 13, No. 2, Page 1-15, https://doi.org/10.33263/BRIAC132.165

ABSTRACT

In this research work, metal-doped MoS_2 of Cobalt and Manganese (Co-MoS_2 and Mn-MoS_2) nanocomposites of different ratios of dopant concentrations were synthesized with a facile hydrothermal technique. The samples were characterized using various instruments to elucidate the properties and novelties of the prepared nanomaterials and likewise to establish their supercapacitive suitability for energy storage devices.

The bibliometric evaluation of the development of literary works involving supercapacitor devices since the use of MoS_2 as the active materials in energy storage (Supercapacitor) was performed. The bibliometric analysis of the studied materials gives us perspectives on the strengths and weaknesses of the materials, which enable us to identify the area of focus and the targeted publication outlets.

The Co-MoS_2 electrode materials (CMS_1 and CMS_3) were electrochemically evaluated for their energy storage performance, the materials exhibit specific capacitances of 164 and 146 Fg^{-1} at 1 Ag^{-1} for the working electrodes, respectively. Also, the energy densities of 3.67 and 2.05 Wh/kg with power densities of 3279.97 and 2960.26 W/kg were calculated for both electrode materials, respectively. While the electrochemical performance of the Mn-doped MoS_2 electrode material showed a pseudo-capacitive behavior, with a specific capacitance of 70.37 Fg^{-1}, and with a corresponding energy density of 3.14 $Whkg^{-1}$ and a power density of 4346.35 Wkg^{-1}.

The general obtained results show that the electrode materials were well prepared and the enhancement of MoS_2 properties is achievable with the transition metal composites. These improved properties of MoS_2 composites showing the suitability of the nanomaterials for the energy storage applications have been explained in this work with possible future works recommended in the report.

Table of Contents

LISTS OF FIGURES

LIST OF TABLES

LIST OF ABBREVIATIONS

Terms/Acronyms/Abbreviations	Definition
AC	Activated carbon
BET	Brunauer-Emmett-Teller
BJH	Barret-Joyner-Halenda
CMS	Cobalt doped MoS_2
CE	Counter Electrode
CV	Cyclic voltammetry
CVD	Chemical vapor deposition
EDLC	Electric double layer capacitor
EIS	Electrochemical impedance spectroscopy
ESR	Equivalent series resistance
FE-SEM	Field emission scanning electron microscopy
GCD	Galvanostatic charge-discharge
LII	Lithium-ion intercalation
LPE	Liquid-phase exfoliation
MMS	Manganese doped MoS_2
NMP	1-methyl-2pyrrolidone
PL	Photoluminescence
RE	Reference Electrode
SBE	Solvent-based exfoliation
SCS	Solution chemistry synthesis
SDS	Sodium dodecyl sulfate

TEM	Transmission electron microscope
TMDs	Transition metals dichalcogenides
XPS	X-ray photoelectron spectroscopy
XRD	X-ray diffraction
WE	Working electrode

Chapter One

Introduction

1.1.MOTIVATION OF STUDY

The environmental risks, high costs and declining availability of fossil fuels has called for the development of sustainable, clean, and green forms of energy. The currently available renewable energy sources are intermittent in nature; such as solar which produce energy only when the sun has higher intensity and wind which requires high wind speed to produce energy. Energy storage technologies, in particular batteries and supercapacitors, could offer efficient and reliable alternative to the currently available energy sources [1,2]. Thus, batteries and supercapacitors, as the two main types of electrochemical energy storage devices, have attracted tremendous attention worldwide for future energy storage applications. Supercapacitors are considered a rapidly growing cutting-edge technology, due to two outstanding features: (1) high power performance, and (2) long-term cycling stability [3–5]. However, the minimal charge storage of supercapacitors, when compared to batteries, restricts their potential future applications [6].

Supercapacitors, or electrochemical capacitors, have attracted intense consideration because of their high-power density, charge-discharge rates and higher magnitude of energy density in comparison to batteries and other conventional capacitors [4]. Supercapacitor, as energy storage devices has many benefits such as environmental friendliness, short-time charge/discharge, and impressive power densities. The importance of supercapacitors could be useful for the optimization of battery-derived hybrid power system and device power performance. The various mechanisms for storing energy have classified the supercapacitor into two groups. The first type is the Electric Double Layer Capacitor (EDLC), which is based on energy charge electrostatic storage. At the electrode/electrolyte interface, no charge is transferred, which can store charges by non-faradaic reactions. In other words, there have been no electrochemical reactions. The second category is

Pseudo-capacitors, which use reactions to transfer charges for storage purposes by faradaic reactions [7].

Recently, efforts have been dedicated in providing new electrode (negative and positive) materials for supercapacitor applications in energy storage devices. Carbon-based materials (such as carbon black, carbon nanotubes, graphene and activated carbon) and transition metals (such as WS_2, MoS_2, and VS_2) are commonly used in energy storage applications. Owing to their intrinsic strength, light weight and excellent electrical conductivity, activated carbon and graphene are the most commonly researched electrode materials for energy storage devices [8,9]. The graphene-like single layered structure of MoS_2 nanosheets has been considered for various energy storage and photocatalysis applications due to their unique morphology, which provides large surface area (27.82, 24.48 and 15.71 m^2/g) and excellent mechanical and electrical properties [10–14].

It has been established in literature that the MoS_2-based supercapacitors have enhanced capacitive performance for supercapacitor applications [15]. The study of its nanocomposite have also been explored ranging from MoS_2/MWCNT composite, Nickel sulfide/MoS_2 (NMS) nanosheets composite, Biomass-derived activated carbon/MoS_2, C/MoS_2 composites, MoS_2/graphene composites and other composites have been reported with improved performance [15–19]. Also, studies have been carried out on electrochemical properties and capacitive efficiency of transition metals such as nickel, cobalt, iron and other graphene composites. However, there are also a few metal-doped composites reported for MoS_2-based supercapacitors such as Nickel [20], Manganese [21], Cobalt [22], and Platinum [23] for improving performance. In this project, we reported one-pot hydrothermally assisted non-modulated synthesis of Cobalt-doped MoS_2 for supercapacitor electrode materials. Likewise, a binder-free mixed-phase of another metal doped MoS_2 (manganese doped MoS_2) for electrochemical performance was also investigated. Finally, an in-

situ crystallites size-dependent of the electrode materials were analyzed to explore how the crystallite sizes of the electrode improving the supercapacitive performance.

1.2.BRIEF OVERVIEW OF MOLYBDENUM SULFIDE (MoS_2)

After the discovery of graphene in 2004 and the developments of graphene-like 2D nanostructures, single-layered transition metal dichalcogenides such as molybdenum sulfide (MoS_2) and tungsten sulfide (WS_2) became materials of choice for the next generation of two-dimensional (2D) materials. This was due to their large intrinsic band gap which made them a perfect replacement for graphene's gapless nature. Moreover, a single-layered transition metal dichalcogenides have narrow bandgap which can be comparable by graphene [24–27]. MoS_2 nanostructures has made numerous advances owing to their unique physical and chemical properties. It has become a promising candidate for eco-friendly applications with cost-effectiveness and efficiency [28]. MoS_2 possesses a graphite-like layered structure with Van der Waal force of attraction (between the S-Mo-S sandwiched layers. The spacing between the interaction of the adjacent layers of Molybdenum between the two Sulphur layers is 0.615 nm that's twice the spacing between the graphite layers (0.335 nm) [29]. These appealing properties of MoS_2, is characterized by optical, electronic, mechanical, magnetic, and valleytronics properties. These properties have resulted in various applications such as energy storage, catalysis, light-harvesting, gas sensor, etc. due to its atomic layered thickness and 2D morphology [30–35].

1.3.OCCURRENCE

The natural occurrence of MoS_2 is from 'molybdenite' which is the principal source of molybdenum. The MoS_2 can be concentrated by foam flotation from the low amount of its ores. Currently, molybdenite is mostly obtained as a byproduct of copper mining [36]. The metal dichalcogenide layer consists of one plane of hexagonally packed metal atoms between two planes

of chalcogenide atoms. In these layers, the chalcogen array around each metal atom is typically octahedral or trigonal prismatic. MoS_2 belongs to the layered dichalcogenides of transition metals of groups *IVb*, *Vb,* and *VIb*, which have attracted interest on account of their highly anisotropic properties [37]. MoS_2 exists in three crystalline structures, i.e., hexagonal (2H), trigonal (3R), and as well as synthetic octahedral (1T) MoS_2 phases, which make it Polytypic materials. Therefore, the 2H structure exists in the space group of $P6_3/mmc$ (a = b = 3.16 Å, c = 12.29 Å) [36], while the 3R structure belongs to the R3m space group (a = b = 3.16 Å and c = 18.37 Å) [38], and the space group of metastable 1T-MoS_2 is P1(a = b = 3.36 Å, c = 6.29 Å) [39]. Also, the structures (2H, 3R, and 1T) have the point groups of D_{6h}, $C_{3v,}$ and D_{6d} with electronic behavior of semiconductor, metal, and semiconductor respectively [40].

1.4.AIM AND OBJECTIVES

This study aims to focus on the enhancement of transition metal-based superconductor materials for improved performance.

The specific objectives of this research will be built on synthesizing molybdenum sulfide (MoS_2) nanomaterials. The functionalization of the composite's compounds of cobalt doped MoS_2 and manganese doped MoS_2 will be accomplished by varying the weight percentage of each composite materials. The structure and properties of the prepared supercapacitor materials and their composites will be elucidated using various spectroscopy methods such as X-ray diffraction (XRD), Field emission scanning electron microscopy (FE-SEM), Raman spectroscopy, X-ray photoemission spectroscopy (XPS), and Brunauer-Emmett-Teller (BET) techniques. The electrochemical performances of the synthesized materials will be investigated using Autolab Electrochemical workstation.

1.5.SCOPE OF THE STUDY

In this research, the synthesis of MoS_2, and their composite materials will be investigated to establish the improvement of supercapacitors electrodes. The supercapacitance properties of the self-assembling electrodes from as-prepared materials will be studied using cyclic voltammetry, galvanostatic charge-discharge, and electrochemical impedance spectroscopy curves for the electrochemical evaluations of the electrodes.

This will be monitored to establish the electronics structure and charge storage capacity of the materials to bring out the nitty-gritty of physics behind the enhancement of the supercapacitor properties.

1.6.ORGANIZATION OF THE THESIS

This thesis entails chapters. The chapters are divided into sections and subsections, to ensure accuracy and conciseness. Within this section, we will discuss the structure of the chapters of this study.

Chapter One introduce supercapacitors as an energy storage device. The motivation of the research, the brief review of the molybdenum sulfide, the aim, and objectives, and the scope of the study were also presented. **Chapter Two** presents the literature review of the recent progress on the MoS_2 based supercapacitors and the bibliometric study of the literature from the inception of using MoS_2 as the active material for supercapacitor. **Chapter Three** detailed the preparation methods, properties and applications of molybdenum sulfide.

Chapter Four provides the detailed working principle of the equipment and instrumentation employed in experimental techniques and the characterization procedures of this research.

In **Chapter Five**, the experimental results and discussions on electrochemical analysis of non-modulated cobalt doped MoS_2 based supercapacitors. **Chapter Six** will present the results and

discussions on the electrochemical performance of the synthesis and characterizations of the manganese doped MoS_2 electrode materials. **Chapter Seven** provides a general summary of the research studies. The published papers to peer-review journals are contained in the **Appendix.**

References

[1] G. Crabtree, The energy-storage revolution, Nature. 526 (2015) S92.

[2] Y. Shabangoli, M.S. Rahmanifar, M.F. El-Kady, A. Noori, M.F. Mousavi, R.B. Kaner, An integrated electrochemical device based on earth-abundant metals for both energy storage and conversion, Energy Storage Mater. 11 (2018) 282–293. https://doi.org/10.1016/j.ensm.2017.09.010.

[3] M.F. El-Kady, Y. Shao, R.B. Kaner, Graphene for batteries, supercapacitors and beyond, Nat. Rev. Mater. 1 (2016) 16033. https://doi.org/10.1038/natrevmats.2016.33.

[4] M.F. El-Kady, M. Ihns, M. Li, J.Y. Hwang, M.F. Mousavi, L. Chaney, A.T. Lech, R.B. Kaner, Engineering three-dimensional hybrid supercapacitors and microsupercapacitors for high-performance integrated energy storage, Proc. Natl. Acad. Sci. U. S. A. 112 (2015) 4233–4238. https://doi.org/10.1073/pnas.1420398112.

[5] Z. Yu, L. Tetard, L. Zhai, J. Thomas, Supercapacitor electrode materials: Nanostructures from 0 to 3 dimensions, Energy Environ. Sci. 8 (2015) 702–730. https://doi.org/10.1039/c4ee03229b.

[6] Y. Wang, Y. Song, Y. Xia, Electrochemical capacitors: Mechanism, materials, systems, characterization and applications, Chem. Soc. Rev. 45 (2016) 5925–5950. https://doi.org/10.1039/c5cs00580a.

[7] P.Y. Chan, S.R. Majid, Metal oxide-based electrode materials for supercapacitor applications, in: Adv. Mater. Their Appl. - Micro to Nano Scale, 2012: pp. 13–30.

[8] Y.X. Chen, K.J. Huang, F. Lin, L.X. Fang, Ultrasensitive electrochemical sensing platform based on graphene wrapping SnO_2 nanocorals and autonomous cascade DNA duplication strategy, Talanta. 175 (2017) 168–176. https://doi.org/10.1016/j.talanta.2017.07.042.

[9] L.C. Gao Lili, Li Xuelian, Li Xiaodong, Cheng Jianli, Wang Bin, Wang Zhiyu, A coaxial yarn electrode based on hierarchical MoS_2 nanosheets/carbon fiber tows for flexible solid-state supercapacitors, RSC Adv. 6 (2016) 57190–57198. https://doi.org/10.1039/x0xx00000x.

[10] D. Merki, X. Hu, Recent developments of molybdenum and tungsten sulfides as hydrogen evolution catalysts, Energy Environ. Sci. 4 (2011) 3878–3888. https://doi.org/10.1039/c1ee01970h.

[11] K. Chang, W. Chen, In situ synthesis of MoS_2/graphene nanosheet composites with extraordinarily high electrochemical performance for lithium ion batteries, Chem. Commun. 47 (2011) 4252–4254. https://doi.org/10.1039/c1cc10631g.

[12] Y. Li, H. Wang, L. Xie, Y. Liang, G. Hong, H. Dai, MoS_2 nanoparticles grown on graphene: An advanced catalyst for the hydrogen evolution reaction, J. Am. Chem. Soc. 133 (2011) 7296–7299. https://doi.org/10.1021/ja201269b.

[13] Z. Yin, H. Li, H. Li, L. Jiang, Y. Shi, Y. Sun, G. Lu, Q. Zhang, X. Chen, H. Zhang, Single-layer MoS_2 phototransistors, ACS Nano. 6 (2012) 74–80. https://doi.org/10.1021/nn2024557.

[14] J.M. Soon, K.P. Loh, Electrochemical double-layer capacitance of MoS_2 nanowall films, Electrochem. Solid-State Lett. 10 (2007) 250–254. https://doi.org/10.1149/1.2778851.

[15] K.J. Huang, L. Wang, Y.J. Liu, Y.M. Liu, H.B. Wang, T. Gan, L.L. Wang, Layered MoS_2-graphene composites for supercapacitor applications with enhanced capacitive performance, Int. J. Hydrogen Energy. 38 (2013) 14027–14034. https://doi.org/10.1016/j.ijhydene.2013.08.112.

[16] X. Yang, L. Zhao, J. Lian, Arrays of hierarchical nickel sulfides/MoS_2 nanosheets supported

on carbon nanotubes backbone as advanced anode materials for asymmetric supercapacitor, J. Power Sources. 343 (2017) 373–382. https://doi.org/10.1016/j.jpowsour.2017.01.078.

[17] D.N. Sangeetha, M. Selvakumar, Active-defective activated carbon/MoS_2 composites for supercapacitor and hydrogen evolution reactions, Appl. Surf. Sci. 453 (2018) 132–140. https://doi.org/10.1016/j.apsusc.2018.05.033.

[18] K.J. Huang, L. Wang, J.Z. Zhang, L.L. Wang, Y.P. Mo, One-step preparation of layered molybdenum disulfide/multi-walled carbon nanotube composites for enhanced performance supercapacitor, Energy. 67 (2014) 234–240. https://doi.org/10.1016/j.energy.2013.12.051.

[19] B. Hu, X. Qin, A.M. Asiri, K.A. Alamry, A.O. Al-Youbi, X. Sun, Synthesis of porous tubular C/MoS_2 nanocomposites and their application as a novel electrode material for supercapacitors with excellent cycling stability, Electrochim. Acta. 100 (2013) 24–28. https://doi.org/10.1016/j.electacta.2013.03.133.

[20] S. Palanisamy, P. Periasamy, K. Subramani, A.P. Shyma, R. Venkatachalam, Ultrathin sheet structure Ni-MoS_2 anode and MnO_2/water dispersion graphene cathode for modern asymmetrical coin cell supercapacitor, J. Alloys Compd. 731 (2018) 936–944. https://doi.org/10.1016/j.jallcom.2017.10.118.

[21] S.S. Singha, S. Rudra, S. Mondal, M. Pradhan, A.K. Nayak, B. Satpati, P. Pal, K. Das, A. Singha, Mn incorporated MoS_2 nanoflowers: A high performance electrode material for symmetric supercapacitor, Electrochim. Acta. 338 (2020). https://doi.org/10.1016/j.electacta.2020.135815.

[22] R. Rohith, M. Manuraj, R.I. Jafri, R.B. Rakhi, Co-MoS_2 nanoflower coated carbon fabric as a flexible electrode for supercapacitor, Mater. Today Proc. (2021).

https://doi.org/10.1016/j.matpr.2020.12.1054.

[23] J. Shao, Y. Li, M. Zhong, Q. Wang, X. Luo, K. Li, W. Zhao, Enhanced-performance flexible supercapacitor based on Pt-doped MoS_2, Mater. Lett. 252 (2019) 173–177. https://doi.org/10.1016/j.matlet.2019.05.124.

[24] J.N. Coleman, M. Lotya, A. O'Neill, S.D. Bergin, P.J. King, U. Khan, K. Young, A. Gaucher, S. De, R.J. Smith, I. V. Shvets, S.K. Arora, G. Stanton, H.Y. Kim, K. Lee, G.T. Kim, G.S. Duesberg, T. Hallam, J.J. Boland, J.J. Wang, J.F. Donegan, J.C. Grunlan, G. Moriarty, A. Shmeliov, R.J. Nicholls, J.M. Perkins, E.M. Grieveson, K. Theuwissen, D.W. McComb, P.D. Nellist, V. Nicolosi, Two-dimensional nanosheets produced by liquid exfoliation of layered materials, Science (80-.). 331 (2011) 568–571. https://doi.org/10.1126/science.1194975.

[25] H.S.S. Ramakrishna Matte, A. Gomathi, A.K. Manna, D.J. Late, R. Datta, S.K. Pati, C.N.R. Rao, MoS_2 and WS_2 analogues of graphene, Angew. Chemie - Int. Ed. 49 (2010) 4059–4062. https://doi.org/10.1002/anie.201000009.

[26] Y.H. Lee, X.Q. Zhang, W. Zhang, M.T. Chang, C. Te Lin, K. Di Chang, Y.C. Yu, J.T.W. Wang, C.S. Chang, L.J. Li, T.W. Lin, Synthesis of large-area MoS_2 atomic layers with chemical vapor deposition, Adv. Mater. 24 (2012) 2320–2325. https://doi.org/10.1002/adma.201104798.

[27] Q.H. Wang, K. Kalantar-Zadeh, A. Kis, J.N. Coleman, M.S. Strano, Electronics and optoelectronics of two-dimensional transition metal dichalcogenides, Nat. Nanotechnol. 7 (2012) 699–712. https://doi.org/10.1038/nnano.2012.193.

[28] G. Zhang, H. Liu, J. Qu, J. Li, Two-dimensional layered MoS_2: Rational design, properties and electrochemical applications, Energy Environ. Sci. 9 (2016) 1190–1209.

https://doi.org/10.1039/c5ee03761a.

[29] Z. Wu, B. Li, Y. Xue, J. Li, Y. Zhang, F. Gao, Fabrication of defect-rich MoS_2 ultrathin nanosheets for application in lithium-ion batteries and supercapacitors, J. Mater. Chem. A. 3 (2015) 19445–19454. https://doi.org/10.1039/c5ta04549e.

[30] K.S. Novoselov, A.K. Geim, S. V Morozov, D. Jiang, Y. Zhang, S. V. Dubonos, I. V Grigorieva, A.A. Firsov, Electric Field Effect in Atomically Thin Carbon Films Supplementary, Science (80-.). 5 (2004) 1–12. https://doi.org/10.1126/science.aab1343.

[31] K.S. Novoselov, D. Jiang, F. Schedin, T.J. Booth, V. V. Khotkevich, S. V. Morozov, A.K. Geim, Two-dimensional atomic crystals, Proc. Natl. Acad. Sci. U. S. A. (2005). https://doi.org/10.1073/pnas.0502848102.

[32] X. Huang, Z. Yin, S. Wu, X. Qi, Q. He, Q. Zhang, Q. Yan, F. Boey, H. Zhang, Graphene-based materials: Synthesis, characterization, properties, and applications, Small. 7 (2011) 1876–1902. https://doi.org/10.1002/smll.201002009.

[33] X. Huang, Z. Zeng, H. Zhang, Metal dichalcogenide nanosheets: Preparation, properties and applications, Chem. Soc. Rev. 42 (2013) 1934–1946. https://doi.org/10.1039/c2cs35387c.

[34] W.J. Zhang, K.J. Huang, A review of recent progress in molybdenum disulfide-based supercapacitors and batteries, Inorg. Chem. Front. 4 (2017) 1602–1620. https://doi.org/10.1039/c7qi00515f.

[35] I.T. Bello, O.A. Oladipo, O. Adedokun, M.S. Dhlamini, Recent advances on the preparation and electrochemical analysis of MoS_2-based materials for supercapacitor applications : A mini-review, Mater. Today Commun. 25 (2020) 101664. https://doi.org/10.1016/j.mtcomm.2020.101664.

[36] E. Benavente, M.A. Santa Ana, F. Mendizábal, G. González, Intercalation chemistry of

molybdenum disulfide, Coord. Chem. Rev. 224 (2002) 87–109. https://doi.org/10.1016/S0010-8545(01)00392-7.

[37] J.A. Wilson, A.D. Yoffe, The transition metal dichalcogenides discussion and interpretation of the observed optical, electrical and structural properties, Adv. Phys. 18 (1969) 193–335. https://doi.org/10.1080/00018736900101307.

[38] B. SCHONFELD, S.C. Moss, J.J. Huang, Anisotropic Mean-Square Displacements (MSD) in Single Crystals of 2H- and 3R-MoS_2, Acta Crystallogr. Sect. B. 39 (1983) 404–407.

[39] M.A. Py, R.R. Haering, STRUCTURAL DESTABILIZATION INDUCED BY LITHIUM INTERCALATION IN MoS_2 AND RELATED COMPOUNDS., Can. J. Phys. 61 (1983) 76–84. https://doi.org/10.1139/p83-013.

[40] D. Mouloua, A. Kotbi, G. Deokar, K. Kaja, M. El Marssi, M.A. El Khakani, M. Jouiad, Recent progress in the synthesis of MoS_2 thin films for sensing, photovoltaic and plasmonic applications: A review, Materials (Basel). 14 (2021). https://doi.org/10.3390/ma14123283.

Chapter Two[1,2]

Literature Review

This chapter has been published in part as:

[1] **Bello, I. T.**, Adio, S. A., Oladipo, A. O., Adedokun, O., Mathevula, L. E., and Dhlamini, M. S. (2021). Molybdenum sulfide-based supercapacitors: from synthetic, bibliometric, and qualitative perspectives. *International Journal of Energy Research*, Vol. 45, Page 12665-12692. https://doi.org/10.1002/er.6690

[2] **Bello, I. T.**, Oladipo, A. O., Adedokun, O., and Dhlamini, M. S. (2020). Recent advances on the preparation and electrochemical analysis of MoS_2-based materials for supercapacitor applications: A mini-review. *Materials Today Communications*, Vol. 25 (2020) 101664. Page 1-9. https://doi.org/10.1016/j.mtcomm.2020.101664

2.0.Introduction

The molybdenum-based supercapacitor is a fast-promising area where researchers are exploring to improve the performance of its electrode materials and their derivatives for energy storage. MoS_2 as an important material for electrochemical devices has recently attracted enormous attention for supercapacitor electrodes as indicated in a large number of research papers [1]. The reports are mainly focused on the properties of MoS_2 with different morphologies as electrode materials for supercapacitors. In this section, the recent development of molybdenum sulfide-based supercapacitors is highlighted. This is to present the evolution of the MoS_2-based supercapacitors from the nanostructured to their composites for their improved efficiencies of the energy storage devices. Likewise, the bibliometric overview of MoS_2-based supercapacitors is presented in this section to elucidate the progress and research outlook of supercapacitors based on MoS_2 materials.

2.1. Recent developments in molybdenum sulfide-based supercapacitor materials

There have been many efforts to commemorate the strength of renewable energies in terms of storage devices for such energies since their sources are attached to one or two factors that can hinder their capacities to perform to the optimum level. Supercapacitors based on molybdenum sulfide are fast-paced fields where researchers are exploring to increase the capacity of their electrode materials and their energy storage derivatives. As an important material for electrochemical devices, molybdenum sulfide has attracted significant attention as a supercapacitor electrode. The most recent improvement in supercapacitors was based on the composition of their active materials, such as its composites, as it was applied to the subject of discussion, MoS_2-based active materials. This section was divided into two, based on the nanostructured and nanocomposites of MoS_2 based electrochemical devices.

2.1.1. Electrochemical Analyses of MoS_2 Nanostructured in Supercapacitor Devices

Molybdenum sulfide nanostructure has been widely employed with enormous applications due to its superiors' characteristics, which can be attributed to the transition metal properties of molybdenum and Sulphur's chemical activity. Recently, Gao *et al*., 2018, described three-dimensional nanospheres of MoS_2 nanosheets through a facile hydrothermal synthesis. The excellent performance of electrochemical outputs was attributed to the improved morphology of MoS_2 nanosheets due to the conferment of the effect of SiO_2 substrates, which provides a large surface area for charge transfer [2]. A simple hydrothermal method was used to prepare MoS_2 nanosheets and the electrochemical data showed an excellent retention capacity of the cyclic stability with an improved specific capacity. The improvement of electrochemical studies has also been accredited to the large specific area, unique two-dimensional (2D) nanostructures of MoS_2 nanosheets, and low series resistance [3]. Krishnamoorthy *et. al*., studied the electrochemical analyses of MoS_2 nanostructure deposited on a stainless-steel substrate. The cyclic voltammetry and galvanostatic charge-discharge studies revealed a specific capacitance of approximately 92.85 F/g and high retention capacity of the cyclic stability analysis after 1000 cycles for the prepared MoS_2 [4]. High capacitance with excellent cycling stability was reported for the binder-free MoS_2 nano worms symmetric supercapacitor. 138 Fg^{-1} of capacitance values were reported at a rate of 1 Ag^{-1} with more than 86% retention over 5000 cycles. A high energy density of 12.26 Wh kg^{-1} at a power density of 0.4 kW kg^{-1} was also reported [5]. Hydrothermal methods for synthesizing MoS_2 nanosheets deposited on titanium plates were described by Wang *et al*., 2017. 93% of cyclic stability retention over 1000 cycles was recorded. The authors agreed that the enhancement of the specific capacitance was due to the composites of MoS_2 [6].

Flower-like MoS_2 microspheres aided with biopolymer-assisted hydrothermal methods were highlighted with a maximum specific capacitance of 145 F/g at 3 A/g and showed good cycle ability with over 100% retention capacitance after 500 cycles [7]. More recently, Javed *et al.,* prepared MoS_2 nanospheres with a typical hydrothermal process, and as-synthesized materials were deposited on carbon cloth to make the supercapacitor device. The electrochemical study performance was associated with the low resistance values observed from electrochemical impedance spectroscopy (EIS) for MoS_2 prepared [8]. Electrochemical analysis of few-layered MoS_2 synthesized by ball milling methods was studied by Pazhamalai *et al*., 2018. The studies show the presence of the pseudocapacitive nature of charge storage via the ion-intercalation/de-intercalation process [9]. A MoS_2-based wire-type supercapacitor was fabricated with few-layered MoS_2 nanosheets synthesized by mechanical milling methods. It was found that a specific capacitance of 119 μF cm^{-1} and an energy density of 8.1 nWh cm^{-1} with cyclic stability of 89.6% retention over 2500 cycles were recorded [10].

2.1.2. Nano-Composites of MoS_2 in Electrochemical Device Analyses

Various efforts have been made to analyze the properties of MoS_2 composites with different morphologies to improve the capacitive performance for supercapacitor applications. The morphology and structural analysis of the layered MoS_2-graphene in a three-dimensional sphere-like structure showed tremendous improvement. The improvement in the electrochemical properties was due to the three-dimensional MoS_2-graphene interconnected conductive network [11].

Patil *et al*., 2016, reported a hybrid MoS_2/graphene oxide for supercapacitor application. The electrochemical studies of the MoS_2/GO hybrid electrode prepared by a facile binder-free approach showed a high specific capacitance at a low scan rate. The high surface area of GO and MoS_2/GO with charge transport was reported to improve the electrochemical performance [12].

Furthermore, MoS_2 deposited by microwave-assisted reduced graphene oxide was studied at different three concentrations and electrochemical studies were taken on all the layered MoS_2/RGO. Firmiano and colleagues concluded that the electrochemical properties can be improved by changing the concentration of MoS_2 for the same hybrid [13].

Composites of MoS_2/Multi-walled carbon nanotube developed from 2-dimensional graphene analog molybdenum sulfide/multi-walled carbon nanotube composites recorded the supercapacitor output. The author related the improved performance to the conductive network of the composites [14]. Supercapacitor application was also demonstrated by the production of porous tubular C/MoS_2 nanocomposites by porous anodic aluminum oxide. Electrochemical analysis of the composite as an electrode material for applications in supercapacitors shows a high specific capacity with long-term cycling stability performances [15].

Recently, Bisset and co-workers reported the characterization of composites MoS_2-graphene using solution-exfoliated methods in a symmetrical coin cell for high-performance supercapacitors with increased charge/discharge cycles up to 800%. The authors found out that electro-activation as a result of ion intercalation offers a significant increase in specific capacitance [16].

Ji and co-workers considered a hybrid preparation of MoS_2/C composites for enhancing the supercapacitor performance through a scalable approach for synthesizing few-layer MoS_2 nanosheets. The electrochemical calculation exhibited a high specific capacity energy storage efficiency and excellent cycling stability retention of 104% after 2000 cycles [17]. 1T-MoS_2@TiO_2/Ti exhibited superior capacitance performance, high energy density, and a high-power density with cycle stability of 97% capacitance retention after 10,000 cycles were observed. The superior performance of the electrochemical studies was associated with the large surface area provided by the array of TiO_2 nanotubes. The fast transfer of electrolyte ions, and electrons due to

the hydrophilicity and conductivity of the 1T-MoS_2 nanosheets, and the direct deposition of TiO_2 nanotubes of titanium foil were also attributed to the performance efficiency [18].

The Biomass-derived activated carbon/MoS_2 nanocomposite was established to have higher specific capacitances for both symmetric and hybrid supercapacitors with the exhibition of good cycle stability [19]. A hierarchical Nickel Sulfides/MoS_2 (NMS) nanosheets composite on carbon nanotubes was invented with favorable specific capacitance and good cycling stability. The assembled NMS/CNT//activated carbon (AC) asymmetric supercapacitor was concluded to be a promising device for energy storage with high specific capacitance. The retention of almost 100% was recorded after 10000 cycles for cycling stability. The improvements recorded for the device were due to the three-dimensional structures that allow electrolyte diffusion and provide fast electron paths to improve its electrochemical properties [20]. MoS_2/RCF composites have been assembled as promising candidates for conductive support for electrodes in energy storage devices. It was deduced that the combination of a negative MoS_2/RCF electrode and a positive MnO_2/RCF electrode enhanced the properties of the device [21].

More Recently, ternary composites of (MoS_2/rGO/PANI) were fabricated for molybdenum-based supercapacitors. The outstanding performance was due to the three components that make the pseudo-capacitance and double-layer capacitance acquired by the composites [22]. Hybrid MoS_2-graphene nanostructures were reported via a facile one-pot chemical method with enhanced electrochemical performance. The electrochemical performance of the device may be associated with the hybridization effect of MoS_2 and graphene [23].

Furthermore, Wang *et. al*. recorded kelp-like layered-structured $NiCo_2S_4$-C-MoS_2 composites for supercapacitors applications in 2018. Hydrothermal and solvothermal methods were used to synthesize the composites with more than 60% of their initial capacitance retained after 1000

charge-discharge cycles. The ternary components of a kept-like layered $NiCo_2S_4$-C-MoS_2 composite showed excellent supercapacitor performance owing to the synergistic effect of their mixture [24]. For high-performance supercapacitors, a cyclic volumetric analysis of a core-sheath holey graphene/graphite composite fiber added with nanosheets of MoS_2 has been studied. The graphene/graphite fiber composite interpolated with MoS_2 nanosheets provided abundant paths for electrolyte ion transfer, large surface area, and fast charge transfer to enhance the electrochemical properties of the device [25]. Maskhiwa *et al*., also observed a high performance for MoS_2/graphene foam composites with expanded activated carbon from graphene. The stability of the supercapacitor cell was attributed to the addition of graphene, which allowed fast charge transfer without weakening the electrode material [26]. In another development, Fan *et al*., 2015, reported an electrochemical analysis of a mesoporous MoS_2/C composite with the structure of a flower-like layer. The values reported in their studies were higher than those previously reported for pure molybdenum sulfide and carbon supercapacitance. The results indicate that the composites can increase the surface area and conductivity of the materials, which in turn enhances the electrochemical performance [27]**.** The overview of the reported works of literature in terms of their specific capacitances values for MoS_2-based supercapacitors ranged from 14.7 F g^{-1} [9] to 1601 F g^{-1} [24], as shown in the summary Table 2.1 [1].

Table 2. 1 Summary of Electrochemical Studies on MoS_2-Based Supercapacitors

MoS_2 Materials	Method of Preparation	Electrochemical Properties	Cyclic stability (%)
MoS_2-G	Hydrothermal	243 F/g@ $1Ag^{-1}$	92.3@1000 cycles
MoS_2/GO–NF	Exfoliation	613 F/g@ 25 mVs^{-1}	98@1000 cycles
MoS_2-RGO	Microwaves	128/265/148 F/g@ 10 mVs^{-1}	92/70@1000 cycles
MoS_2/MWCNT	Hydrothermal	452.7 F/g@ $1Ag^{-1}$	95@1000 cycles
C/MoS_2 nanocomposite	Hydrothermal	210 F/g@ $1Ag^{-1}$	80@1000 cycles
MoS_2/C composites	Microwave-Hydrothermal	589/364 F/g@ $0.5/20Ag^{-1}$	104@2000 cycles
MoS_2 nanosheets	Hydrothermal	129.2 F/g@ $1Ag^{-1}$	85@500 cycles
MoS_2 nanostructure	Hydrothermal	106 F/g@ $5mVs^{-1}$	93.8@1000 cycles
MoS_2 nicrospheres	Biopolymer-assisted Hydrothermal	145 F/g@ $3Ag^{-1}$	100@500 cycles
MoS_2/GF//AEG	Hydrothermal	59 F/g@ $1Ag^{-1}$	95@2000 cycles
MoS_2 hierarchical nanospheres	Hydrothermal	368 F/g@ 5 mVs^{-1}	95@5000 cycles
1T-MoS_2@TiO_2/Ti	Hydrothermal	428.1 F/g@ $0.2Ag^{-1}$	97@10000 cycles
DAC/MoS_2	Hydrothermal	261/193 F/g@ 2 mVs^{-1}	89/88@5000 cycles
NMS/CNT// (AC)	Glucose-assisted Hydrothermal	108 F/g@ $0.5Ag^{-1}$	100@10000 cycles
MoS_2/RCF composite	Hydrothermal	225 F/g@ $0.5Ag^{-1}$	81@2000 cycles

MoS_2/rGO/PANI	Hydrothermal-Polymerization	570 F/g@ $1Ag^{-1}$	78.6@500 cycles
Hybrid MoS_2-graphene nanostructures	Hydrothermal	756 F/g@ $0.5Ag^{-1}$	88@10000 cycles
3D-MoS_2 nanosheets	Hydrothermal	683 F/g@ $1Ag^{-1}$	85.1@10000 cycles
$NiCo_2S_4$-C-MoS_2 composite	Hydrothermal-Solvothermal	1601 F/g@ $0.5Ag^{-1}$	60@1000
few-layered MoS_2	Ball Milling	14.7 F/g@ $0.75Ag^{-1}$	91.2@5000 cycles
graphite composite/MoS_2 nanosheets	Hydrothermal	421F/cm^{-3}@ 5 mVs^{-1}	51@3000 cycles
MoS_2 nanoworms	Hydrothermal	138 F/g@ $1Ag^{-1}$	86@5000 cycles
MoS_2/C composite	Hydrothermal	201.4 F/g@ $0.2Ag^{-1}$	94@1000 cycles
MoS_2-titanium plate	Hydrothermal	133 F/g@ $1Ag^{-1}$	93@1000 cycles
MoS_2 based wire-type	Ball Milling-Exfoliation	119 μFcm^{-1}@2.5μA	89.36@2500 cycles

2.2. Bibliometric Review of MoS_2-Based Supercapacitors

Although there are several appraisals of Molybdenum Sulfide (MoS_2) based on supercapacitors. Nevertheless, a comprehensive overview of MoS_2-based supercapacitors using bibliometric techniques has been presented in recent times. In 2009, Lufrano and Staitis presented a bibliometric study of the literature in the supercapacitors field between 1994 and 2008 [28]. Meanwhile, the evolution of using MoS_2 as active material in supercapacitors devices began in 2007, so their studies might not have covered the current progress in the recent literature on MoS_2-based supercapacitors for bibliometric analysis. Therefore, their work could not have shown how far the MoS_2-based supercapacitors have grown since 2007.

2.2.1. Bibliometric Study

A bibliometric study is the collection of methods for analyzing the scientific and technical works of literature empirically [29]. The bibliometric analysis examines scientific publications through a set of procedures, such as publishing reports of different journals, countries, organizations, writers, and citation analyses, and identifies methods that focus more on quantitative analysis and research evolution [30]. The use of bibliometrics or scientometrics spreads increasingly to all fields of study. At a time when the focus on scientific contributions generates broad, diverse, and divisive research sources, with the emphasis on the voluminous research items based on empirical contributions [31,32]. This hinders the ability to gain information from a collection of previous research papers and actively collect data. Literature reviews are therefore increasingly playing a key role in refining previous study results to use the current knowledge base efficiently, advance a line of research, and provide evidence-based perspective into the practice of professional judgment and competence exercise and maintenance [33]. To understand and coordinate earlier observations, researchers use numerous qualitative and quantitative literature

review methods. Among these approaches, bibliometrics provides a systematic, clear, and reproducible analysis mechanism based on statistical measurements of science, or scientific operation [34–36].

The bibliometric method employed in this field of study is a powerful tool for research in the quantitative analysis of the application of mathematics and statistical methods to academics' publications such as books, journals, and other media of communication [36]. Bibliometric analysis has been widely adopted for tracing the relationships among quotations from academic journals.

Content and citation analyses are two methods used in bibliometric analyses. The content review aims to classify current hotspots based on author keyword frequencies and other distributions. Bibliometric studies generally provide a useful tool for moving from the micro (scientist and institute) to the macro (national and global) level. Besides, the research patterns and current issues in the fields of study can be established by using such a method [37–41]. While citation analysis can be referred to as the link between citing and cited works in a specific research field and allows us to identify core literature, journals, countries, etc. [42].

The impact factor (IF) and H-index are the two major indicators to measure the quality of the journal, thus closely related to the bibliometric analysis. The impact factor measures the average number of citations received in a particular year by papers published in the journal during the two preceding years. It was regarded as a standardized means of evaluating the quality of journals and was put in place by the Institute of Scientific Information (ISI) [43,44]. In 2005, Hirsch introduced the H-index as a quantitative method to measure the total effective output of a researcher with strengths of simplicity and immediate intuitive meaning. The h-index is an objective measure and has a predictive value with one calculation. Giving an estimation of the relevance, significance,

and specific impact of cumulative research contributions by a scientist. The index may also be used by authors, journals, and institutions [45,46]. The impact factor used in this study was obtained from the 2019 journal citation reports of clarivate analytics.

2.2.1.1. Methods and Data Collection

In this study, R-package software (R-studio, Bibliometric, and Biblioshiny) was used to perform bibliometric analysis. It can extract basic information from each searched paper, including details about the authors (names, countries, and institutions), year of publication and journal, total citation times, and keywords, enabling a thorough analysis of key features of relevant research results.

2.2.1.2. Data Collection

All documents used in this study were retrieved from the Scopus database (www.scopus.com), which has been adjudged as the most popular literature data bank in academia. Four keywords; (TITLE-ABS-KEY (molybdenum AND sulfide) OR TITLE-ABS- KEY (molybdenum AND sulphide) OR TITLE-ABS-KEY (mos2) AND TITLE-ABS-KEY (supercapacitor)) were chosen to search the recent publications from 2007-2020. Out of the total 467 retrieved publications, peer-reviewed articles have 432, 9 conference papers, 19 review papers, 2 book chapters, 2 errata, 2 conference proceedings, and 1 note. English is the major language used in the retrieved publications, accounting for 98.7%, this is responsible for the global coverage of the research output and the remaining 1.3% is the Chinese language, which suggests the commitment and dominance of the authors with a Chinese background in the research field.

2.3. Result and Discussions

2.3.1. Main Information and Patterns of the Publications

The description of the total retrieved publications is presented in Table 2.2. The total documents of 467 from 139 sources of the publication revealed more than 1900 and 800 keywords plus and Author's keywords, respectively. The studied publications are between the period January 2007 to April 2020 with average citations per document of 32.48 and more than 1400 authors, which implies the research is progressing towards the enhancement of the MoS_2-based supercapacitors. The results are shown for the documents per author, authors per document, co-authors per document, and collaboration index from the main information details accounted for progress made so far within the review years.

Figure 2.1 shows the general patterns of the publications. The total number of annual publications (TNO) gradually increased between 2007-2020. However, the figure shows that there are no publications between 2008 to 2013, after the first publication by Soon and Loh in 2007 [47]. The non-availability of research documents between those years can be attributed to the understudy of MoS_2 effects on the enhancement of the supercapacitor, which was later translated to an increase in the publication output from 2013. The highest publications output was reported in 2017, 2018, and 2019 with 93, 93, and 116 documents, respectively. Documents retrieved so far for 2020 were the fourth-highest documents that show the prospect of the MoS_2-based supercapacitor as of April 2020.

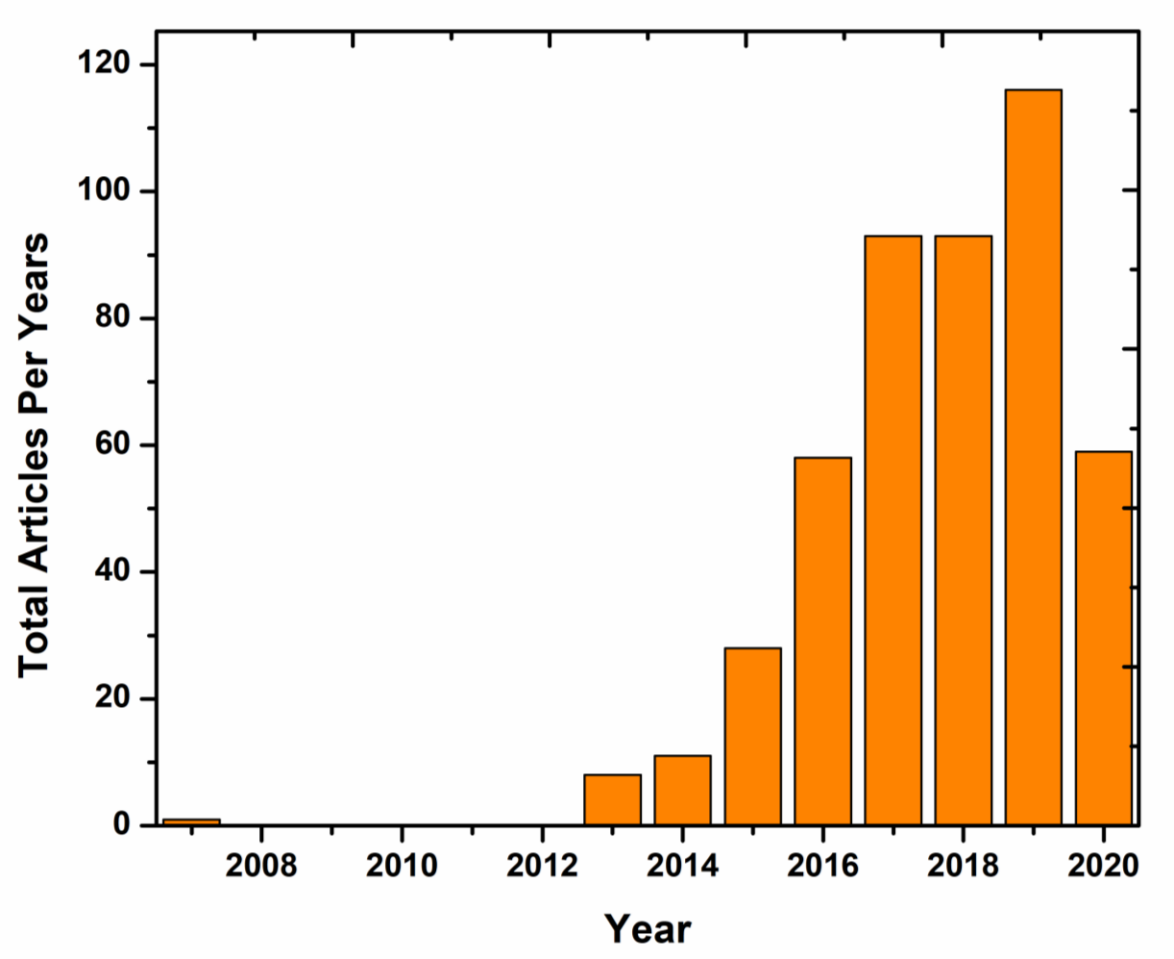

Figure 2. 1 General patterns of the publications.

Table 2. 2 Main information of the retrieved publications.

Description	Results
Documents	467
Sources (Journals, Books, etc.)	139
Keywords Plus (ID)	1955
Author's Keywords (DE)	802
Period	2007 - 2020
Average citations per document	32.48
Authors	1475
Author Appearances	2738
Authors of single-authored documents	5
Authors of multi-authored documents	1470
Single-authored documents	7
Documents per Author	0.317
Authors per Document	3.16
Co-Authors per Documents	5.86
Collaboration Index	3.2

2.3.2. Performance of different Journals

The total number of journals that have published articles on MoS_2-based supercapacitors was 139. The lists of the 20 most relevant journals using the h-index and other performance indicators are summarized in Table 2.3. Considering the total publications associated with MoS_2-based supercapacitors over the 14 years, the top 20 journals contributed more than 14%, inferring the

spread distribution of these publications and a general interest in Molybdenum Sulfide-based supercapacitors devices. In terms of the total number of publications (TNP), Electrochimica Acta, Journal of Alloys and Compounds, RSC Advances, Journal of Materials Chemistry A, and ACS Applied Materials and Interfaces are the five most influential journals with 41, 32, 24, 20, and 16 articles, respectively. Electrochimica Acta has the highest h-index value (17), which shows that Electrochimica Acta is one of the strategic journals with a substantial impact on electrochemical research. However, the Journal of Materials Chemistry A ranked 4th by the number of publications but has the second-highest h-index (14). The Journal of Alloys and Compounds ranked 2nd in terms of articles had an h-index of 13, followed by RSC Advance and ACS Applied Materials and Interfaces with the same h-index of 12 but ranked 3rd and 5th by the number of articles, respectively. The highest total citation was recorded for Electrochimica Acta, which shows its importance to the research field, as presented in Table 2.3. However, the Journal of ACS Applied Materials and Interfaces has the second-highest citations number but is ranked 4th by the number of articles and h-index values, implying the quality of the journal in terms of annual citation.

Table 2. 3 The lists of the 20 most relevant journals.

N/S	Source	h_index	IF	TC	NP	PY_start
1	Electrochimica Acta	17	5.38	1163	41	2013
2	Journal of Alloys and Compounds	13	4.17	509	32	2015
3	RSC Advances	12	3.04	319	24	2015
4	Journal of Materials Chemistry A	14	10.73	681	20	2015
5	ACS Applied Materials and Interfaces	12	8.45	1113	16	2015
6	Chemical Engineering Journal	8	8.35	176	14	2017
7	Journal of Power Sources	9	7.46	713	12	2013
8	Materials Letters	6	3.01	94	10	2014
9	New Journal of Chemistry	6	3.06	234	10	2014
10	Small	8	10.85	780	10	2013
11	Advanced Energy Materials	6	24.88	431	8	2014
12	Applied Surface Science	6	5.15	114	8	2017
13	International Journal of Hydrogen Energy	4	4.08	286	8	2013
14	Nano Energy	6	15.54	514	8	2014
15	Inorganic Chemistry Frontiers	4	5.93	115	7	2017
16	Journal of Colloid and Interface Science	7	6.36	150	7	2017
17	Scientific Reports	6	4.12	201	7	2016
18	Acs Applied Energy Materials	3	-	47	6	2018
19	Ceramics International	3	3.45	34	6	2017
20	Energy Storage Materials	3	2.04	121	6	2017

The source growth of publications of MoS_2-based ultracapacitors across the top five journals is shown in Figure 2.2. As shown in Figure 2.2, an increasing number of publications on MoS_2-based ultracapacitors are observed. This trend might reflect the importance of MoS_2-based ultracapacitors as an accepted method to improve the performance of electrochemical storage devices. Electrochimica Acta has the highest number of publications shared in electrochemical studies, which showed its significance in the research field.

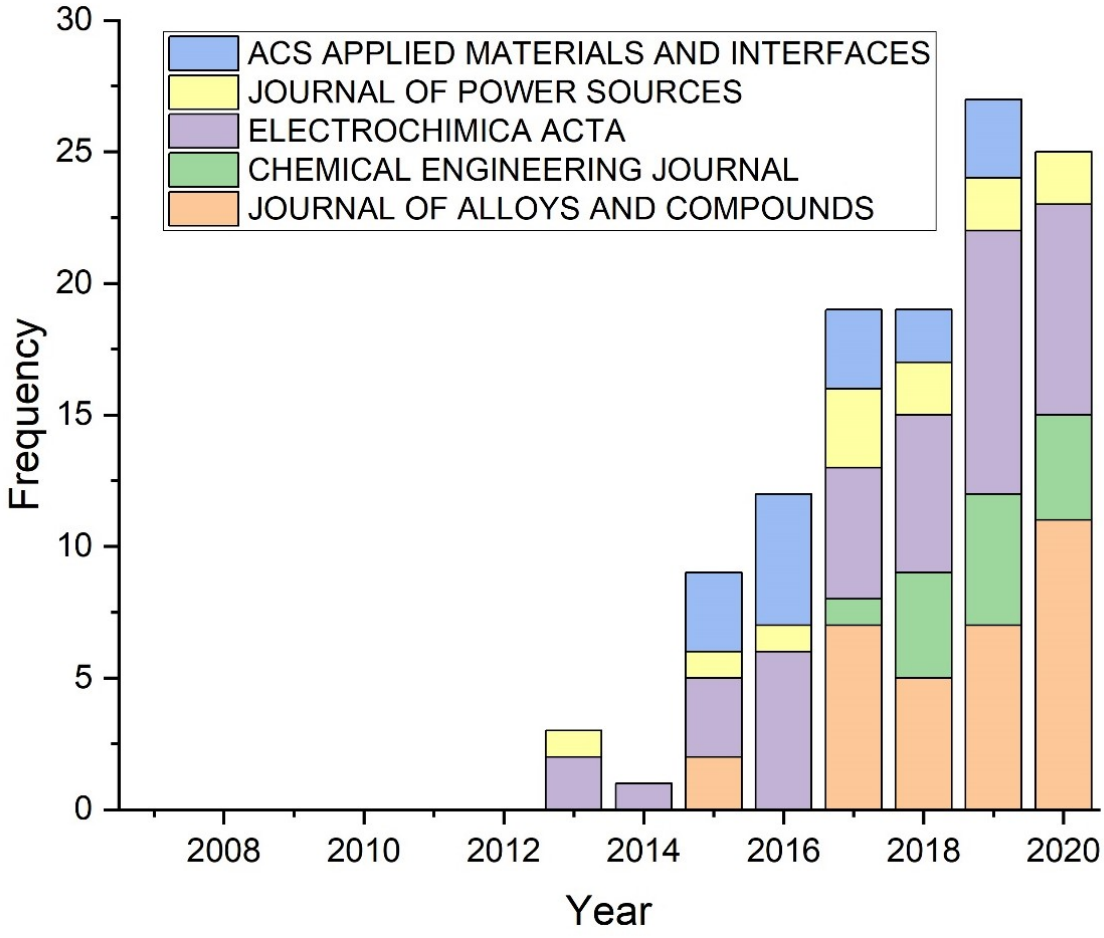

Figure 2. 2 Source dynamics of publications of MoS_2-based ultracapacitors across the top five journals.

2.3.3. Characteristics of the Authors

2.3.3.1. Authors' Performances

A total number of 1475 authors contributed to the research on MoS_2-based supercapacitors. Figure 2.3 shows the top 10 most prolific authors with their total number of publications and h-indexes. The smallest publications for the 10^{th} author are 13 publications, while the total publications for the first author among the top 10 most productive authors are 32. More than 50% of these authors belong to the top ten most productive countries, implying the authors' better productivity in the research field. Out of these authors, Prof. Zhang Y is the most productive author, with 32 articles, followed by Prof. Wang Y with 22 articles, and the next three authors have the same number of publications (16 articles). From the h-index point of view, Prof. Zhang Y has the highest h-index value of 20, which shows that he has higher academic performance with scientific quality and most of his works are generally acknowledged. Prof. Wang Y is the second-most productive author in terms of publications and has a relatively low h-index (8) compared to the fourth (Wang J) and fifth (Wang X) authors with 10 h-indexes. This only means that his works did not receive enough citations, which can be due to the source of his publications and the quality of the research.

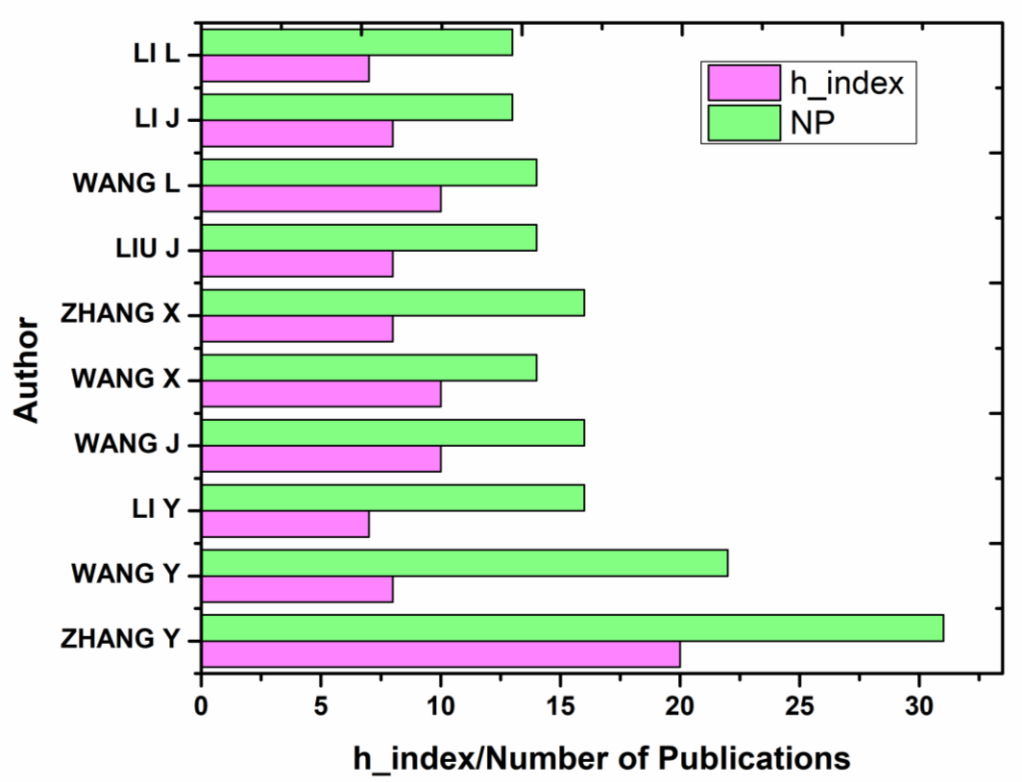

Figure 2. 3 The top 10 most productive authors.

2.3.3.2. Most Cited Authors

Table 2.4 details the list of the top 20 most cited authors with their number of publications, h-index values, the total number of citations, and citations per paper. With all the indicators in Table 2.4, Prof. Zhang Y remains the most prolific author among the authors who contributed to this research with the highest number of global citations. Followed by Li J ranked 2nd in terms of global citation, but ranked 9th and 3rd by the number of articles and h-index, respectively. Wang J. ranked the 3rd most cited author based on the global citation indicator with 16 articles and h-index 8. The ranking of the authors listed in Table 2.4 is based on the number of their citations. However, there is a difference in the ranking of the authors' h-indexes and publications, which is likely to be associated with their collaboration efforts in the research study.

Table 2. 4 Details of the top 20 most cited authors.

Ranks	Authors	Articles	h_index	TC	Cites/Articles
1	Zhang Y	32	20	1581	4.5554
2	Li J	13	8	1010	2.0079
3	Wang J	16	10	987	2.1357
4	Wang L	14	10	838	2.4472
5	Zhang X	16	8	801	2.4718
6	Ma L	12	10	647	2.025
7	Wang X	16	10	484	2.1907
8	Liu H	11	6	421	1.7845
9	Liu J	15	8	363	2.2723
10	Li Y	16	7	354	2.0858
11	Li L	13	7	346	1.8874
12	Zhang J	13	8	319	1.7556
13	Wang Y	22	8	289	4.1615
14	Yang X	12	6	268	2.3278
15	Zhang Z	12	6	255	1.7682
16	Li X	13	5	208	1.864
17	Li Z	11	6	160	2.075
18	Liu Y	13	6	136	2.3206
19	Wang H	13	6	125	1.9159
20	Li H	12	4	93	1.5552

2.3.3.3. Authors' Collaborations

Figure 2.4 presents the collaboration clusters between the active authors contributing to the study of MoS_2-based supercapacitors. The 5 most active research groups are shown according to their academic collaborative relationships in five clusters. Each cluster represents a group of collaborated authors. The largest author node belongs to Prof. Zhang Y and the most collaborated works within his cluster are with the other three authors (Zhang L, Wang S, and Wang R). The activeness of the collaborated works can be related to the thickness of the cluster lines linking authors to each. The second, third, and fourth authors' nodes belong to Wang X, Zhang X, and Wang Y with their respective collaborative relationships, while the fifth authors' nodes belong to Zhang C with just three collaborations. However, some isolated nodes were removed because there was no collaboration with other authors. The VOSviewer computer tool was initiated for the graphical representation in building the bibliometric network with various parameters thus, allowing the bibliometric system construction with different settings.

Figure 2. 4 Top 5 most active collaborative clusters authors.

2.4.The Features of Countries and Institutions

2.4.1. Countries' Characteristics

A total number of 467 documents were studied for countries and affiliated institutes in the Scopus database. Between 2007-2020, 29 countries have contributed to the publications of research articles on MoS_2-based supercapacitors. Figure 2.5 shows the country's scientific productions of MoS_2-based supercapacitors' research based on geographical location. China produced 520 publications on MoS_2-based supercapacitors within the period of study (2007-2020), indicating its interest in improving energy storage optimization. Other countries, such as India (151), South Korea (105), the USA (78), Singapore (40), Australia (20), UK (19), are the countries that have contributed to the study of electrochemical devices using MoS_2 as an active material. Additional studies on supercapacitors using MoS_2 were found in many other countries like Taiwan,

Saudi Arabia, Germany, and Italy with greater than 10 research outputs, and Japan with only 10 research documents. Only two countries from the African continent, Egypt (10) and South Africa (7), were found in the supercapacitors of MoS_2 devices. The number of publications from one country represents the country's focus and overall strengths in its related fields of research.

Table 2.5 shows the top 15 most relevant countries according to some indicators, such as the total number of articles, total global citations, and average article citations or average citation per year. China is the most productive country with the highest stake in all indicators, indicating its investment in energy storage development. India is the second most ranked productive country by the number of publications but ranked 6^{th} by the total citations. The disparities between the rank of the number of publications and global total citations, likely indicate the quality of the research and sources of publication.

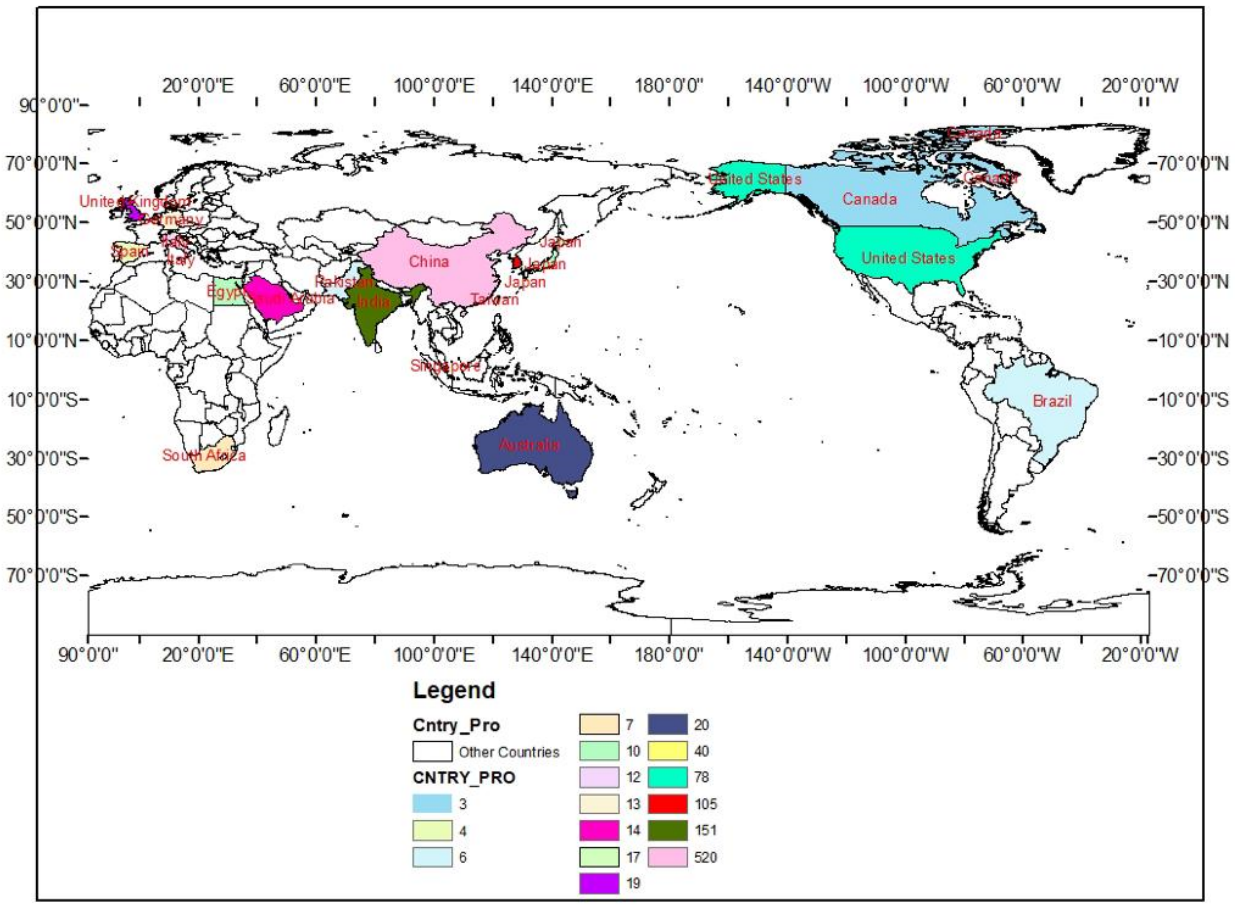

Figure 2. 5 The Geographical Spread of Country Scientific Production.

Table 2. 5 The top 15 most relevant countries.

Rank	Country	Publication Frequency	Total Citations	Average Citations per Years
1	China	520	2890	38.5
2	India	151	356	13.2
3	South Korea	105	1057	24.6
4	USA	78	1867	207.4
5	Singapore	40	1618	124.5
6	Australia	20	0	0
7	UK	19	492	82
8	Taiwan	17	61	15.2
9	Saudi Arabia	14	0	0
10	Germany	13	93	46.5
11	Italy	12	196	32.7
12	Egypt	10	0	0
13	Japan	10	62	31
14	South Africa	7	2	2
15	Brazil	6	266	266

2.4.2. Academic Cooperation

The importance of academic collaboration between countries is that they can share many innovative ideas. Furthermore, it enhances their way of understanding and experience in the search for a creative solution and knowledge advancement. Collaborations between developed and developing countries usually provide access to sophisticated technologies with a series of experiences that might not be available in developing countries. Figure 2.6 shows the academic cooperative relationship between the top 16 collaborative countries. As shown in Figure 2.6, the collaboration strength is represented by the size of the circle. The bigger the circle, the more international active the country is. The thickness of the line joining one country to others corresponds to the collaborative frequencies between them. China is the most internationally active country in cooperative publications with Saudi Arabia, India, Korea, the United Kingdom, the United States, Pakistan, Singapore, Germany, Australia, Canada, and Japan. China and the USA have the highest collaborative frequency, which indicates that both countries (as the economic power of the world) have more interest in improving and diversifying their energy storage technologies with better research collaborations. There are also some collaborative frequencies between the UK, the USA, and China. Interestingly, there are some cooperative improvements between Saudi Arabia, Malaysia, Korea, India, and Egypt. Some isolated nodes were removed from the cluster because there was no link with other countries.

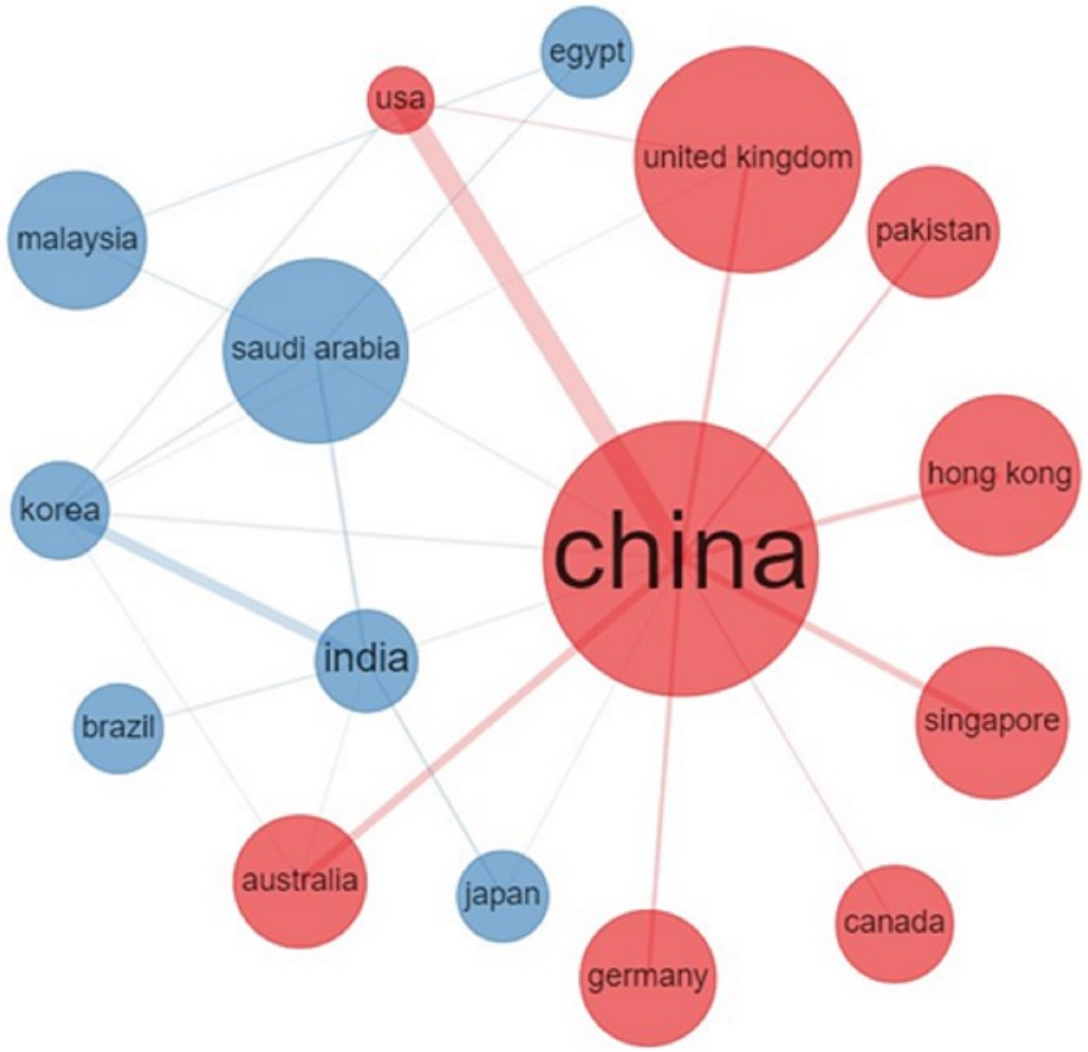

Figure 2. 6 The academic cooperative relationship between the top 16 countries.

2.4.3. Institutions' Performances

The 20 most relevant institutions are shown in Table 2.6. All of them are from the top five most productive countries, except the United Kingdom. Among the top 20 most creative institutions, fourteen are located in China, indicating that Chinese universities are more active in the research field, which also reflects their collaborative relationships with researchers from both developed and developing countries. Two institutions from Singapore and the USA, respectively, and one each from England and South Korea. Nanyang Technological University, Singapore is the

most productive university with the highest number of publications (22). Thus, it is not surprising that a Singaporean University ranked first, which may be likely due to its collaborative relationships with many universities in the region. Jiangsu University, China, and Jeju National University, South Korea ranked 2nd and 3rd most relevant universities with 18 and 16 publications, respectively. It must be also noted that the overbearing of Chinese universities in the top 20 shows the great attention of their government and researchers in the development of energy storage technologies.

Table 2. 6 Top 20 most relevant institutions.

Rank	Affiliations	Articles	Country
1	Nanyang Technological University	22	Singapore
2	Jiangsu University	18	China
3	Jeju National University	16	South Korea
4	Tsinghua University	13	China
5	Xinyang Normal University	12	China
6	University of Chinese Academy of Sciences	11	China
7	University of Manchester	11	England
8	Shanghai Jiao Tong University	10	China
9	South China University of Technology	10	China
10	Tongji University	10	China
11	China University of Geosciences	9	China
12	National University of Singapore	9	Singapore
13	Tianjin University	9	China
14	Jilin University	8	China
15	Lanzhou Institute of Chemical Physics	8	China
16	Nanjing University	8	China
17	Rice University	8	USA
18	Southern Illinois University	8	USA
19	Taiyuan University of Technology	8	China
20	Tianjin University of Technology and Education	8	China

2.5. Keywords

Keywords reflect the priority of the authors' main research area and therefore allow the reader to identify the specific articles' key research contents. Keyword reviews were carried out to identify the core study patterns in MoS_2-based supercapacitors. Figure 2.7 represents the 10 most frequently used keywords of the total 1955 keywords with a cumulative appearance of 8343 times. The top 10 most frequent words appeared (1892 times), accounting for 22.7% of the appearance of the total keyword from the analyzed publications. This indicates that these 10 most frequent words are the hotspot areas of the study of supercapacitors using molybdenum sulfide. Among these keywords, the molybdenum compound appeared 337 times, supercapacitor (305 times), layered semiconductors (228 times), capacitance (199 times), sulfur compounds (184 times), electrodes (167 times), electrochemical performance (134 times), nanosheets (120 times), electrochemical electrodes (110 times), and graphene (108 times). Other keywords that appear more than 50 times are specific capacitance, molybdenum disulfide, electrolytes, high specific capacitances, supercapacitor electrodes, energy storage, electric discharges, asymmetric supercapacitor, MoS_2, and nanocomposites.

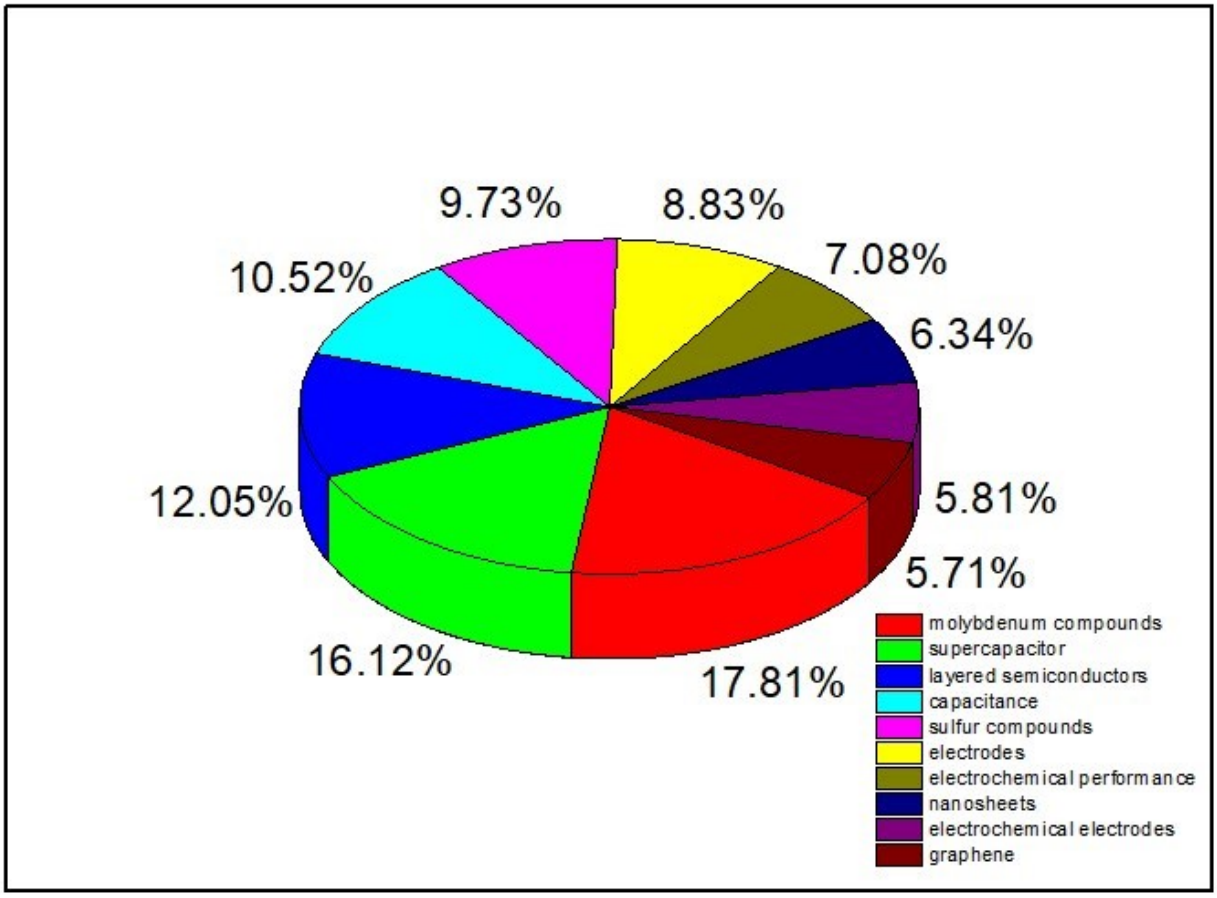

Figure 2. 7 Top 10 most frequently used keywords.

2.6. Most Cited Articles

Table 2.7 presents the top 20 most cited articles for the period under consideration (2007-2020), comprising the title of the articles, name of the journal, number of total citations, total citations per year, and the country of the first authors. The effect of publications and the influence of the authors can be measured by differences in the number of citations or references in a year [48]. As presented in Table 2.7, eight authors were from China, four from the USA and Singapore, two from India, and the remaining two authors are from Brazil and the United Kingdom. The most frequently cited articles among the listed articles had 1157 total citations and the highest total citations per year of 192.83 times. It was published in Nature Nanotechnology, titled "Metallic 1T

phase MoS_2 nanosheets as supercapacitor electrode materials". This paper presents the exfoliation of MoS_2 nanosheets containing a high concentration of the metallic 1T phase electrode to improve the electrochemical properties [49]. The second most cited article is "Nanostructured metal sulfides for energy storage", published in 2014 in Nanoscale with 529 total citations and a total citation per year of 75.57 times. This paper highlights a general overview and the importance of nanostructures and summarizes the recent progress on nanostructured metal sulfides [50]. The third most cited article is "Growth of polypyrrole ultrathin films on MoS_2 monolayers as high-performance supercapacitor electrodes". It was published in Advanced Materials in 2015 with 439 total citations and citations per year of 73.17 times. The paper revealed scalable solution-based methods to grow polypyrrole ultrathin films on MoS_2 monolayer electrodes with high capacitance performance [51]. Among the remaining 17 articles listed in Table 2.7, three had more than 300 citations, eight had more than 200 citations, and the remaining six had more than 150 citations.

Table 2. 7 The top 20 most cited articles.

Rank	Paper	Journal	Year	Total Citations	TC per Year	Country
1	Metallic 1T phase MoS_2 nanosheets as supercapacitor electrode materials	Nature Nanotechnology	2015	1157	192	USA
2	Nanostructured metal sulfides for energy storage	Nanoscale	2014	529	75	China
3	Growth of polypyrrole ultrathin films on MoS_2 monolayers as high-performance supercapacitor electrodes	Advanced Materials	2015	439	73	China
4	Edge-Oriented MoS_2 Nanoporous Films as Flexible Electrodes for Hydrogen Evolution Reactions and Supercapacitor Devices	Advanced Materials	2014	378	54	USA
5	2D space-confined synthesis of few-layer MoS_2 anchored on carbon nanosheet for lithium-ion battery anode	ACS Nano	2015	368	61	China
6	Direct laser-patterned micro-supercapacitors from paintable MoS_2 films	Small	2013	308	38	USA

7	Two-dimensional (2D) layered MoS_2: rational design, properties, and electrochemical applications	Energy & Environmental Science	2016	296	59	China
8	In situ intercalative polymerization of pyrrole in graphene analogue of MoS_2 as advanced electrode material in supercapacitor	Journal of Power Sources	2013	290	36	India
9	Electrochemical double-layer capacitance of MoS_2 nanowall films	Electrochemical and Solid State Letters	2007	272	19	Singapore
10	Supercapacitor electrodes obtained by directly bonding 2D MoS_2 on reduced graphene oxide	Advanced Energy Materials	2014	266	38	Brazil
11	Hybrid fibers made of molybdenum disulfide, reduced graphene oxide, and multi-walled carbon nanotubes for solid-state, flexible, asymmetric supercapacitors	Angewandte Chemie International Edition	2015	252	42	Singapore

12	Layered MoS_2–graphene composites for supercapacitor applications with enhanced capacitive performance	International Journal of Hydrogen Energy	2013	239	29	China
13	Comparative study of potential applications of graphene, MoS_2, and other two-dimensional (2D) materials in energy devices, sensors, and related areas	ACS Applied Materials & Interfaces	2015	222	37	India
14	Characterization of MoS_2–graphene composites for high-performance coin cell supercapacitors	ACS Applied Materials & Interfaces	2015	206	34	United Kingdom
15	Synthesis of polyaniline/2-dimensional graphene analog MoS_2 composites for high-performance supercapacitor	Electrochimica Acta	2013	188	23	China
16	High performance solid state flexible supercapacitor based on molybdenum sulfide hierarchical nanospheres	Journal of Power Sources	2015	178	29	China
17	$Ni3S_2$@MoS_2 core/shell nanorod arrays on Ni foam for high-performance electrochemical energy storage	Nano Energy	2014	173	24	Singapore

18	Two-dimensional (2D) water-coupled metallic MoS_2 with nanochannels for ultrafast supercapacitors	Nano Letters	2017	153	38	USA
19	One-Pot Synthesis of Tunable Crystalline $Ni3S_4$@ Amorphous MoS_2 Core/Shell Nanospheres for High-Performance Supercapacitors	Small	2015	152	25	Singapore
20	One-step preparation of layered molybdenum disulfide/multi-walled carbon nanotube composites for enhanced performance supercapacitor	Energy	2014	152	21	China

2.7. Summary

The recent progress in the electrochemical performance of the MoS_2-based supercapacitors shows that their efficiencies are based on the fundamental formation of composite materials from different types of two-dimensional (2D) nanomaterials to resolve the drawbacks and unstable features. The bibliometric analysis of the evolution of literary works related to its supercapacitor devices since the usage of MoS_2 as the active materials in energy storage (Supercapacitor) was evaluated. The bibliometric studies will guide researchers to explore the previously prioritized areas and encourage future collaborations. The realization of advanced storage capacity from flexible and wearable supercapacitors should be achievable soon with the current pace at which the study of MoS_2-based supercapacitors is growing.

References

[1] I.T. Bello, O.A. Oladipo, O. Adedokun, M.S. Dhlamini, Recent advances on the preparation and electrochemical analysis of MoS_2-based materials for supercapacitor applications : A mini-review, Mater. Today Commun. 25 (2020) 101664. https://doi.org/10.1016/j.mtcomm.2020.101664.

[2] Y.P. Gao, K.J. Huang, X. Wu, Z.Q. Hou, Y.Y. Liu, MoS_2 nanosheets assembling three-dimensional nanospheres for enhanced-performance supercapacitor, J. Alloys Compd. 741 (2018) 174–181. https://doi.org/10.1016/j.jallcom.2018.01.110.

[3] K.J. Huang, J.Z. Zhang, G.W. Shi, Y.M. Liu, Hydrothermal synthesis of molybdenum disulfide nanosheets as supercapacitors electrode material, Electrochim. Acta. (2014). https://doi.org/10.1016/j.electacta.2014.04.007.

[4] K. Krishnamoorthy, G.K. Veerasubramani, S. Radhakrishnan, S.J. Kim, Supercapacitive properties of hydrothermally synthesized sphere like MoS_2 nanostructures, Mater. Res. Bull. 50 (2014) 499–502. https://doi.org/10.1016/j.materresbull.2013.11.019.

[5] Neetika, A. Sanger, V.K. Malik, R. Chandra, One step sputtered grown MoS_2 nanoworms binder free electrodes for high performance supercapacitor application, Int. J. Hydrogen Energy. 43 (2018) 11141–11149. https://doi.org/10.1016/j.ijhydene.2018.05.005.

[6] L. Wang, Y. Ma, M. Yang, Y. Qi, Titanium plate supported MoS_2 nanosheet arrays for supercapacitor application, Appl. Surf. Sci. 396 (2017) 1466–1471. https://doi.org/10.1016/j.apsusc.2016.11.193.

[7] L. Ma, L.M. Xu, X.P. Zhou, X.Y. Xu, Biopolymer-assisted hydrothermal synthesis of flower-like MoS_2 microspheres and their supercapacitive properties, Mater. Lett. 132 (2014) 291–294. https://doi.org/10.1016/j.matlet.2014.06.108.

[8] M.S. Javed, S. Dai, M. Wang, D. Guo, L. Chen, X. Wang, C. Hu, Y. Xi, High performance solid state flexible supercapacitor based on molybdenum sulfide hierarchical nanospheres, J. Power Sources. 285 (2015) 63–69. https://doi.org/10.1016/j.jpowsour.2015.03.079.

[9] P. Pazhamalai, K. Krishnamoorthy, S. Manoharan, S.J. Kim, High energy symmetric supercapacitor based on mechanically delaminated few-layered MoS_2 sheets in organic electrolyte, J. Alloys Compd. 771 (2019) 803–809. https://doi.org/10.1016/j.jallcom.2018.08.203.

[10] K. Krishnamoorthy, P. Pazhamalai, G.K. Veerasubramani, S.J. Kim, Mechanically delaminated few layered MoS_2 nanosheets based high performance wire type solid-state symmetric supercapacitors, J. Power Sources. 321 (2016) 112–119. https://doi.org/10.1016/j.jpowsour.2016.04.116.

[11] K.J. Huang, L. Wang, Y.J. Liu, Y.M. Liu, H.B. Wang, T. Gan, L.L. Wang, Layered MoS_2-graphene composites for supercapacitor applications with enhanced capacitive performance, Int. J. Hydrogen Energy. 38 (2013) 14027–14034. https://doi.org/10.1016/j.ijhydene.2013.08.112.

[12] U.M. Patil, M.S. Nam, S. Kang, J.S. Sohn, H.B. Sim, S. Kang, S.C. Jun, Fabrication of ultra-high energy and power asymmetric supercapacitors based on hybrid 2D MoS_2/graphene oxide composite electrodes: A binder-free approach, RSC Adv. 6 (2016) 43261–43271. https://doi.org/10.1039/c6ra00670a.

[13] E.G. Da Silveira Firmiano, A.C. Rabelo, C.J. Dalmaschio, A.N. Pinheiro, E.C. Pereira, W.H. Schreiner, E.R. Leite, Supercapacitor electrodes obtained by directly bonding 2D MoS_2 on reduced graphene oxide, Adv. Energy Mater. 4 (2014) 1–8. https://doi.org/10.1002/aenm.201301380.

[14] K.J. Huang, L. Wang, J.Z. Zhang, L.L. Wang, Y.P. Mo, One-step preparation of layered molybdenum disulfide/multi-walled carbon nanotube composites for enhanced performance supercapacitor, Energy. 67 (2014) 234–240. https://doi.org/10.1016/j.energy.2013.12.051.

[15] B. Hu, X. Qin, A.M. Asiri, K.A. Alamry, A.O. Al-Youbi, X. Sun, Synthesis of porous tubular C/MoS_2 nanocomposites and their application as a novel electrode material for supercapacitors with excellent cycling stability, Electrochim. Acta. 100 (2013) 24–28. https://doi.org/10.1016/j.electacta.2013.03.133.

[16] M.A. Bissett, I.A. Kinloch, R.A.W. Dryfe, Characterization of MoS_2-Graphene Composites for High-Performance Coin Cell Supercapacitors, ACS Appl. Mater. Interfaces. 7 (2015) 17388–17398. https://doi.org/10.1021/acsami.5b04672.

[17] H. Ji, C. Liu, T. Wang, J. Chen, Z. Mao, J. Zhao, W. Hou, G. Yang, Porous Hybrid Composites of Few-Layer MoS_2 Nanosheets Embedded in a Carbon Matrix with an Excellent Supercapacitor Electrode Performance, Small. 11 (2015) 6480–6490. https://doi.org/10.1002/smll.201502355.

[18] J. Zhou, M. Guo, L. Wang, Y. Ding, Z. Zhang, Y. Tang, C. Liu, S. Luo, 1T-MoS_2 nanosheets confined among TiO_2 nanotube arrays for high performance supercapacitor, Chem. Eng. J. 366 (2019) 163–171. https://doi.org/10.1016/j.cej.2019.02.079.

[19] D.N. Sangeetha, M. Selvakumar, Active-defective activated carbon/MoS_2 composites for supercapacitor and hydrogen evolution reactions, Appl. Surf. Sci. 453 (2018) 132–140. https://doi.org/10.1016/j.apsusc.2018.05.033.

[20] X. Yang, L. Zhao, J. Lian, Arrays of hierarchical nickel sulfides/MoS_2 nanosheets supported on carbon nanotubes backbone as advanced anode materials for asymmetric supercapacitor,

J. Power Sources. 343 (2017) 373–382. https://doi.org/10.1016/j.jpowsour.2017.01.078.

[21] C. Zhao, Y. Zhou, Z. Ge, C. Zhao, X. Qian, Facile construction of MoS_2/RCF electrode for high-performance supercapacitor, Carbon N. Y. 127 (2018) 699–706. https://doi.org/10.1016/j.carbon.2017.11.052.

[22] L.Z. Bai, Y.H. Wang, S.S. Cheng, F. Li, Z.Y. Zhang, Y.Q. Liu, Synthesis and electrochemical performance of molybdenum disulfide-reduced graphene oxide-polyaniline ternary composites for supercapacitors, Front. Chem. 6 (2018) 1–7. https://doi.org/10.3389/fchem.2018.00218.

[23] D. Vikraman, K. Karuppasamy, S. Hussain, A. Kathalingam, A. Sanmugam, J. Jung, H.S. Kim, One-pot facile methodology to synthesize MoS_2-graphene hybrid nanocomposites for supercapacitors with improved electrochemical capacitance, Compos. Part B Eng. 161 (2019) 555–563. https://doi.org/10.1016/j.compositesb.2018.12.143.

[24] D. Wang, W. Zhu, Y. Yuan, G. Du, J. Zhu, X. Zhu, G. Pezzotti, Kelp-like structured $NiCo_2S_4$-C-MoS_2 composite electrodes for high performance supercapacitor, J. Alloys Compd. 735 (2018) 1505–1513. https://doi.org/10.1016/j.jallcom.2017.11.249.

[25] C. Wang, S. Zhai, Z. Yuan, J. Chen, X. Zhang, Q. Huang, Y. Wang, X. Liao, L. Wei, Y. Chen, A core-sheath holey graphene/graphite composite fiber intercalated with MoS_2 nanosheets for high-performance fiber supercapacitors, Electrochim. Acta. 305 (2019) 493–501. https://doi.org/10.1016/j.electacta.2019.03.084.

[26] T.M. Masikhwa, M.J. Madito, A. Bello, J.K. Dangbegnon, N. Manyala, High performance asymmetric supercapacitor based on molybdenum disulphide/graphene foam and activated carbon from expanded graphite, J. Colloid Interface Sci. 488 (2017) 155–165. https://doi.org/10.1016/j.jcis.2016.10.095.

[27] L.Q. Fan, G.J. Liu, C.Y. Zhang, J.H. Wu, Y.L. Wei, Facile one-step hydrothermal preparation of molybdenum disulfide/carbon composite for use in supercapacitor, Int. J. Hydrogen Energy. 40 (2015) 10150–10157. https://doi.org/10.1016/j.ijhydene.2015.06.061.

[28] F. Lufrano, P. Staiti, A bibliometric analysis of the international literature in supercapacitors, Int. J. Electrochem. Sci. 4 (2009) 173–186.

[29] Bibliometrics and citation analysis : from the Science citation index to cybermetrics - Ghent University Library, (n.d.). https://lib.ugent.be/en/catalog/rug01:001668507#reference-details (accessed June 12, 2020).

[30] X. Liu, L. Zhang, S. Hong, Global biodiversity research during 1900-2009: A bibliometric analysis, Biodivers. Conserv. 20 (2011) 807–826. https://doi.org/10.1007/s10531-010-9981-z.

[31] M. Aria, C. Cuccurullo, bibliometrix: An R-tool for comprehensive science mapping analysis, J. Informetr. 11 (2017) 959–975. https://doi.org/10.1016/j.joi.2017.08.007.

[32] R.B. Briner, D. Denyer, Systematic Review and Evidence Synthesis as a Practice and Scholarship Tool, in: Oxford Handb. Evidence-Based Manag., 2012. https://doi.org/10.1093/oxfordhb/9780199763986.013.0007.

[33] D.M. Rousseau, The Oxford Handbook of Evidence-Based Management, 2012. https://doi.org/10.1093/oxfordhb/9780199763986.001.0001.

[34] R.N. Broadus, Toward a definition of “bibliometrics,” Scientometrics. 12 (1987) 373–379. https://doi.org/10.1007/BF02016680.

[35] V.P. Diodato, P. Gellatly, Dictionary of Bibliometrics, 2013. https://doi.org/10.4324/9780203714133.

[36] Alan Pritchard, Statistical Bibliography or Bibliometrics?, J. Doc. 25 (1969) 348–349.

[37] G. Mao, X. Liu, H. Du, J. Zuo, L. Wang, Way forward for alternative energy research: A bibliometric analysis during 1994-2013, Renew. Sustain. Energy Rev. 48 (2015) 276–286. https://doi.org/10.1016/j.rser.2015.03.094.

[38] G. Mao, H. Zou, G. Chen, H. Du, J. Zuo, Past, current and future of biomass energy research: A bibliometric analysis, Renew. Sustain. Energy Rev. 52 (2015) 1823–1833. https://doi.org/10.1016/j.rser.2015.07.141.

[39] W. Zhi, L. Yuan, G. Ji, Y. Liu, Z. Cai, X. Chen, A bibliometric review on carbon cycling research during 1993–2013, Environ. Earth Sci. 74 (2015) 6065–6075. https://doi.org/10.1007/s12665-015-4629-7.

[40] H. Chen, Y.S. Ho, Highly cited articles in biomass research: A bibliometric analysis, Renew. Sustain. Energy Rev. 49 (2015) 12–20. https://doi.org/10.1016/j.rser.2015.04.060.

[41] F. Zhou, H.C. Guo, Y.S. Ho, C.Z. Wu, Scientometric analysis of geostatistics using multivariate methods, Scientometrics. 73 (2007) 265–279. https://doi.org/10.1007/s11192-007-1798-5.

[42] A. Pilkington, J. Meredith, The evolution of the intellectual structure of operations management-1980-2006: A citation/co-citation analysis, J. Oper. Manag. 27 (2009) 185–202. https://doi.org/10.1016/j.jom.2008.08.001.

[43] G. Buela-Casal, I. Zych, What do the scientists think about the impact factor?, Scientometrics. 92 (2012) 281–292. https://doi.org/10.1007/s11192-012-0676-y.

[44] E. Garfield, The history and meaning of the journal impact factor, J. Am. Med. Assoc. 295 (2006) 90–93. https://doi.org/10.1001/jama.295.1.90.

[45] J.E. Hirsch, An index to quantify an individual's scientific research output, Proc. Natl.

Acad. Sci. U. S. A. 102 (2005) 16569–16572. https://doi.org/10.1073/pnas.0507655102.

[46] J.E. Hirsch, Does the h index have predictive power?, Proc. Natl. Acad. Sci. U. S. A. 104 (2007) 19193–19198. https://doi.org/10.1073/pnas.0707962104.

[47] J.M. Soon, K.P. Loh, Electrochemical double-layer capacitance of MoS2 nanowall films, Electrochem. Solid-State Lett. 10 (2007) 250–254. https://doi.org/10.1149/1.2778851.

[48] J. Li, M.H. Wang, Y.S. Ho, Trends in research on global climate change: A Science Citation Index Expanded-based analysis, Glob. Planet. Change. 77 (2011) 13–20. https://doi.org/10.1016/j.gloplacha.2011.02.005.

[49] M. Acerce, D. Voiry, M. Chhowalla, Metallic 1T phase MoS_2 nanosheets as supercapacitor electrode materials, Nat. Nanotechnol. 10 (2015) 313–318. https://doi.org/10.1038/nnano.2015.40.

[50] X. Rui, H. Tan, Q. Yan, Nanostructured metal sulfides for energy storage, Nanoscale. 6 (2014) 9889–9924. https://doi.org/10.1039/c4nr03057e.

[51] H. Tang, J. Wang, H. Yin, H. Zhao, D. Wang, Z. Tang, Growth of polypyrrole ultrathin films on mos_2 monolayers as high-performance supercapacitor electrodes, Adv. Mater. 27 (2015) 1117–1123. https://doi.org/10.1002/adma.201404622.

Chapter Three[31,2]

Preparation, Properties, and Applications of Molybdenum Sulfide

This chapter has been published in part as:

[1] **Bello, I. T.**, Oladipo, A. O., Adedokun, O., and Dhlamini, M. S. (2020). Recent advances on the preparation and electrochemical analysis of MoS_2-based materials for supercapacitor applications: A mini-review. *Materials Today Communications*, Vol. 25 (2020) 101664. Page 1-9. https://doi.org/10.1016/j.mtcomm.2020.101664

[2] **Bello, I. T.**, Adio, S. A., Oladipo, A. O., Adedokun, O., Mathevula, L. E., and Dhlamini, M. S. (2021). Molybdenum sulfide-based supercapacitors: from synthetic, bibliometric, and qualitative perspectives. *International Journal of Energy Research*, Vol. 45, Page 12665-12692. https://doi.org/10.1002/er.6690

3.1. Introduction

The recent advances in the synthesis techniques, properties, and applications of molybdenum sulfide (MoS_2) were detailed in this section. The general methods of preparing MoS_2 in terms of the top-down and bottom-up techniques were also highlighted. The characterized properties of the MoS_2 such as bulk, optical, electronic, mechanical, magnetic, and valleytronic properties were also discussed with their respective applications. This is to have a better understanding of the material used in this study.

3.2. Preparation Methods

The two general approaches employed for synthesizing a few- or mono- and multi-layer 2D nanomaterials and MoS_2 can be categorized into top-down and bottom-up approaches. The top-down approach depends on the exfoliation of layered bulk materials, it includes mechanical and liquid phase exfoliation methods that employ physical and solvent assisted processes, respectively. On the other hand, the bottom-up methods rely on metal salts as precursors to produce a nanosheets material via chemical reactions. The fascinating and significant properties of MoS_2 nanostructures have led to the design of several preparation techniques, such as wet chemical synthesis (Hydrothermal and Solvothermal) [1,2], chemical vapor deposition [3,4], electrochemical Li-intercalation and exfoliation [5,6], and mechanical exfoliation [7–11].

3.2.1. Top-down Approaches

The top-down approach depends on the exfoliation of layered bulk materials, it includes mechanical and liquid phase exfoliation methods that employ physical- and solvent-assisted processes, respectively. Other top-down approaches include Solvent-based exfoliation, Surfactant-assisted exfoliation, Ion-intercalation/exfoliation, electrochemical lithiation-intercalation, and other sonication methods.

3.2.1.1.Mechanical Exfoliation

The mechanical exfoliation of MoS_2 nanostructure and other graphene-like 2D materials was derived from the exfoliation of graphene from bulk graphite using a simple "Scotch Tape method" [12,13]. This method has been traditionally used for intrinsic sheet production and fundamental study, owing to the highest quality of monolayer (2D materials) occurring from mechanical exfoliation techniques to study the pristine properties and device performances [14]. Some of the mechanical exfoliation methods include anodic bonding and micro-exfoliation techniques. The anodic bonding method was proposed by Karim *et al*., as a general method for synthesizing high-quality 2D materials. A larger and comparably controllable size of a few-layer MoS_2 ($10 - 100\ \mu m$) was obtained using the anodic bonding method [15]. In the same vein, micro-exfoliation methods have been used to produce MoS_2 monolayers that are applicable in ultrasensitive photodetectors [16], metal-insulator transition, mobility engineering [17], analog [18], and digital circuits [19]. However, the van der Waals bond of many transition metals dichalcogenides (TMDs) to a typical substrate (SiO_2) was found to be much weaker than that of graphene, which makes the lateral size of the obtained flakes to be very small. These results can be improved by slightly modifying the exfoliation methods to produce a large area of MoS_2 flakes [20]. A monolayer of MoS_2 with a lateral size ($10 - 100\ \mu m$) was reported by Magda *et al*., [20], by substituting the MoS_2-substrate to improve the adhesion between the sulfur atoms. The mechanism shows that sulfur can strongly bind to gold than to SiO_2 substrates. The disadvantage of this mechanism is that the as-exfoliated MoS_2 flakes must be transferred to another substrate for application purposes, which requires low electrical conductivity. Additionally, the mechanical exfoliation method is not suitable for large-scale production because it offers a very low yield and is limited in controlling the size and number of layers. That is why this method is limited to the synthesis of MoS_2 at a

laboratory scale for fundamental research. A schematic diagram of mechanical methods is shown in Figure 3.1 [21].

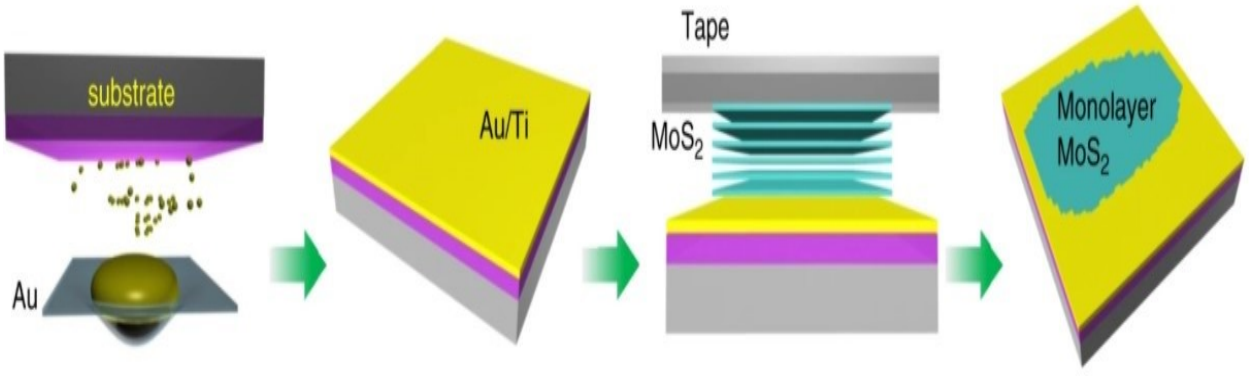

Figure 3. 1 Schematic Diagram of Mechanical Exfoliation Methods.

3.2.1.2.Liquid-Phase Exfoliation

Liquid-phase exfoliation (LPE) is a class of solvent-assisted exfoliation methods. The method is like the mechanical exfoliation techniques. The main distinction is the wet chemistry which involves sonicating bulk materials in organic solvents. LPE is easy to implement for the exfoliation of layered materials, including solvent-based and ion intercalation exfoliation [22–25]. The nature of the solvents used has been established to mainly affected the product of exfoliation. When the surface tension of the solvent matches that of immersed layered bulk materials, it reduces the economic cost of exfoliation. Furthermore, the process results in high stability with a reduced level of and with high stability aggregation and re-stacking [26]. Solvent-based exfoliation (SBE) was first reported by Coleman's group in 2011, in which a single- and few-layer MoS_2 was exfoliated by sonication of submerged bulk MoS_2 in the organic solvent [24]. The result showed that 1-methyl-2pyrrolidone (NMP) was the most active solvent for exfoliation of MoS_2 with the solvent surface tension around 40 mJm^{-2}. Later, O'Neill *et al*. further optimized the SBE method by systematically controlling the starting mass, sonication time, centrifugation conditions, and

sonication power, resulting in a higher concentration of exfoliated MoS_2 and relatively increased lateral size [27]. However, the toxicity and difficulty in the separation of nanosheets from NMP are impediments, which can be unfavorable for certain applications [28,29]. The development of different exfoliation methods using an aqueous solution or volatile solvent is imperative, to overcome the problems associated with NMP. Recently, Zhang *et al*. proposed an alternative solvent for exfoliating MoS_2 nanosheets via a mixture of ethanol and water [30]. Significantly, the non-toxic mixture of water and ethanol are solvents that can be easily dispersed. Besides, another mixture of solvents has been demonstrated to exfoliate MoS_2 nanosheets under different conditions, such as a mixture of chloroform and acetonitrile [31], in which a few-layer MoS_2 nanosheet with 0.4 mg/mL concentration was obtained. Similarly, Lu *et al.*, also proposed that the mixture of H_2O_2 and NMP could be an excellent replacement solvent for exfoliating MoS_2 nanosheets but unexpected oxidation of MoS_2 nanosheets has been a major drawback [32].

3.2.1.3.Surfactant-assisted Exfoliation Methods

Surfactant-assisted exfoliation methods are another class of liquid phase exfoliation aided by organic compounds. It has been categorized as an alternative way of isolating MoS_2 nanosheets [33,34]. Significantly, exfoliation of MoS_2 can be achieved when small organic molecules, polymers, or surfactants with high adsorption energy on the basal plane of MoS_2 nanosheets are used. For example, Coleman *et al.*, employed sodium cholate as an ionic surfactant to support the exfoliation and stabilization of MoS_2 nanosheets, leading to the formation of sodium cholate-coated MoS_2 nanosheets. The exfoliated MoS_2 was stable in an aqueous solution and can simply form a composite with carbon nanotubes and graphene [33]. Huang's group similarly demonstrated the exfoliation of MoS_2 nanosheets using an alkylamine-assisted liquid sonication technique with different alkyl chains. It was observed that butylamine in NMP was effective in increasing the

exfoliation yield. The obtained MoS_2 nanosheets were stable in sequences of polar and nonpolar organic solvents [35]. More recently, Han *et al*., reported the use of bovine serum albumin (BSA) as the exfoliating and stabilizing agent to produce MoS_2 nanosheets in water. The result showed that BSA can adsorb onto MoS_2 layers to form a composite (MoS_2-BSA) that possesses good biocompatibility and a higher binding capacity in comparison to pesticides [36]. On the other hand, Liu *et al*., demonstrated that polyvinylpyrrolidone (PVP) can be used in ethanol to improve the exfoliation of MoS_2 nanosheets from its bulk materials. They found that PVP could easily be adsorbed on the MoS_2 surfaces, due to its excellent solubility thereby forming PVP-coated MoS_2 composite nanosheets [34].

3.2.1.4.Ion-intercalation/exfoliation Methods

Ion-intercalation/exfoliation methods are another way of improving the exfoliated layered material's efficiency through inorganic ions intercalators. Due to the small interlayer space of MoS_2, only alkali-metal ions and Lewis bases with small radii can penetrate the interlayer space of bulk MoS_2 materials [37]. Lithium-ion intercalation (LII) is one of the most effective and generally accepted intercalators for exfoliating MoS_2 nanosheets resulting in high throughput nanosheets. In the LII method, an intercalated MoS_2 can be obtained in three steps, firstly, the intercalation of lithium into the interlayer space of bulk MoS_2 is followed by exfoliation, and thereafter the sonication of the intercalated compound. Importantly, it should be noted that there is a phase structural transformation of Li-ion intercalation of MoS_2 from hexagonal (2H) to octahedral (1T) phase [5,38–41]. Chhowalla *et al*., reported a non-controllable Li-ion intercalated single-layer MoS_2 using n-butyllithium as the source of intercalation [39,41]. Loh's group recently demonstrated a two-step process of expansion and intercalation technique to obtain high-quality

intercalated single-layer MoS_2 nanosheets [42]. However, the process may be hazardous due to the possibility of self-explosion of intercalators (Li, Na, and K) in the air.

3.2.1.5.Electrochemical Lithiation-intercalation Methods

More recently, Huang *et al*. developed a more efficient and highly controllable method of intercalating MoS_2 via an electrochemical lithiation-intercalation of bulk MoS_2, which indicated some advantages compared to the aforementioned methods [5]. The experimental setup of the electrochemical lithiation-intercalation is shown in Figure 3.2. Briefly, bulk MoS_2 was integrated with a test cell as the cathode, and lithium ions were provided from the lithium foil used as the anode. After the completion of the lithium intercalation process, the intercalated compound was washed with acetone and ultrasonicated in ethanol or water to remove the residual electrolyte. The MoS_2 2D nanosheets were successfully exfoliated and isolated respectively. A similar electrochemical method for the structural evolution of intercalated MoS_2 by controlling Na^+ was recently reported [43]. Likewise, Dravid and colleagues have recently demonstrated the controllable recovery of the semiconducting properties of the MoS_2 nanosheets treated with Li directly in solution [44]. Generally, the product of this method was dramatically improved in comparison to mechanical exfoliation. Liquid phase exfoliation presents a simple low-cost process, producing relatively high-quality, large quantities of 2D nanosheets. It was therefore considered to be the most appropriate method for large-scale industrial production of single- to few-layer 2D materials at a low expense [24].

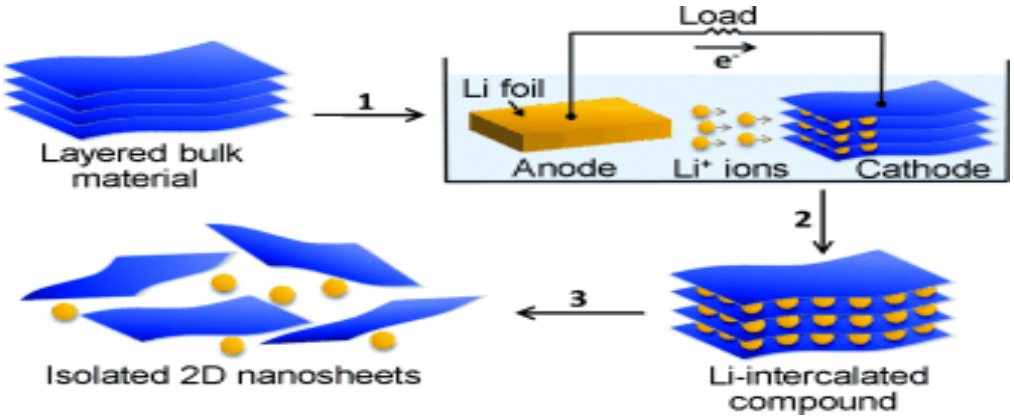

Figure 3. 2 Experimental setup of the electrochemical lithiation-intercalation.

3.2.1.6.Other Sonication Methods

There are few other sonication methods to enhance the efficacy of the exfoliation of MoS_2 nanosheets through external forces. Typically, the shear force generated from mechanical grinding could be used to detach the MoS_2 layer from bulk materials, thus promoting the exfoliation of MoS_2 nanosheets [45]. This method was reported by Wong et al., which combined grinding and sonication techniques to prepare a highly concentrated solution of MoS_2 nanosheets from bulk MoS_2 powder [45]. Similarly, a grinding-assisted sonication process was employed to exfoliate MoS_2 from the mixture of sodium dodecyl sulfate (SDS), water, and NMP solution [46,47]. Also, Kalantar and colleagues investigated the effect of different solvents and their advantages on the exfoliation of MoS_2 nanosheets using the grinding-assisted exfoliation method. It was discovered that the solvents play a critical role in determining the yield of exfoliation as well as the layer sizes and thickness [48]. Wei and colleagues have recently demonstrated that the "quenching cracks" induced by liquid nitrogen could greatly enhance the exfoliation efficiency of MoS_2 nanosheets, as the quenching cracks induced by instant cooling could break the van der Waals forces between the adjacent layers of MoS_2 [49]. Nonetheless, caution must be taken when using this method since careful handling of liquid nitrogen is required. Alternatively, electrochemical exfoliation using a

two-electrode cell can be employed. Lee *et al*. reported the use of two-electrode cells for MoS_2 nanosheets exfoliation from bulk MoS_2 crystal [50]. However, there is some degree of oxidation of the exfoliated MoS_2 nanosheets during the electrochemical exfoliation and the obtained nanosheets were multi-layers instead of single-layer nanosheets.

3.2.2. Bottom-up Approach

The bottom-up methods rely on metal salts as precursors to produce a nanosheets material via chemical reactions. Among the generally accepted bottom-up techniques are chemical vapor deposition, hydrothermal, solvothermal, and Hot-injection methods.

3.2.2.1.Chemical Vapor Deposition (CVD)

The chemical vapor deposition (CVD) method has been widely accepted as the most suitable method to prepare high-quality and controllable MoS_2 among all the synthesis techniques. The formation of highly uniform, large surface area MoS_2 using the CVD method is most compatible with the existing semiconductor fabrication processes. This method directly highlights the heterostructures layered formation that can be devoid of injection of interfacial contamination during layer by the layer transfer process, and continuous preparation of a single film with a certain thickness [51–53]. The starting precursors currently used for the preparation of MoS_2 include Molybdenum (Mo) based powder [54,55], Molybdenum Sulfide (MoS_2) powder [56], deposited molybdenum (Mo) based film [57,58] and ammonium molybdates [4]. The sulfurization of the Mo-based compound was first reported by Lain-Jong et al., [54], to prepare large-area single-layer MoS_2 films on SiO_2 (silicon dioxide) substrate at room temperature through the CVD method. Solid precursors of MoO_3 and sulfur were used with a graphene-like pretreated SiO_2 substrate to increase the nucleation points (Figure 3.3a). Recently, Yu and coworkers also demonstrated a self-limiting CVD technique to grow uniform MoS_2 films under the pressure of around 2-Torr. The

starting reactant used for the sulfurization procedure was Molybdenum chloride ($MoCl_5$) [55]. Yongjie and colleagues further improve large areas of uniform MoS_2 via sulfurization of Mo and Mo oxides using the CVD method. Briefly, they employed electron beam evaporation to pre-deposited a thin layer of Mo (~1-5 nm) on SiO_2 substrate, followed by sulfur vaporization of the substrate in a tube furnace at 750 ^{0}C. The thickness of the obtained MoS_2 was bi- or tri-layer with an interlayer spacing of approximately 6.6 ± 0.2 Å [58]. The resulting MoS_2 of both Lain-Jong and Yongjie groups were found to display excellent electrical properties.

Alternatively, another operational method to prepare MoS_2 with high controllability on a wafer-scale was through simple thermal decomposition of $(NH_4)_2MoS_4$, called thermolysis. In 2012, a bi- or tri-layer of continuous MoS_2 films on insulating substrates was prepared through the thermolysis method (Figure 3.3b) by Liu's group [4]. It was found that the crystallization and electrical behavior of the samples improved significantly due to the second-step high-temperature sulfurization process. Importantly, they noted that the key factor that must be carefully monitored is to have homogeneous dip-coated precursor films on the substrate. Very recently, Wu and colleagues proposed a vapor-solid growth mechanism as a forthright approach to synthesizing MoS_2 from MoS_2 powder. The schematic preparation setup of monolayer MoS_2 films on various substrates is shown in (Figure 3.3c). While figure 3.3d shown the furnace schematic set-up of as-grown MoS_2 nanosheets on graphene. The nanosheets exhibited good Photoluminescence (PL) polarization in the ambient environment. The sample uniformity was the major limitation of this method due to the random nucleation of MoS_2 crystal causing the presence of the thicker zones [56].

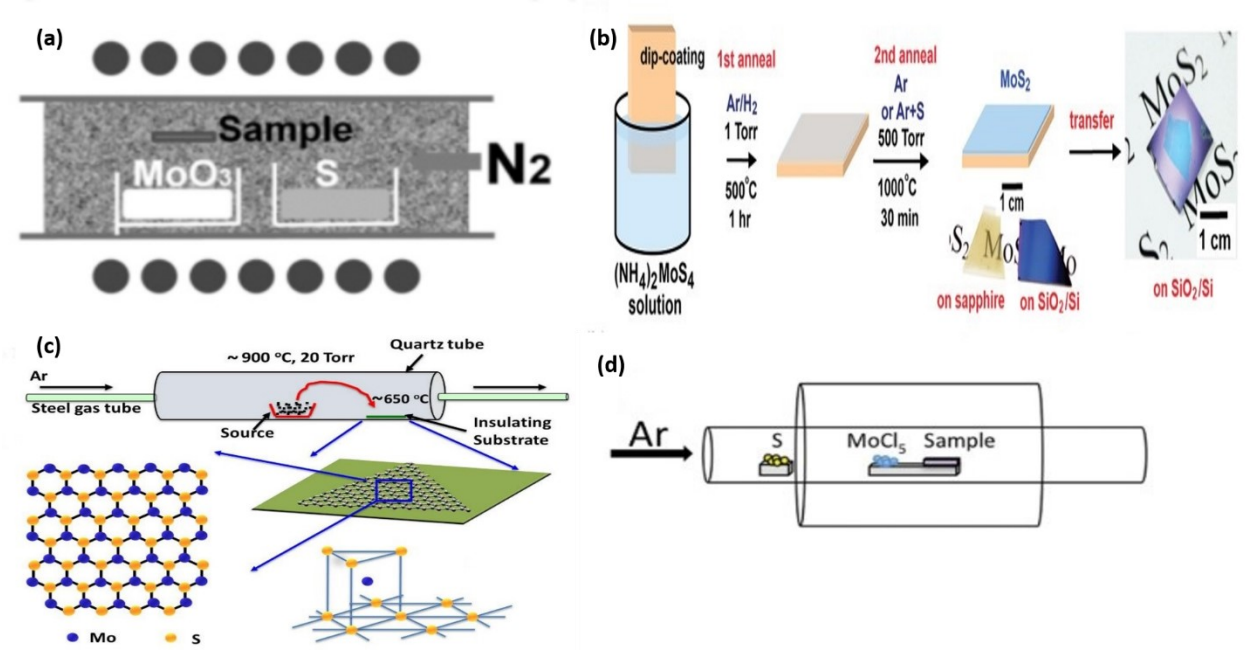

Figure 3. 3 (a) CVD sulfurization MoO_3 with Sulfur, (b) Schematic diagram of Thermolysis, (c) Growth setup of Vapor-solid Mechanism, (d) furnace set up for growth MoS_2.

Some of the reactions involving typical CVD methods are [51]:

$$MoO_3 + 2H_2S + H_2 = MoS_2 + 3H_2O \quad (1)$$

$$8MoO_3 + 24H_2S = 8MoS_2 + 24H_2O + S_8 \quad (2)$$

$$16MoO_3 + 7S_8 = 16MoS_2 + 24SO_2 \quad (3)$$

3.2.2.2. Solution Chemical Synthesis

Solution chemistry synthesis (SCS) methods have been explored to synthesize MoS_2 nanosheets of different sizes and thicknesses. Hydrothermal and solvothermal methods are the two typical approaches of the SCS used to prepare MoS_2 nanosheets using metal salts as starting precursors [59,60]. Both techniques are analogs to each other as they are usually conducted under high temperature and pressure in a sealed vessel (bomb or autoclave). Hydrothermal methods use

water while solvothermal employ organic solvents, as their respective medium of preparations. Owing to its simplicity and wide-ranging applicability, the hydrothermal method has attracted great attention for the synthesis of MoS_2 [60–62]. For instance, Rao *et al*., employed a hydrothermal method to synthesize MoS_2 nanosheets at a high temperature of 453 K using MoO_3 and KSCN as the molybdenum and sulfur sources respectively [59]. The preparation of defect-rich MoS_2 nanosheets was recently reported, where thiourea was used as a reducing and stabilizing agent to obtain ultrathin MoS_2 nanosheets via the hydrothermal method [63]. More recently, ammonium molybdate ($(NH_4)_2MoS_4$) and sulfur powder were used to obtain three-dimensional (3D) tubular structures of MoS_2 through the hydrothermal method [60]. It is worth noting that MoS_2 nanosheets obtained from hydrothermal methods usually aggregate to form nanoflowers [64] and nanotubes [60] structures. However, the hydrothermal method is not easy to obtain well-dispersed single-layer MoS_2 nanosheets, since the ultrathin 2D nanosheets can be easily achieved. Very often, the powders are post-annealed at high temperatures to improve their crystalline quality and purity [26,51]. The schematic representation of solution chemical synthesis of preparing MoS_2 nanosheets is shown in figure 3.4(a, b).

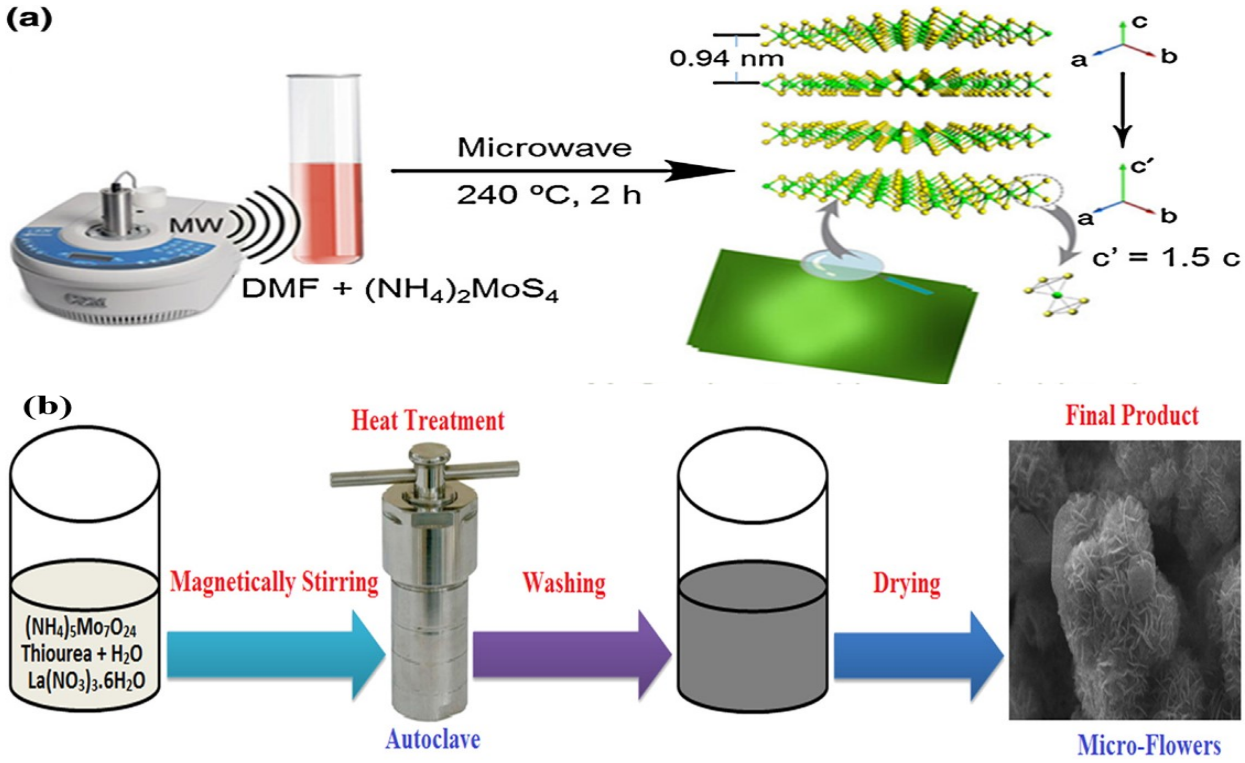

Figure 3. 4 (a) microwave-assisted solvothermal methods, (b) Hydrothermal methods.

3.2.2.3.Hot Injection Methods

A hot injection is another method established for the preparation of MoS_2 nanosheets. This reaction is normally performed in an organic high-boiling mixture (100 ℃ – 500 ℃), where the efficient nucleation and growth process takes place. Organic ligands are specifically used to control the morphology and size, as well as improve the dispersibility of the MoS_2 nanosheets obtained. Synthesis of free-standing MoS_2 nanosheets by decomposition of ammonium tetrathiomolybdate in oleylamine at high temperature (360 ℃) was reported by Altavilla *et al*., [65]. Concisely, the precursor (ammonium tetrathiomolybdate) was stirred in Oleylamine at 100 ℃ for 15 min under N_2 atmosphere, and the mixture was further heated up to 360 ℃. The resulting nanosheets were coated with oleylamine, which stabilized their suspension and prevented their oxidation and aggregation. Likewise, Rao *et al*., demonstrated the preparation of MoS_2

nanosheets under N_2 flow using molybdic acid and thiourea at a high temperature of 773 K [59]. The above-mentioned methods can be used for large-scale synthesis of MoS_2 nanosheets, however, the required inert gas makes its preparation conditions rigid, with difficulty in removing ligands coated on MoS_2 nanosheets. Hence, these challenges affect electron transport and mainly limit their use in catalysis and electronics fields. Many chemical processes of the solution begin at nearly room temperature and atmospheric pressure, where post-annealing is mostly used. Depending on the preparation methods, the products can be either a powder or a thin film [4,66–69]. An infographic representation of the synthesis methods of MoS_2 was shown in figure 3.5, and the summary of the synthesis methods of MoS_2 is presented in Table 3.1 [70].

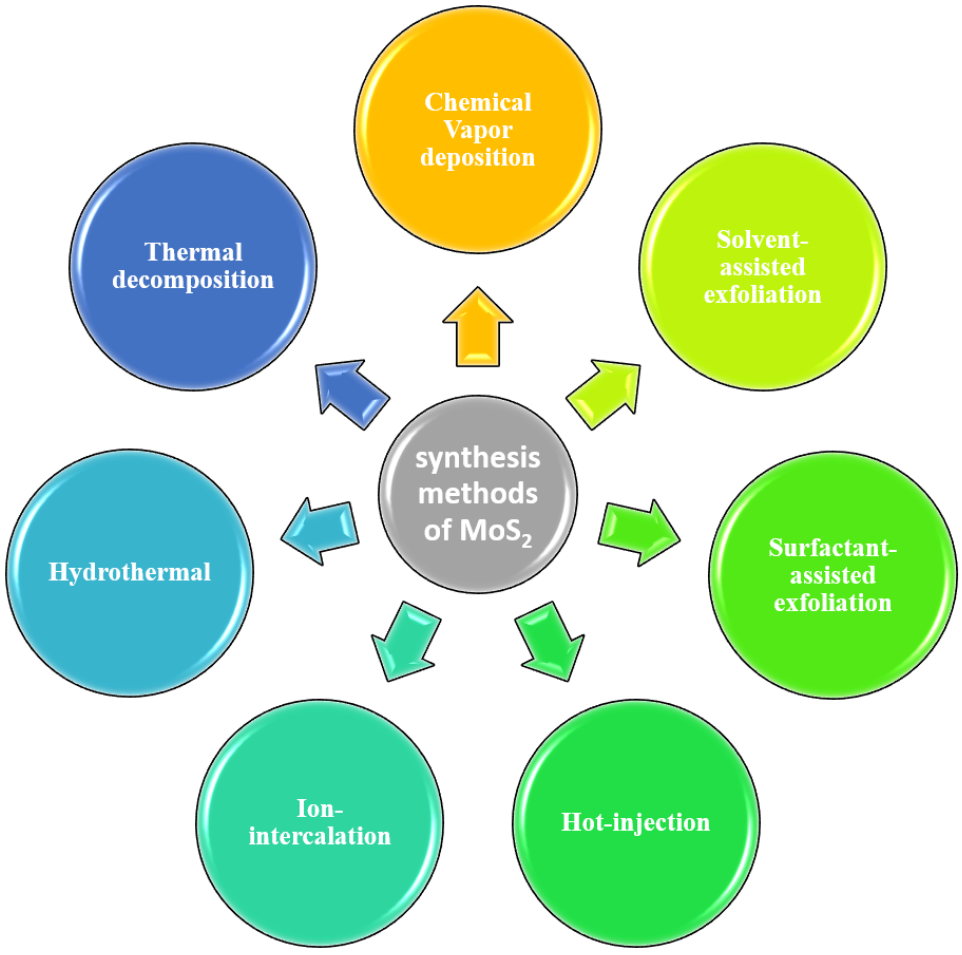

Figure 3. 5 Infographic representation of synthesis methods of MoS_2.

Table 3. 1 Summary of the synthesis methods of MoS_2

Synthetic methods	Precursors	Nanostructures	Morphology
Chemical Vapor deposition:			
Sulfurization of Mo based Compound	MoO_3, S, MoO_3 nanoribbons, S	nanosheets	Monolayer
Sulfurization of Mo and Mo based oxides	Mo Film, S MoO_2 flakes, S	nanosheets	Mono-to-few layers, Rhomboid shape
Thermal decomposition	$(NH_4)_2MoS_4$, S	nanosheets	2-3 layers
Hydrothermal	$(NH_4)_2MoO_4/CH_4N_2S$	nanoflowers/ nanotubes	Single-layer
Ion-intercalation	MoS_2/NMP	nanosheets	Single-/few-layer
Hot-injection	$(NH_4)_2MoS_4$/oleylamine	nanosheets	2-3 layers
Surfactant-assisted exfoliation	MoS_2/PVP	nanosheets	Few-layer
Solvent-assisted exfoliation	Bulk MoS_2/H_2O_2-NMP	Porous nanosheets	Few-layer

3.2.3. Properties of MoS_2

The bulk properties and other various properties of MoS_2 such as optical, electronic, mechanical, magnetic, and valleytronics have been extensively studied owing to their two-dimensional (2D) layered material nature. The exceptional properties of the bulk MoS_2 from the other features have been highlighted below.

3.2.3.1.Bulk Properties

The natural occurrence of MoS_2 in its bulk form, is a molybdenite mineral, with a shiny solid and a dark appearance. They possessed a weak interlayers force of attractions that easily allow sheets to slide over one another. The weak attraction force makes them regularly employed as lubricants. Also, in high vacuum applications bulk MoS_2 is often used as a replacement for graphite, but graphite has a higher maximum operating temperature than MoS_2 [71]. As a semiconductor with an indirect bandgap (~1.2 eV), bulk MoS_2 has a lower bandgap compared to its monolayer form with a direct bandgap of ~1.8 eV, which has limited its applicability in the optoelectronics industry [72]. Recently, special consideration has been given to the production of single-layer MoS_2 from its bulk, as the transition owing to its interesting properties in the monolayer state [7,24,73].

3.2.3.2.Electronic Properties

As iterated in Section 3.3.2.1, the indirect bandgap of bulk MoS_2 increases upon thinning from the bulk layers resulting in a direct bandgap of 1.8 eV. Although the narrow bandgap indicates good potential, it is still lower than the direct bandgap of silicon (1.12 eV) [74]. The bandgap of MoS_2 is grossly affected by mechanical strains, thus changes from direct to indirect bandgap and upgraded to a metallic material from a semiconducting one. The projected density of states (PDOS) of a monolayer MoS_2 possessed some peaks that distinguished it from bulk MoS_2, as their PDOS is almost the same [75]. The electronic properties of material change when doped with other types

of materials. Therefore, a monolayer MoS_2 doped with scandium, chromium, and copper changes to an n-type semiconductor and changes to a p-type semiconductor when doped with Zinc or Nickel [76]. Similarly, Titanium doped MoS_2 changes p-type to n-type (or vice-versa) semiconductor-based on the dopant concentration and sites of doping. MoS_2 behaves as a p-type material when the doping concentration of Ti is below 2.04% and behaves as an n-type when the doping concentration is around 3.57%. This is because the covalent bond between MoS_2 and Ti is strong, thereby increasing the surface dipole moment which induces the reduction of the electron affinity to 0.49 eV when substitutional chemical doping is applied. The Fermi level shifts towards the conduction band at a high doping concentration of 7.69% and merges into the conduction band, where the surface dipole moment decreases and the electron affinity increases, shifting the Fermi level above the conduction band. MoS_2 transforms into a ferromagnetic half-metal with a spin polarization of 1 (arb. unit) in this situation, which is promising for spintronics application. On the other hand, for the three doping concentrations (2.04%, 3.57%, 7.69%), interstitial doping of Ti did not demonstrate any change in electrical characteristics [77].

3.2.3.3.Optical Properties

When a certain wavelength passes through a material, the parameters that determine its response are the absorption coefficient and refractive index. The distance at which a spectrum penetrates the material before being absorbed is controlled by the absorption coefficient, and it indicates a high attenuation to the applied wave. Semiconductors do not have the required energy to move electrons from one excitation state to another (i.e., valence band to conduction band), thereby having a low absorption coefficient for long wavelengths. Likewise, they have a high absorption coefficient for high energy and frequency spectrum (short wavelengths). In terms of absorption coefficient, MoS_2 has a moderately large coefficient for a certain range of wavelengths (400 to 500

nm) with a sharp decay at 500 nm [78]. The tunable bandgap of the MoS_2 that changes with size and structure, is the main factor behind its wide range of applications, which infer from the tunable photoresponsivity from different bandgap, response time, and specific detectivity [79]. The high refractive index (>2) of both bulk and monolayers MoS_2, perfect its usage in coating applications. MoS_2 has different photoluminescence (PL) activity since the PL spectra are influenced by doping, structure, and bandgap of the material. A single layer of MoS_2 has a PL peak exciton (A) and its PL properties can be improved by adding an H_2O_2 solution, which serves as a strong oxidizer with the MoS_2 crystalline structure remaining unchanged [80]. The ratio of the number of emitted photons to the number of generated electron-hole pairs, which is PL quantum yield (QY) are known to be relatively low for the TMDs and they are between 0.01 to 6%. Amani *et. al*., were able to enhance the QY of MoS_2 to a near-unity of 95% through the chemical treatment of an organic superacid. They observed a lifetime of MoS_2 carriers to be around 10.8 ns, which allows it to be applied in solar cells and high-performance lasers [81].

3.2.3.4.Magnetic Properties

The non-magnetization properties of TMDs are well established [82]. However, the advances in the study of electron spin properties of one of the promising candidates of TMDs such as MoS_2 become a must, as the scientific communities are progressing toward nanotechnology and nanoscale materials. So, the tunability of semiconductor features can be achieved, when we successfully added magnetism to them [83]. There have been attempts to induce magnetism into TMDS by various researchers [76,83,84]. For instance, Liang *et al*., 2017, reported a magnetic characteristic of a bulk MoS_2 via an electrical spin injection and detection. A two-terminal spin-valve configuration geometry was used to prove the electrical spin and detection in the conduction band of a semiconducting bulk MoS_2. It was observed that MoS_2 possesses a long spin diffusion

length of about 235 nm and the electron spin-relaxation in MoS_2 can be influenced by an in-plane spin polarization [84]. The magnetism studies using muon spin rotation and scanning tunneling semiconducting were also reported in semiconducting molybdenum dichalcogenides [83]. The presence of a large and homogeneous internal magnetic field was observed and randomly distributed metal vacancies and chalcogen-metal antisites in the lattice at the sub-percent level were also established. In the same vein, semi-metallic ferromagnetism and a unity spin polarization were observed for MoS_2 when doped with Scandium in Tsai and Li's work [76]. The progress recorded so far on the magnetic properties of MoS_2 has shown that the material is a favorable candidate and opens a new way for the study of TMDs in spintronics applications.

3.2.3.5.Valleytronics Properties

Valleytronics is the process of exploring a semiconductor's degrees of freedom for spin-based information processing and data storage applications. TMDs especially MoS_2 have been presented as the material to be investigated beyond their electronic technologies, by using their degrees of freedom for the application of information processing or storage [85]. The electronic band structure of MoS_2 exhibits maxima energy in the valence band and minima in the conduction band, at both K and K' (commonly referred to as -K) points in the Brillouin zone. The energy gap between these two discrete 'valleys' is the same, yet they are distinct in position in momentum space. Angular momentum shifts of +1 for the K-point and -1 for the K' point are required for optical transitions in these valleys. Excitons can thus be purposefully excited into a valley using circularly polarized light, with right-handed (σ+) polarized light exciting excitons in the K valley and left-handed (σ-) polarized light excitons in the K' valley [86]. Light emitted by exciton recombination in the K valley is σ+ polarized, while light emitted by exciton recombination in the K' valley is σ- polarized. These valleys provide a degree of freedom known as 'valley pseudospin,' which could

be utilized in 'valleytronic' devices because they can be addressed individually [87]. Furthermore, at the K and K' points, the spin-orbit split valence band has opposing signs of spin for each of the valleys. This means that the valley pseudospin and charge carrier spin degrees of freedom are related (spin-valley coupling), and charge carrier spin and valley attributes can be controlled optically - through excitation polarization (to choose the valley) and energy (to choose the spin) [88,89]. Excitons in MoS_2 have a valley lifespan of a few picoseconds (the amount of time they stay in their original valley before scattering out). The valley lifespan of electrons exceeds 100 nanoseconds, while the lifetime of holes may be substantially longer. This is the amount of time it takes to accomplish logic operations with the valley pseudospin, and it should be as large as possible for practical applications [90].

3.2.3.6.Mechanical Properties

Comparing the mechanical properties of the bulk MoS_2 with its monolayer structure, a monolayer MoS_2 has more flexibility than its bulk counterpart with Young's modulus of 0.24 TPa. It also has good elasticity properties similar to that of graphene oxide and high strength less than that of graphene, with 0.33 ±0.07 TPa values of its Young's modulus [53]. The deformation and bandgap shift that used to occur in the crystalline structure of other semiconductors when subjected to strain, was prevented in MoS_2 semiconductors due to their flexibility. Nevertheless, the phase transformation of MoS_2 from semiconductor to metal and its electronic characteristics can be altered by a mechanical strain. This changes a MoS_2 monolayer from a direct bandgap to an indirect bandgap and the structural deformation and the transformation to metal can occur in MoS_2, when high strain values are applied [91].

3.3. Applications

Among the layered metal dichalcogenides such as MoS_2, WS_2, TiS_2, and other various transition metals-based materials that have been previously studied in various applications, MoS_2 was extensively investigated in recent times [92–95]. The high electrical conductivity, sheet-like, and surface morphology make it exhibit good capacitive properties [96–99]. MoS_2 heterostructures have demonstrated high-performance ability in photocatalysis applications such as photocatalytic decomposition and adsorption of organic dyes and photocatalytic hydrogen production. It has also been reported to enhance a solid lubricant under severe conditions in tribological applications [92,95]. Additionally, some three-dimensional (3D) structures comprising pristine 2D MoS_2 nanosheets demonstrated good robustness, which efficiently preserves the individual nanosheets with a largely exposed surface area, thereby achieving the full quality of 2D MoS_2 [100–103]. MoS_2 nanosheets and their composites have been comprehensively applied to improve the performance of supercapacitors [104–112], batteries [113,114], solar cells [115–117], sensors [118,119], hydrogen evolution [120–124], photothermal and chemotherapy of cancer [125,126], nano-electronics [127–129], thermoelectric and thermal management [130,131], lubrications [132–134], and dehyrosulfurization [135,136].

3.4. Summary

This chapter examined the methods of synthesis of MoS_2 nanomaterials. In the top-down approach to synthesizing MoS_2, mechanical exfoliation produced the best quality of MoS_2 materials but it offers very low yields with the problem of controlling the size and number of layers. Solvent-assisted exfoliation methods were also regarded as an easy process but the nature of the solvent has been the major factor affecting the product of exfoliation. On the other hand, both CVD and solution chemical methods in the bottom-up approaches have been widely accepted as the most

suitable techniques to synthesize controllably, and high-quality materials on a large scale at a low cost. Hydrothermal methods have been regarded as the most attractive way of synthesizing MoS_2 nanosheets because of their simplicity and wide range of applicability with relatively high electrochemical performance. The hydrothermal method was adopted in the synthesis of the electrode materials used in this study due to its general acceptability.

References

[1] W. Zhou, Z. Yin, Y. Du, X. Huang, Z. Zeng, Z. Fan, H. Liu, J. Wang, H. Zhang, Synthesis of few-layer MoS_2 nanosheet-coated TiO_2 nanobelt heterostructures for enhanced photocatalytic activities, Small. 9 (2013) 140–147. https://doi.org/10.1002/smll.201201161.

[2] K. Chang, W. Chen, L -Cysteine-assisted synthesis of layered MoS_2/graphene composites with excellent electrochemical performances for lithium ion batteries, ACS Nano. 5 (2011) 4720–4728. https://doi.org/10.1021/nn200659w.

[3] Y. Shi, W. Zhou, A.Y. Lu, W. Fang, Y.H. Lee, A.L. Hsu, S.M. Kim, K.K. Kim, H.Y. Yang, L.J. Li, J.C. Idrobo, J. Kong, Van der Waals epitaxy of MoS_2 layers using graphene as growth templates, Nano Lett. 12 (2012) 2784–2791. https://doi.org/10.1021/nl204562j.

[4] K.K. Liu, W. Zhang, Y.H. Lee, Y.C. Lin, M.T. Chang, C.Y. Su, C.S. Chang, H. Li, Y. Shi, H. Zhang, C.S. Lai, L.J. Li, Growth of large-area and highly crystalline MoS_2 thin layers on insulating substrates, Nano Lett. 12 (2012) 1538–1544. https://doi.org/10.1021/nl2043612.

[5] Z. Zeng, Z. Yin, X. Huang, H. Li, Q. He, G. Lu, F. Boey, H. Zhang, Single-layer semiconducting nanosheets: High-yield preparation and device fabrication, Angew. Chemie - Int. Ed. 50 (2011) 11093–11097. https://doi.org/10.1002/anie.201106004.

[6] Z. Zeng, T. Sun, J. Zhu, X. Huang, Z. Yin, G. Lu, Z. Fan, Q. Yan, H.H. Hng, H. Zhang, An effective method for the fabrication of few-layer-thick inorganic nanosheets, Angew. Chemie - Int. Ed. 51 (2012) 9052–9056. https://doi.org/10.1002/anie.201204208.

[7] K.S. Novoselov, D. Jiang, F. Schedin, T.J. Booth, V. V. Khotkevich, S. V. Morozov, A.K. Geim, Two-dimensional atomic crystals, Proc. Natl. Acad. Sci. U. S. A. (2005). https://doi.org/10.1073/pnas.0502848102.

[8] Z. Yin, H. Li, H. Li, L. Jiang, Y. Shi, Y. Sun, G. Lu, Q. Zhang, X. Chen, H. Zhang, Single-

layer MoS_2 phototransistors, ACS Nano. 6 (2012) 74–80. https://doi.org/10.1021/nn2024557.

[9] H. Li, G. Lu, Z. Yin, Q. He, H. Li, Q. Zhang, H. Zhang, Optical identification of single- and few-layer MoS 2 sheets, Small. 8 (2012) 682–686. https://doi.org/10.1002/smll.201101958.

[10] H. Li, G. Lu, Y. Wang, Z. Yin, C. Cong, Q. He, L. Wang, F. Ding, T. Yu, H. Zhang, Mechanical exfoliation and characterization of single- and few-layer nanosheets of WSe2, TaS_2, and $TaSe_2$, Small. 9 (2013) 1974–1981. https://doi.org/10.1002/smll.201202919.

[11] H. Li, Z. Yin, Q. He, H. Li, X. Huang, G. Lu, D.W.H. Fam, A.I.Y. Tok, Q. Zhang, H. Zhang, Fabrication of single- and multilayer MoS_2 film-based field-effect transistors for sensing NO at room temperature, Small. 8 (2012) 63–67. https://doi.org/10.1002/smll.201101016.

[12] K.S. Novoselov, A.K. Geim, S. V Morozov, D. Jiang, Y. Zhang, S. V. Dubonos, I. V Grigorieva, A.A. Firsov, Electric Field Effect in Atomically Thin Carbon Films Supplementary, Science (80-.). 5 (2004) 1–12. https://doi.org/10.1126/science.aab1343.

[13] H. Li, J. Wu, Z. Yin, H. Zhang, Preparation and applications of mechanically exfoliated single-layer and multilayer MoS_2 and WSe_2 nanosheets, Acc. Chem. Res. 47 (2014) 1067–1075. https://doi.org/10.1021/ar4002312.

[14] B. Radisavljevic, A. Radenovic, J. Brivio, V. Giacometti, A. Kis, Single-layer MoS_2 transistors, Nat. Nanotechnol. (2011). https://doi.org/10.1038/nnano.2010.279.

[15] K. Gacem, M. Boukhicha, Z. Chen, A. Shukla, High quality 2D crystals made by anodic bonding: A general technique for layered materials, Nanotechnology. 23 (2012). https://doi.org/10.1088/0957-4484/23/50/505709.

[16] O. Lopez-Sanchez, D. Lembke, M. Kayci, A. Radenovic, A. Kis, Ultrasensitive photodetectors based on monolayer MoS_2, Nat. Nanotechnol. 8 (2013) 497–501.

https://doi.org/10.1038/nnano.2013.100.

[17] B. Radisavljevic, A. Kis, Mobility engineering and a metal-insulator transition in monolayer MoS_2, Nat. Mater. 12 (2013) 815–820. https://doi.org/10.1038/nmat3687.

[18] A. Phys, Small-signal amplifier based on single-layer, 043103 (2014).

[19] B. Radisavljevic, M.B. Whitwick, A. Kis, Integrated circuits and logic operations based on single-layer MoS_2, ACS Nano. 5 (2011) 9934–9938. https://doi.org/10.1021/nn203715c.

[20] G.Z. Magda, J. Petõ, G. Dobrik, C. Hwang, L.P. Biró, L. Tapasztó, Exfoliation of large-area transition metal chalcogenide single layers, Sci. Rep. 5 (2015) 3–7. https://doi.org/10.1038/srep14714.

[21] Y. Huang, Y.H. Pan, R. Yang, L.H. Bao, L. Meng, H.L. Luo, Y.Q. Cai, G.D. Liu, W.J. Zhao, Z. Zhou, L.M. Wu, Z.L. Zhu, M. Huang, L.W. Liu, L. Liu, P. Cheng, K.H. Wu, S.B. Tian, C.Z. Gu, Y.G. Shi, Y.F. Guo, Z.G. Cheng, J.P. Hu, L. Zhao, G.H. Yang, E. Sutter, P. Sutter, Y.L. Wang, W. Ji, X.J. Zhou, H.J. Gao, Universal mechanical exfoliation of large-area 2D crystals, Nat. Commun. 11 (2020). https://doi.org/10.1038/s41467-020-16266-w.

[22] R. Ganatra, Q. Zhang, N. Centre, E. Engineering, Few-layer MoS2: a promising layered semiconductor, ACS Nano. 8 (2014) 4074–4099.

[23] V. Nicolosi, M. Chhowalla, M.G. Kanatzidis, M.S. Strano, J.N. Coleman, Liquid exfoliation of layered materials, Science (80-.). 340 (2013) 72–75. https://doi.org/10.1126/science.1226419.

[24] J.N. Coleman, M. Lotya, A. O'Neill, S.D. Bergin, P.J. King, U. Khan, K. Young, A. Gaucher, S. De, R.J. Smith, I. V. Shvets, S.K. Arora, G. Stanton, H.Y. Kim, K. Lee, G.T. Kim, G.S. Duesberg, T. Hallam, J.J. Boland, J.J. Wang, J.F. Donegan, J.C. Grunlan, G. Moriarty, A. Shmeliov, R.J. Nicholls, J.M. Perkins, E.M. Grieveson, K. Theuwissen, D.W.

McComb, P.D. Nellist, V. Nicolosi, Two-dimensional nanosheets produced by liquid exfoliation of layered materials, Science (80-.). 331 (2011) 568–571. https://doi.org/10.1126/science.1194975.

[25] A. Ciesielski, P. Samorì, Graphene via sonication assisted liquid-phase exfoliation, Chem. Soc. Rev. 43 (2014) 381–398. https://doi.org/10.1039/c3cs60217f.

[26] X. Zhang, Z. Lai, C. Tan, H. Zhang, Solution-Processed Two-Dimensional MoS_2 Nanosheets: Preparation, Hybridization, and Applications, Angew. Chemie - Int. Ed. 55 (2016) 8816–8838. https://doi.org/10.1002/anie.201509933.

[27] A. O'Neill, U. Khan, J.N. Coleman, Preparation of high concentration dispersions of exfoliated MoS_2 with increased flake size, Chem. Mater. 24 (2012) 2414–2421. https://doi.org/10.1021/cm301515z.

[28] Y. Hernandez, V. Nicolosi, M. Lotya, F.M. Blighe, Z. Sun, S. De, I.T. McGovern, B. Holland, M. Byrne, Y.K. Gun'ko, J.J. Boland, P. Niraj, G. Duesberg, S. Krishnamurthy, R. Goodhue, J. Hutchison, V. Scardaci, A.C. Ferrari, J.N. Coleman, High-yield production of graphene by liquid-phase exfoliation of graphite, Nat. Nanotechnol. 3 (2008) 563–568. https://doi.org/10.1038/nnano.2008.215.

[29] H.M. Solomon, B.A. Burgess, G.L. Kennedy, R.E. Staples, 1-methyl-2-pyrrolidone (nmp): Reproductive and developmental toxicity study by inhalation in the rat, Drug Chem. Toxicol. 18 (1995) 271–293. https://doi.org/10.3109/01480549509014324.

[30] K.G. Zhou, N.N. Mao, H.X. Wang, Y. Peng, H.L. Zhang, A mixed-solvent strategy for efficient exfoliation of inorganic graphene analogues, Angew. Chemie - Int. Ed. (2011). https://doi.org/10.1002/anie.201105364.

[31] S.L. Zhang, H. Jung, J.S. Huh, J.B. Yu, W.C. Yang, Efficient exfoliation of MoS2with

volatile solvents and their application for humidity sensor, J. Nanosci. Nanotechnol. 14 (2014) 8518–8522. https://doi.org/10.1166/jnn.2014.9984.

[32] L. Dong, S. Lin, L. Yang, J. Zhang, C. Yang, D. Yang, H. Lu, Spontaneous exfoliation and tailoring of MoS_2 in mixed solvents, Chem. Commun. 50 (2014) 15936–15939. https://doi.org/10.1039/c4cc07238c.

[33] R.J. Smith, P.J. King, M. Lotya, C. Wirtz, U. Khan, S. De, A. O'Neill, G.S. Duesberg, J.C. Grunlan, G. Moriarty, J. Chen, J. Wang, A.I. Minett, V. Nicolosi, J.N. Coleman, Large-scale exfoliation of inorganic layered compounds in aqueous surfactant solutions, Adv. Mater. 23 (2011) 3944–3988. https://doi.org/10.1002/adma.201102584.

[34] J. Liu, Z. Zeng, X. Cao, G. Lu, L.H. Wang, Q.L. Fan, W. Huang, H. Zhang, Preparation of MoS_2-polyvinylpyrrolidone nanocomposites for flexible nonvolatile rewritable memory devices with reduced graphene oxide electrodes, Small. 8 (2012) 3517–3522. https://doi.org/10.1002/smll.201200999.

[35] B. Mao, Y. Yuan, Y. Shao, B. Yang, Z. Xiao, J. Huang, Alkylamine assisted ultrasound exfoliation of MoS_2 nanosheets and organic photovoltaic application, Nanosci. Nanotechnol. Lett. 6 (2014) 685–691. https://doi.org/10.1166/nnl.2014.1827.

[36] G. Guan, S. Zhang, S. Liu, Y. Cai, M. Low, C.P. Teng, I.Y. Phang, Y. Cheng, K.L. Duei, B.M. Srinivasan, Y. Zheng, Y.W. Zhang, M.Y. Han, Protein induces layer-by-layer exfoliation of transition metal dichalcogenides, J. Am. Chem. Soc. 137 (2015) 6152–6155. https://doi.org/10.1021/jacs.5b02780.

[37] E. Benavente, M.A. Santa Ana, F. Mendizábal, G. González, Intercalation chemistry of molybdenum disulfide, Coord. Chem. Rev. 224 (2002) 87–109. https://doi.org/10.1016/S0010-8545(01)00392-7.

[38] M. Chhowalla, H.S. Shin, G. Eda, L.J. Li, K.P. Loh, H. Zhang, The chemistry of two-dimensional layered transition metal dichalcogenide nanosheets, Nat. Chem. 5 (2013) 263–275. https://doi.org/10.1038/nchem.1589.

[39] G. Eda, H. Yamaguchi, D. Voiry, T. Fujita, M. Chen, M. Chhowalla, Photoluminescence from chemically exfoliated MoS_2, Nano Lett. 11 (2011) 5111–5116. https://doi.org/10.1021/nl201874w.

[40] X. Huang, Z. Zeng, S. Bao, M. Wang, X. Qi, Z. Fan, H. Zhang, Solution-phase epitaxial growth of noble metal nanostructures on dispersible single-layer molybdenum disulfide nanosheets, Nat. Commun. 4 (2013) 1–8. https://doi.org/10.1038/ncomms2472.

[41] G. Eda, T. Fujita, H. Yamaguchi, D. Voiry, M. Chen, M. Chhowalla, Coherent atomic and electronic heterostructures of single-layer MoS_2, ACS Nano. 6 (2012) 7311–7317. https://doi.org/10.1021/nn302422x.

[42] J. Zheng, H. Zhang, S. Dong, Y. Liu, C. Tai Nai, H. Suk Shin, H. Young Jeong, B. Liu, K. Ping Loh, High yield exfoliation of two-dimensional chalcogenides using sodium naphthalenide, Nat. Commun. 5 (2014) 1–7. https://doi.org/10.1038/ncomms3995.

[43] X. Wang, X. Shen, Z. Wang, R. Yu, L. Chen, Atomic-scale clarification of structural transition of MoS_2 upon sodium intercalation, ACS Nano. 8 (2014) 11394–11400. https://doi.org/10.1021/nn505501v.

[44] S.S. Chou, Y.K. Huang, J. Kim, B. Kaehr, B.M. Foley, P. Lu, C. Dykstra, P.E. Hopkins, C.J. Brinker, J. Huang, V.P. Dravid, Controlling the metal to semiconductor transition of MoS_2 and WS_2 in solution, J. Am. Chem. Soc. 137 (2015) 1742–1745. https://doi.org/10.1021/ja5107145.

[45] Y. Yao, L. Tolentino, Z. Yang, X. Song, W. Zhang, Y. Chen, C.P. Wong, High-

concentration aqueous dispersions of MoS_2, Adv. Funct. Mater. 23 (2013) 3577–3583. https://doi.org/10.1002/adfm.201201843.

[46] J.Y. Wu, M.N. Lin, L. De Wang, T. Zhang, Photoluminescence of MoS_2 prepared by effective grinding-assisted sonication exfoliation, J. Nanomater. 2014 (2014) 1–7. https://doi.org/10.1155/2014/852735.

[47] Y. Yao, Z. Lin, Z. Li, X. Song, K.S. Moon, C.P. Wong, Large-scale production of two-dimensional nanosheets, J. Mater. Chem. 22 (2012) 13494–13499. https://doi.org/10.1039/c2jm30587a.

[48] E.P. Nguyen, B.J. Carey, T. Daeneke, J.Z. Ou, K. Latham, S. Zhuiykov, K. Kalantar-Zadeh, Investigation of two-solvent grinding-assisted liquid phase exfoliation of layered MoS_2, Chem. Mater. 27 (2015) 53–59. https://doi.org/10.1021/cm502915f.

[49] D. Van Thanh, C.C. Pan, C.W. Chu, K.H. Wei, Production of few-layer MoS_2 nanosheets through exfoliation of liquid N_2-quenched bulk MoS_2, RSC Adv. 4 (2014) 15586–15589. https://doi.org/10.1039/c4ra00297k.

[50] N. Liu, P. Kim, J.H. Kim, J.H. Ye, S. Kim, C.J. Lee, Large-area atomically thin MoS_2 nanosheets prepared using electrochemical exfoliation, ACS Nano. 8 (2014) 6902–6910. https://doi.org/10.1021/nn5016242.

[51] J. Sun, X. Li, W. Guo, M. Zhao, X. Fan, Y. Dong, C. Xu, J. Deng, Y. Fu, Synthesis methods of two-dimensional MoS_2: A brief review, Crystals. 7 (2017) 1–11. https://doi.org/10.3390/cryst7070198.

[52] X. Huang, Z. Zeng, H. Zhang, Metal dichalcogenide nanosheets: Preparation, properties and applications, Chem. Soc. Rev. 42 (2013) 1934–1946. https://doi.org/10.1039/c2cs35387c.

[53] X. Li, H. Zhu, Two-dimensional MoS_2: Properties, preparation, and applications, J. Mater.

1 (2015) 33–44. https://doi.org/10.1016/j.jmat.2015.03.003.

[54] Y.H. Lee, X.Q. Zhang, W. Zhang, M.T. Chang, C. Te Lin, K. Di Chang, Y.C. Yu, J.T.W. Wang, C.S. Chang, L.J. Li, T.W. Lin, Synthesis of large-area MoS_2 atomic layers with chemical vapor deposition, Adv. Mater. 24 (2012) 2320–2325. https://doi.org/10.1002/adma.201104798.

[55] Y. Yu, C. Li, Y. Liu, L. Su, Y. Zhang, L. Cao, Controlled scalable synthesis of uniform, high-quality monolayer and few-layer MoS_2 films, Sci. Rep. 3 (2013) 1–6. https://doi.org/10.1038/srep01866.

[56] S. Wu, C. Huang, G. Aivazian, J.S. Ross, D.H. Cobden, X. Xu, Vapor-solid growth of high optical quality MoS_2 monolayers with near-unity valley polarization, ACS Nano. 7 (2013) 2768–2772. https://doi.org/10.1021/nn4002038.

[57] Y.C. Lin, W. Zhang, J.K. Huang, K.K. Liu, Y.H. Lee, C. Te Liang, C.W. Chu, L.J. Li, Wafer-scale MoS_2 thin layers prepared by MoO_3 sulfurization, Nanoscale. 4 (2012) 6637–6641. https://doi.org/10.1039/c2nr31833d.

[58] Y. Zhan, Z. Liu, S. Najmaei, P.M. Ajayan, J. Lou, Large-area vapor-phase growth and characterization of MoS_2 atomic layers on a SiO_2 substrate, Small. 8 (2012) 966–971. https://doi.org/10.1002/smll.201102654.

[59] H.S.S. Ramakrishna Matte, A. Gomathi, A.K. Manna, D.J. Late, R. Datta, S.K. Pati, C.N.R. Rao, MoS_2 and WS_2 analogues of graphene, Angew. Chemie - Int. Ed. 49 (2010) 4059–4062. https://doi.org/10.1002/anie.201000009.

[60] P.P. Wang, H. Sun, Y. Ji, W. Li, X. Wang, Three-dimensional assembly of single-layered Mos2, Adv. Mater. 26 (2014) 964–969. https://doi.org/10.1002/adma.201304120.

[61] C.N.R. Rao, H.S.S. Ramakrishna Matte, U. Maitra, Graphen-analoge anorganische

Schichtmaterialien, Angew. Chemie. 125 (2013) 13400–13424. https://doi.org/10.1002/ange.201301548.

[62] B.L. Cushing, V.L. Kolesnichenko, C.J. O'Connor, Recent advances in the liquid-phase syntheses of inorganic nanoparticles, Chem. Rev. 104 (2004) 3893–3946. https://doi.org/10.1021/cr030027b.

[63] J. Xie, H. Zhang, S. Li, R. Wang, X. Sun, M. Zhou, J. Zhou, X.W. Lou, Y. Xie, Defect-rich MoS_2 ultrathin nanosheets with additional active edge sites for enhanced electrocatalytic hydrogen evolution, Adv. Mater. 25 (2013) 5807–5813. https://doi.org/10.1002/adma.201302685.

[64] Y. Lu, X. Yao, J. Yin, G. Peng, P. Cui, X. Xu, MoS_2 nanoflowers consisting of nanosheets with a controllable interlayer distance as high-performance lithium ion battery anodes, RSC Adv. 5 (2015) 7938–7943. https://doi.org/10.1039/c4ra14026e.

[65] C. Altavilla, M. Sarno, P. Ciambelli, A novel wet chemistry approach for the synthesis of hybrid 2D free-floating single or multilayer nanosheets of MS2@oleylamine (M=Mo, W), Chem. Mater. 23 (2011) 3879–3885. https://doi.org/10.1021/cm200837g.

[66] H. Liao, Y. Wang, S. Zhang, Y. Qian, A solution low-temperature route to MoS_2 fiber, Chem. Mater. 13 (2001) 6–8. https://doi.org/10.1021/cm000602h.

[67] X. Li, W. Zhang, Y. Wu, C. Min, J. Fang, Solution-processed MoSx as an efficient anode buffer layer in organic solar cells, ACS Appl. Mater. Interfaces. 5 (2013) 8823–8827. https://doi.org/10.1021/am402105d.

[68] I. Bezverkhy, P. Afanasiev, M. Lacroix, Aqueous preparation of highly dispersed molybdenum sulfide, Inorg. Chem. 39 (2000) 5416–5417. https://doi.org/10.1021/ic000627i.

[69] P. Afanasiev, C. Geantet, C. Thomazeau, B. Jouget, Molybdenum polysulfide hollow microtubules grown at room temperature from solution, Chem. Commun. (2000) 1001–1002. https://doi.org/10.1039/b001406k.

[70] I.T. Bello, S.A. Adio, A.O. Oladipo, O. Adedokun, L.E. Mathevula, M.S. Dhlamini, Molybdenum sulfide-based supercapacitors: From synthetic, bibliometric, and qualitative perspectives, Int. J. Energy Res. (2021) 12665–12692. https://doi.org/10.1002/er.6690.

[71] S. Ahmad, S. Mukherjee, A Comparative Study of Electronic Properties of Bulk MoS_2 and Its Monolayer Using DFT Technique: Application of Mechanical Strain on MoS_2 Monolayer, Graphene. 03 (2014) 52–59. https://doi.org/10.4236/graphene.2014.34008.

[72] K.F. Mak, C. Lee, J. Hone, J. Shan, T.F. Heinz, Atomically thin MoS_2: A new direct-gap semiconductor, Phys. Rev. Lett. 105 (2010) 136805-1-136805–4. https://doi.org/10.1103/PhysRevLett.105.136805.

[73] P. Joensen, R.F. Frindt, S.R. Morrison, Single-layer MoS_2, Mater. Res. Bull. 21 (1986) 457–461. https://doi.org/10.1016/0025-5408(86)90011-5.

[74] Y.P. Venkata Subbaiah, K.J. Saji, A. Tiwari, Atomically Thin MoS_2 : A Versatile Nongraphene 2D Material , Adv. Funct. Mater. 26 (2016) 2046–2069. https://doi.org/10.1002/adfm.201504202.

[75] E.S. Kadantsev, P. Hawrylak, Electronic structure of a single MoS_2 monolayer, Solid State Commun. 152 (2012) 909–913. https://doi.org/10.1016/j.ssc.2012.02.005.

[76] Y.C. Tsai, Y. Li, Impact of Doping Concentration on Electronic Properties of Transition Metal-Doped Monolayer Molybdenum Disulfide, IEEE Trans. Electron Devices. 65 (2018) 733–738. https://doi.org/10.1109/TED.2017.2782667.

[77] O. Samy, S. Zeng, M.D. Birowosuto, A. El Moutaouakil, A review on MoS_2 properties,

synthesis, sensing applications and challenges, Crystals. 11 (2021) 1–24. https://doi.org/10.3390/cryst11040355.

[78] S.N.M. Halim, S.N.F. Zuikafly, M.F.M. Taib, F. Ahmad, First Principles Study on Electronic and Optical Properties of Graphene/MoS_2 for Optoelectronic Application, IEEE Int. Conf. Semicond. Electron. Proceedings, ICSE. 2020-July (2020) 29–32. https://doi.org/10.1109/ICSE49846.2020.9166878.

[79] H.S. Nalwa, A review of molybdenum disulfide (MoS_2) based photodetectors: From ultra-broadband, self-powered to flexible devices, RSC Adv. 10 (2020) 30529–30602. https://doi.org/10.1039/d0ra03183f.

[80] Y. Cheng, J.Z. Wang, X.X. Wei, D. Guo, B. Wu, L.W. Yu, X.R. Wang, Y. Shi, Tuning Photoluminescence Performance of Monolayer MoS_2 via H_2O_2 Aqueous Solution, Chinese Phys. Lett. 32 (2015). https://doi.org/10.1088/0256-307X/32/11/117801.

[81] M. Amani, D.H. Lien, D. Kiriya, J. Xiao, A. Azcatl, J. Noh, S.R. Madhvapathy, R. Addou, K.C. Santosh, M. Dubey, K. Cho, R.M. Wallace, S.C. Lee, J.H. He, J.W. Ager, X. Zhang, E. Yablonovitch, A. Javey, Near-unity photoluminescence quantum yield in MoS_2, Science (80-.). 350 (2015) 1065–1068. https://doi.org/10.1126/science.aad2114.

[82] R.M. dos Santos, W.F. da Cunha, R.T. de Sousa Junior, W.F. Giozza, L.A. Ribeiro Junior, Tuning magnetic properties of penta-graphene bilayers through doping with boron, nitrogen, and oxygen, Sci. Rep. 10 (2020) 1–8. https://doi.org/10.1038/s41598-020-73901-8.

[83] Z. Guguchia, A. Kerelsky, D. Edelberg, S. Banerjee, F. Von Rohr, D. Scullion, M. Augustin, M. Scully, D.A. Rhodes, Z. Shermadini, H. Luetkens, A. Shengelaya, C. Baines, E. Morenzoni, A. Amato, J.C. Hone, R. Khasanov, S.J.L. Billinge, E. Santos, A.N. Pasupathy,

Y.J. Uemura, Magnetism in semiconducting molybdenum dichalcogenides, Sci. Adv. 4 (2018) 1–9. https://doi.org/10.1126/sciadv.aat3672.

[84] S. Liang, H. Yang, P. Renucci, B. Tao, P. Laczkowski, S. Mc-Murtry, G. Wang, X. Marie, J.M. George, S. Petit-Watelot, A. Djeffal, S. Mangin, H. Jaffrès, Y. Lu, Electrical spin injection and detection in molybdenum disulfide multilayer channel, Nat. Commun. 8 (2017) 1–9. https://doi.org/10.1038/ncomms14947.

[85] J.R. Schaibley, H. Yu, G. Clark, P. Rivera, J.S. Ross, K.L. Seyler, W. Yao, X. Xu, Valleytronics in 2D materials, Nat. Rev. Mater. 1 (2016) 1–15. https://doi.org/10.1038/natrevmats.2016.55.

[86] T. Cao, G. Wang, W. Han, H. Ye, C. Zhu, J. Shi, Q. Niu, P. Tan, E. Wang, B. Liu, J. Feng, Valley-selective circular dichroism of monolayer molybdenum disulphide, Nat. Commun. 3 (2012). https://doi.org/10.1038/ncomms1882.

[87] X. Xu, W. Yao, D. Xiao, T.F. Heinz, Spin and pseudospins in layered transition metal dichalcogenides, Nat. Phys. 10 (2014) 343–350. https://doi.org/10.1038/nphys2942.

[88] F. Bussolotti, H. Kawai, Z.E. Ooi, V. Chellappan, D. Thian, A.L.C. Pang, K.E.J. Goh, Roadmap on finding chiral valleys: Screening 2d materials for valleytronics, Nano Futur. 2 (2018). https://doi.org/10.1088/2399-1984/aac9d7.

[89] D. Xiao, G. Bin Liu, W. Feng, X. Xu, W. Yao, Coupled spin and valley physics in monolayers of MoS_2 and other group-VI dichalcogenides, Phys. Rev. Lett. 108 (2012) 1–5. https://doi.org/10.1103/PhysRevLett.108.196802.

[90] S.A. Vitale, D. Nezich, J.O. Varghese, P. Kim, N. Gedik, P. Jarillo-Herrero, D. Xiao, M. Rothschild, Valleytronics: Opportunities, Challenges, and Paths Forward, Small. 14 (2018) 1–15. https://doi.org/10.1002/smll.201801483.

[91] M. Ghorbani-Asl, N. Zibouche, M. Wahiduzzaman, A.F. Oliveira, A. Kuc, T. Heine, Electromechanics in MoS_2 and WS_2: Nanotubes vs. monolayers, Sci. Rep. 3 (2013) 1–8. https://doi.org/10.1038/srep02961.

[92] W. Zhou, Z. Yin, Y. Du, X. Huang, Z. Zeng, Z. Fan, H. Liu, J. Wang, H. Zhang, Synthesis of few-layer MoS_2 nanosheet-coated TiO_2 nanobelt heterostructures for enhanced photocatalytic activities, Small. 9 (2013) 140–147. https://doi.org/10.1002/smll.201201161.

[93] W. Ho, J.C. Yu, J. Lin, J. Yu, P. Li, Preparation and photocatalytic behavior of MoS_2 and WS_2 nanocluster sensitized TiO_2, Langmuir. 20 (2004) 5865–5869. https://doi.org/10.1021/la049838g.

[94] M.S. Whittingham, Lithium batteries and cathode materials, Chem. Rev. 104 (2004) 4271–4301. https://doi.org/10.1021/cr020731c.

[95] L. Rapoport, N. Fleischer, R. Tenne, Applications of WS_2 (MoS_2) inorganic nanotubes and fullerene-like nanoparticles for solid lubrication and for structural nanocomposites, J. Mater. Chem. 15 (2005) 1782–1788. https://doi.org/10.1039/b417488g.

[96] Z. Wu, B. Li, Y. Xue, J. Li, Y. Zhang, F. Gao, Fabrication of defect-rich MoS_2 ultrathin nanosheets for application in lithium-ion batteries and supercapacitors, J. Mater. Chem. A. 3 (2015) 19445–19454. https://doi.org/10.1039/c5ta04549e.

[97] S. Deng, Y. Zhong, Y. Zeng, Y. Wang, Z. Yao, F. Yang, S. Lin, X. Wang, X. Lu, X. Xia, J. Tu, Directional Construction of Vertical Nitrogen-Doped 1T-2H $MoSe_2$/Graphene Shell/Core Nanoflake Arrays for Efficient Hydrogen Evolution Reaction, Adv. Mater. 29 (2017) 1700748-1-1700748–8. https://doi.org/10.1002/adma.201700748.

[98] N. Choudhary, M. Patel, Y.H. Ho, N.B. Dahotre, W. Lee, J.Y. Hwang, W. Choi, Directly deposited MoS_2 thin film electrodes for high performance supercapacitors, J. Mater. Chem.

A. (2015). https://doi.org/10.1039/c5ta08095a.

[99] S.S. Karade, D.P. Dubal, B.R. Sankapal, MoS_2 ultrathin nanoflakes for high performance supercapacitors: Room temperature chemical bath deposition (CBD), RSC Adv. 6 (2016) 39159–39165. https://doi.org/10.1039/c6ra04441g.

[100] L. Zhang, H. Bin Wu, Y. Yan, X. Wang, X.W. Lou, Hierarchical MoS_2 microboxes constructed by nanosheets with enhanced electrochemical properties for lithium storage and water splitting, Energy Environ. Sci. 7 (2014) 3302–3306. https://doi.org/10.1039/c4ee01932f.

[101] J. Zhou, J. Qin, N. Zhao, C. Shi, E.Z. Liu, F. He, J. Li, C. He, Salt-template-assisted synthesis of robust 3D honeycomb-like structured MoS_2 and its application as a lithium-ion battery anode, J. Mater. Chem. A. 4 (2016) 8734–8741. https://doi.org/10.1039/c6ta02565j.

[102] J. Wang, J. Liu, J. Luo, P. Liang, D. Chao, L. Lai, J. Lin, Z. Shen, MoS_2 architectures supported on graphene foam/carbon nanotube hybrid films: Highly integrated frameworks with ideal contact for superior lithium storage, J. Mater. Chem. A. 3 (2015) 17534–17543. https://doi.org/10.1039/c5ta03870g.

[103] X.-Y. Yu, H. Hu, Y. Wang, H. Chen, X.W.D. Lou, Ultrathin MoS_2 Nanosheets Supported on N-doped Carbon Nanoboxes with Enhanced Lithium Storage and Electrocatalytic Properties , Angew. Chemie. 127 (2015) 7503–7506. https://doi.org/10.1002/ange.201502117.

[104] W.J. Zhang, K.J. Huang, A review of recent progress in molybdenum disulfide-based supercapacitors and batteries, Inorg. Chem. Front. 4 (2017) 1602–1620. https://doi.org/10.1039/c7qi00515f.

[105] D. (David) Xia, F. Gong, X. Pei, W. Wang, H. Li, W. Zeng, M. Wu, D. V. Papavassiliou,

Molybdenum and tungsten disulfides-based nanocomposite films for energy storage and conversion: A review, Chem. Eng. J. 348 (2018) 908–928. https://doi.org/10.1016/j.cej.2018.04.207.

[106] S.S. Karade, D.P. Dubal, B.R. Sankapal, MoS_2 ultrathin nanoflakes for high performance supercapacitors: Room temperature chemical bath deposition (CBD), RSC Adv. (2016). https://doi.org/10.1039/c6ra04441g.

[107] G. Zhang, H. Liu, J. Qu, J. Li, Two-dimensional layered MoS_2: Rational design, properties and electrochemical applications, Energy Environ. Sci. 9 (2016) 1190–1209. https://doi.org/10.1039/c5ee03761a.

[108] L. Wang, Y. Ma, M. Yang, Y. Qi, Titanium plate supported MoS_2 nanosheet arrays for supercapacitor application, Appl. Surf. Sci. 396 (2017) 1466–1471. https://doi.org/10.1016/j.apsusc.2016.11.193.

[109] Y. Zhao, X. He, R. Chen, Q. Liu, J. Liu, J. Yu, H. Zhang, H. Dong, M. Zhang, R. Li, J. Wang, Flexible all-solid-state asymmetric supercapacitor based on three-dimensional MoS_2/Ketjen black nanoflower arrays, Int. J. Hydrogen Energy. 44 (2019) 13690–13699. https://doi.org/10.1016/j.ijhydene.2019.03.171.

[110] R.B. Pujari, A.C. Lokhande, A.R. Shelke, J.H. Kim, C.D. Lokhande, Chemically deposited nano grain composed MoS_2 thin films for supercapacitor application, J. Colloid Interface Sci. 496 (2017) 1–7. https://doi.org/10.1016/j.jcis.2016.11.026.

[111] I.T. Bello, K.O. Otun, G. Nyongombe, O. Adedokun, G.L. Kabongo, M.S. Dhlamini, Synthesis , Characterization , and Supercapacitor Performance of a Mixed-Phase Mn-Doped MoS_2 Nanoflower, Nanomaterials. 12 (2022) 1–12.

[112] I.T. Bello, K.O. Otun, G. Nyongombe, O. Adedokun, G.L. Kabongo, M.S. Dhlamini, Non-

modulated synthesis of cobalt-doped MoS_2 for improved supercapacitor performance, Int. J. Energy Res. (2022) 1–11. https://doi.org/10.1002/er.7765.

[113] Z.A. Ghazi, X. He, A.M. Khattak, N.A. Khan, B. Liang, A. Iqbal, J. Wang, H. Sin, L. Li, Z. Tang, MoS_2/Celgard Separator as Efficient Polysulfide Barrier for Long-Life Lithium–Sulfur Batteries, Adv. Mater. 29 (2017) 1–6. https://doi.org/10.1002/adma.201606817.

[114] Y. Wang, B. Chen, D.H. Seo, Z.J. Han, J.I. Wong, K.K. Ostrikov, H. Zhang, H.Y. Yang, MoS_2-coated vertical graphene nanosheet for high-performance rechargeable lithium-ion batteries and hydrogen production, NPG Asia Mater. 8 (2016). https://doi.org/10.1038/am.2016.44.

[115] E. Singh, K.S. Kim, G.Y. Yeom, H.S. Nalwa, Atomically thin-layered molybdenum disulfide (MoS_2) for bulk-heterojunction solar cells, ACS Appl. Mater. Interfaces. 9 (2017) 3223–3245. https://doi.org/10.1021/acsami.6b13582.

[116] M.L. Tsai, S.H. Su, J.K. Chang, D.S. Tsai, C.H. Chen, C.I. Wu, L.J. Li, L.J. Chen, J.H. He, Monolayer MoS_2 heterojunction solar cells, ACS Nano. 8 (2014) 8317–8322. https://doi.org/10.1021/nn502776h.

[117] D.Q. Zheng, Z. Zhao, R. Huang, J. Nie, L. Li, Y. Zhang, High-performance piezo-phototronic solar cell based on two-dimensional materials, Nano Energy. 32 (2017) 448–453. https://doi.org/10.1016/j.nanoen.2017.01.005.

[118] M. Park, Y.J. Park, X. Chen, Y.K. Park, M.S. Kim, J.H. Ahn, MoS_2-Based Tactile Sensor for Electronic Skin Applications, Adv. Mater. 28 (2016) 2556–2562. https://doi.org/10.1002/adma.201505124.

[119] Y.H. Wang, K.J. Huang, X. Wu, Recent advances in transition-metal dichalcogenides based electrochemical biosensors: A review, Biosens. Bioelectron. 97 (2017) 305–316.

https://doi.org/10.1016/j.bios.2017.06.011.

[120] Q. Lu, Y. Yu, Q. Ma, B. Chen, H. Zhang, 2D Transition-Metal-Dichalcogenide-Nanosheet-Based Composites for Photocatalytic and Electrocatalytic Hydrogen Evolution Reactions, Adv. Mater. 28 (2016) 1917–1933. https://doi.org/10.1002/adma.201503270.

[121] B. Lai, S.C. Singh, J.K. Bindra, C.S. Saraj, A. Shukla, T.P. Yadav, W. Wu, S.A. McGill, N.S. Dalal, A. Srivastava, C. Guo, Hydrogen evolution reaction from bare and surface-functionalized few-layered MoS_2 nanosheets in acidic and alkaline electrolytes, Mater. Today Chem. 14 (2019) 1–14. https://doi.org/10.1016/j.mtchem.2019.100207.

[122] K. Zhang, Y. Liu, B. Wang, F. Yu, Y. Yang, L. Xing, J. Hao, J. Zeng, B. Mao, W. Shi, S. Yuan, Three-dimensional interconnected MoS_2 nanosheets on industrial 316L stainless steel mesh as an efficient hydrogen evolution electrode, Int. J. Hydrogen Energy. 44 (2019) 1555–1564. https://doi.org/10.1016/j.ijhydene.2018.11.172.

[123] B. Mao, B. Wang, F. Yu, K. Zhang, Z. Zhang, J. Hao, J. Zhong, Y. Liu, W. Shi, Hierarchical MoS_2 nanoflowers on carbon cloth as an efficient cathode electrode for hydrogen evolution under all pH values, Int. J. Hydrogen Energy. 43 (2018) 11038–11046. https://doi.org/10.1016/j.ijhydene.2018.04.226.

[124] A. Chen, R. Cui, Y. He, Q. Wang, J. Zhang, J. Yang, X. Li, Self-assembly of hollow MoS_2 microflakes by one-pot hydrothermal synthesis for efficient electrocatalytic hydrogen evolution, Appl. Surf. Sci. 411 (2017) 210–218. https://doi.org/10.1016/j.apsusc.2017.03.184.

[125] T. Liu, C. Wang, X. Gu, H. Gong, L. Cheng, X. Shi, L. Feng, B. Sun, Z. Liu, Drug delivery with PEGylated MoS_2 nano-sheets for combined photothermal and chemotherapy of cancer, Adv. Mater. 26 (2014) 3433–3440. https://doi.org/10.1002/adma.201305256.

[126] S. Zhu, L. Gong, J. Xie, Z. Gu, Y. Zhao, Design, Synthesis, and Surface Modification of Materials Based on Transition-Metal Dichalcogenides for Biomedical Applications, Small Methods. 1 (2017) 1700220. https://doi.org/10.1002/smtd.201700220.

[127] H.J. Chuang, B. Chamlagain, M. Koehler, M.M. Perera, J. Yan, D. Mandrus, D. Tománek, Z. Zhou, Low-Resistance 2D/2D Ohmic Contacts: A Universal Approach to High-Performance WSe_2, MoS_2, and $MoSe_2$ Transistors, Nano Lett. 16 (2016) 1896–1902. https://doi.org/10.1021/acs.nanolett.5b05066.

[128] R. Kappera, D. Voiry, S.E. Yalcin, B. Branch, G. Gupta, A.D. Mohite, M. Chhowalla, Phase-engineered low-resistance contacts for ultrathin MoS_2 transistors, Nat. Mater. 13 (2014) 1128–1134. https://doi.org/10.1038/nmat4080.

[129] A. Nourbakhsh, A. Zubair, R.N. Sajjad, T.K.G. Amir, W. Chen, S. Fang, X. Ling, J. Kong, M.S. Dresselhaus, E. Kaxiras, K.K. Berggren, D. Antoniadis, T. Palacios, MoS_2 Field-Effect Transistor with Sub-10 nm Channel Length, Nano Lett. 16 (2016) 7798–7806. https://doi.org/10.1021/acs.nanolett.6b03999.

[130] F. Gong, X. Liu, Y. Yang, D. Xia, W. Wang, H.M. Duong, D. V. Papavassiliou, Z. Xu, J. Liao, M. Wu, A facile approach to tune the electrical and thermal properties of graphene aerogels by including bulk MoS_2, Nanomaterials. 7 (2017). https://doi.org/10.3390/nano7120420.

[131] J. Peng, G. Zhang, B. Li, Thermal management in MoS2 based integrated device using near-field radiation, Appl. Phys. Lett. 107 (2015). https://doi.org/10.1063/1.4932125.

[132] Y. Liu, K. Hu, E. Hu, J. Guo, C. Han, X. Hu, Double hollow MoS_2 nano-spheres: Synthesis, tribological properties, and functional conversion from lubrication to photocatalysis, Appl. Surf. Sci. 392 (2017) 1144–1152. https://doi.org/10.1016/j.apsusc.2016.09.132.

[133] K. Gong, X. Wu, G. Zhao, X. Wang, Nanosized MoS_2 deposited on graphene as lubricant additive in polyalkylene glycol for steel/steel contact at elevated temperature, Tribol. Int. 110 (2017) 1–7. https://doi.org/10.1016/j.triboint.2017.01.024.

[134] Y. Huang, L. Liu, J. Lv, J. Yang, J. Sha, Y. Chen, MoS_2 solid-lubricating film fabricated by atomic layer deposition on Si substrate, AIP Adv. 8 (2018). https://doi.org/10.1063/1.5021051.

[135] O.Y. Gutiérrez, S. Singh, E. Schachtl, J. Kim, E. Kondratieva, J. Hein, J.A. Lercher, Effects of the support on the performance and promotion of (Ni)MoS_2 catalysts for simultaneous hydrodenitrogenation and hydrodesulfurization, ACS Catal. 4 (2014) 1487–1499. https://doi.org/10.1021/cs500034d.

[136] S. Rangarajan, M. Mavrikakis, On the Preferred Active Sites of Promoted MoS2 for Hydrodesulfurization with Minimal Organonitrogen Inhibition, ACS Catal. 7 (2017) 501–509. https://doi.org/10.1021/acscatal.6b02735.

Chapter Four

Equipment and Instrumentation

4.1. Instrumentation

This section detailed the working principle of the equipment and instruments employed in characterizing the prepared electrode materials used in this study. The following techniques were used to elucidate the properties of the synthesized electrode materials. Brunauer-Emmett-Teller (BET) (prosimetra, TriStar II 3020 version 2.00) was employed to determine the surface area, the morphology and microstructure studies were carried out by Field emission scanning electron microscopy (FE-SEM JSM-7800 F, JOEL Ltd.) and the structural defects and the vibrational states of the materials were analyzed by Raman spectroscopy (HORIBA scientific XploRA). X-ray diffraction (Rigaku Smartlab), TEM, and XPS techniques were respectively utilized to determine the crystallinity, internal imaging structure, and elemental composition of the materials. The electrochemical performance of the electrode materials was studied using Autolab (PGSTAT302N) electrochemical working station. All the characterizations were under ambient temperature.

4.2. Brunauer-Emmett-Teller (BET)

The Brunauer-Emmett-Teller (BET) surface area analysis model was first reported by Brunauer et. al., 1938. It was named BET from the initials of the scientists (Brunauer-Emmett-Teller) who proposed the model [1]. BET is used to determine the surface area, and pore size distribution in a porous material and to predict moisture sorption of solids. Generally, depending on the nature of the material and type of sorption isotherm, the BET model can properly define their relative isothermal humidity to an accuracy of approximately 50%.

Equation 4.1 can be used to evaluate the surface area of material and define optimal moisture content for drying and storage stability of materials [2].

$$\frac{a_w}{R(1-a_w)} = \frac{1}{\alpha R_o} + \frac{\alpha-1}{\alpha R_o}\alpha_w, \quad (4.1).$$

where R is the moisture regain, R_o is the monolayer moisture regain, a_w is the water activity, and α is approximately equal to the net heat of sorption.

The BET working principles utilize a nitrogen data template for surface area analysis. Nitrogen data is used because of its high purity and strong interaction with most materials [3]. Due to the weak contact between gaseous and solid phases, the surface is cooled with liquid N_2 to obtain detectable levels of adsorption. The pressure of nitrogen gas is gradually increased, causing more molecules to attach to the surface [4]. The higher the surface area accessible for gas adsorption, the smaller the pores, which is determined by closely observing the volume and pressure of the gas at a constant temperature. Figure 4.1 shows the schematic of the volumetric system for measuring BET surface area using nitrogen gas adsorption [5]. In this study, a BET surface analyzer (prosimetra, TriStar II 3020 version 2.00), was employed to measure the surface areas of the electrode materials.

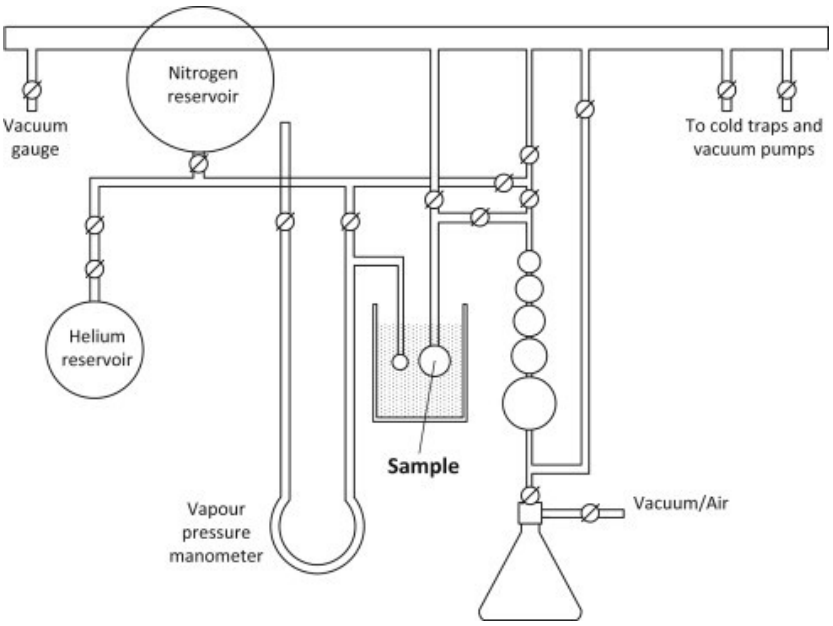

Figure 4. 1 Schematic diagram of a volumetric system for measuring BET surface area using nitrogen gas adsorption [5].

4.3. Field Emission Scanning Electron Spectroscopy (FE-SEM)

Since the invention of the electron microscope (EM) in 1931, the microscopical study of both biological and non-biological samples has been transformed. Advances in electron microscopy techniques, including scanning EM and transmission EM, have broadened their usefulness in a range of fields, including drug toxicity research, mechanism development, crime site investigation, and nano-molecule characterization [6]. FE-SEM spectroscopy is an imaging technique to characterize the morphology and microstructure of nanomaterial. It is frequently employed to provide information on the morphology, topography, and composition of various kinds of materials using electron beam analysis with up to 5,00,000 times magnifications [7]. To form an image in an FE-SEM machine, the surface of the material will be scanned with an electron beam, after being carbon-coated to avoid the charging effect when the material interacts with the beam's radiation. Thus, emitting sequences of radiations and exploited to display the morphology of the nanomaterials [8].

The Scanning Electron Microscope (SEM) operates on the premise of using kinetic energy to generate signals from electron interactions. Secondary electrons, backscattered electrons, and diffracted backscattered electrons are all types of electrons used to observe crystalline elements and photons [6]. An image is created using secondary and backscattered electrons. The primary role of the secondary electrons generated by the specimen is to detect the shape and topography of the specimen, whilst the backscattered electrons exhibit a contrast in the composition of the specimen's constituents [9]. The FE-SEM equipment used to study the microstructure and morphology of the electrode materials procured from Joel of the JSM-7800F model, which operates between the voltage range of 0.5 t0 30 kV. Figure 4.2 shows the schematic working principle of Scanning Electron Spectroscopy (SEM) [10].

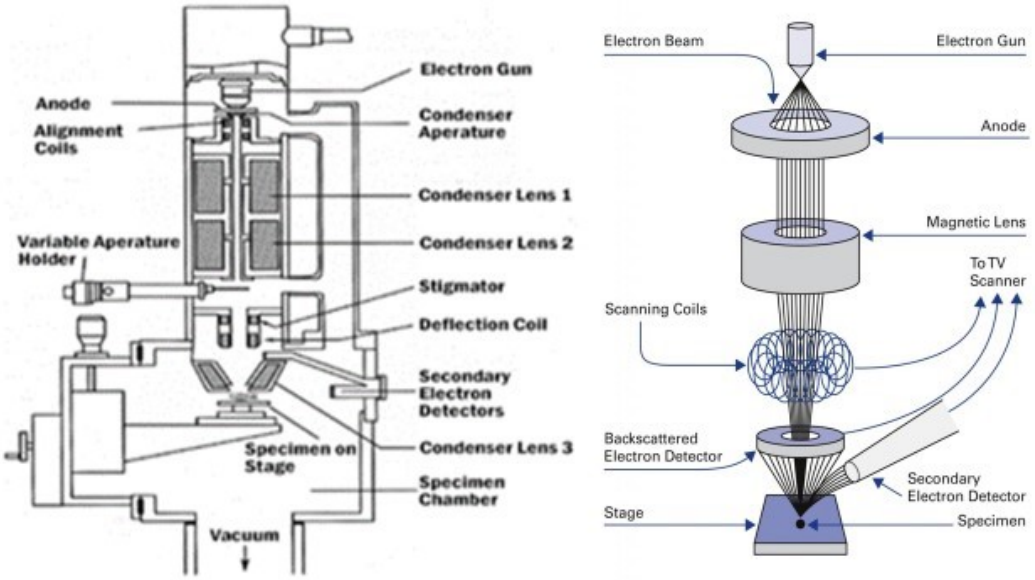

Figure 4. 2 The schematic working principle of Scanning Electron Spectroscopy (SEM) [10].

4.4. Raman spectroscopy

The vibrational states of various molecules were first investigated with Raman scattering in the 1930s after it was first observed in 1928. The generational progress of laser sources and new monochromators and detectors in the last two decades has provided a wide range of Raman spectroscopy applicability to the solution of different problems of technological interest. It is regularly used with infrared spectroscopy, for vibrational spectra acquisition [11]. Raman spectroscopy is a technique for characterizing materials that depend on the scattering of inelastic monochromatic light from a laser source focused on the sample. When the monochromatic light interacts with a sample, the rate of photons in the laser causes a transition in the monochromatic light. The sample absorbed and emitted these photons from the laser light, providing information on the sample's defect. There is a shift in the speed of the emitted photons when compared to monochromatic frequency. The Raman effect describes this shift. The effect of rotation and

vibration is likewise affected by this shift [11,12]. The graphical representation of the working principle of Raman Spectroscopy is shown in figure 4.3 [11].

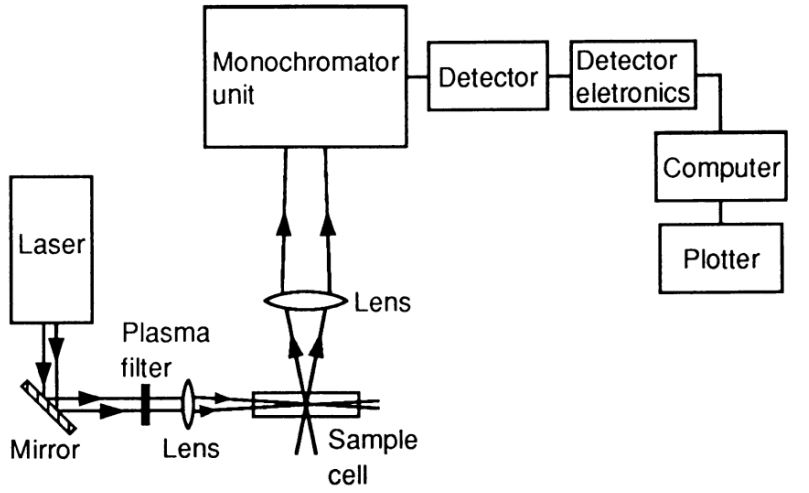

Figure 4. 3 Graphical representation of Raman Spectroscopy working principle [11].

4.5. Transmission Electron Microscopy (TEM)

Since its first discovery in 1931 by Ernst Ruska [13], the study of modern-day science has been significantly influenced by the transmission electron microscope (TEM) analytical technique. The electron beam and the high vacuum and radiation damages were the major limitations that hindered its usability. However, the development of sample preparation methods made TEM to playing an important role in nanomaterial and material sciences [14]. The TEM creates a wide spectrum of signals, allowing the collection of images and a variety of spectra from a single isolated area of the specimen. TEM is a technique for characterizing material to obtain structural dislocations, crystal structure, grain boundaries, as well as chemical analysis [15]. High-resolution images are obtained from TEM analysis when a high-energy beam of an electron is incident on a thin sample. The interaction between the electron beam and the sample causes an interactions between electrons

and the atoms [15]. The composition, defects, and layers growth in a semiconductor can be examined by TEM, and the high-resolution types (HRTEMs) can be used to further analyze the shape, density, size, and quality of quantum dots wells, and wires. Most importantly, TEM can reveal the finest details of the internal structure (individual atoms) of a material, because of its basic working principle of a light microscope, which uses electrons instead of light [16]. Figure 4.4 shows the schematic diagram of the TEM microscope [7].

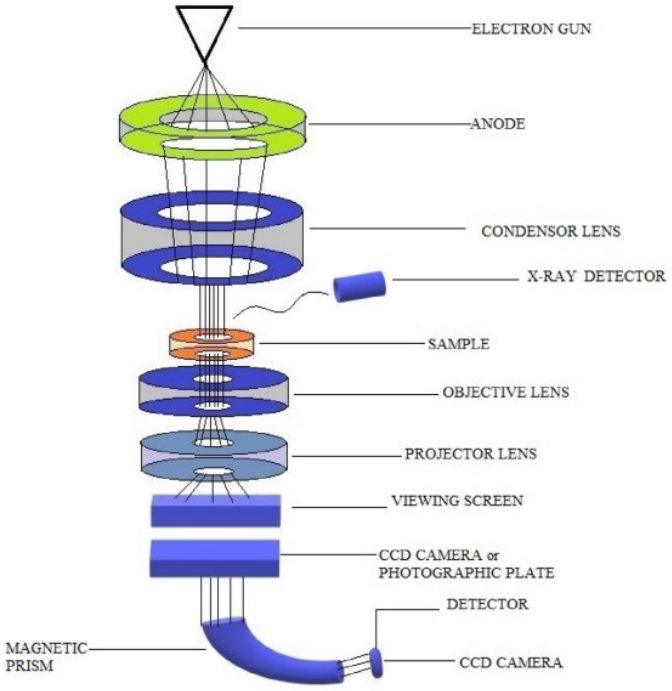

Figure 4. 4 The schematic diagram of the TEM microscope [7].

4.6. X-ray diffraction (XRD)

X-ray diffraction (XRD) is a common technique for determining the diffraction pattern of a nanomaterial. The analytical technique of X-ray diffraction (XRD) is based on the diffraction of X-rays by crystalline materials. X-ray diffraction is an elastic scattering (without loss of photon energy) that results in increasing interference of the studied structured material [17]. X-ray diffraction (XRD) is used to probe the crystal structure, crystalline phases, and crystallite size of

the materials. Furthermore, the X-ray spectrum produced in a cathode ray tube is reliant on the bombardment of intense electrons, which are then filtered to create radiation that is focused on the material. The constructive interference between X-ray monochromatic beams and crystalline materials produces an XRD diffracted pattern, which is a representative blueprint of the material characterized [17]. Constructive interference is created by the interaction of incident rays with the material, which obeys Bragg's Law [18] and results in diffracted patterns. Bragg's Law is the fundamental equation on which XRD operates and is given as;

$$n\boldsymbol{\lambda} = 2d\sin\theta, \tag{4.2}$$

where n is the reflection number, λ is the X-ray wavelength, d is the lattice distance and θ is the diffracted angle. Similarly, the crystalline size of the material can be calculated using the Debye Scherrer's equation [19] given as:

$$D = k\lambda/\beta\cos\theta, \tag{4.3}$$

where D is the crystallite size, k is ~0.9, λ is the wavelength of x-ray (1.54 Å), β is the full width at half maximum and θ is Bragg's angle.

The X-ray diffractometer facility used in the characterization of the electrode materials used in this study was procured from Rigaku Smartlab. The wavelength (λ=0.154 nm) with Cu K_α-line radiation was used during the measurements. A schematic representation of Bragg's Law equation is shown in figure 4.5.

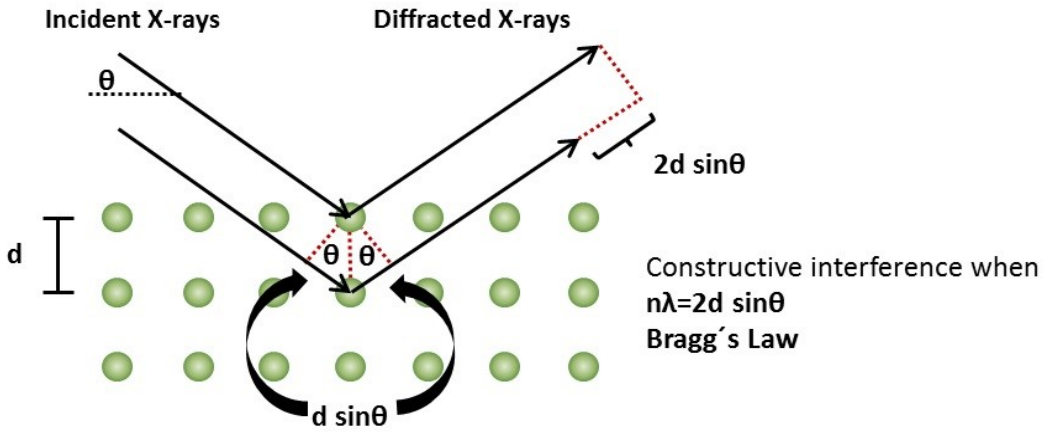

Figure 4. 5 Schematic representation of the Bragg's Law equation.

4.7. X-ray Photoelectron Spectroscopy (XPS)

XPS techniques are used to examine the chemical and electronic states, and the elemental composition of materials. The working principle of XPS is based on the photoelectric effect, which involves the emission of photoelectrons from the surface of a material [20]. X-ray photoelectron spectroscopy (XPS) is a surface-sensitive analytical technique that involves bombarding a material's surface with x-rays and measuring the kinetic energy of the emitted electrons [21]. Surface sensitivity and the capacity to reveal chemical state information from the elements in the sample are two important properties of this approach that make it powerful as an analytical tool. XPS has been used to analyze the surfaces of materials and can identify all elemental components except hydrogen and helium because they have an extremely small photoelectron cross-section for photoemission [21]. The details of how core electrons are been ejected from a characterized material are shown in Figure 4.6.

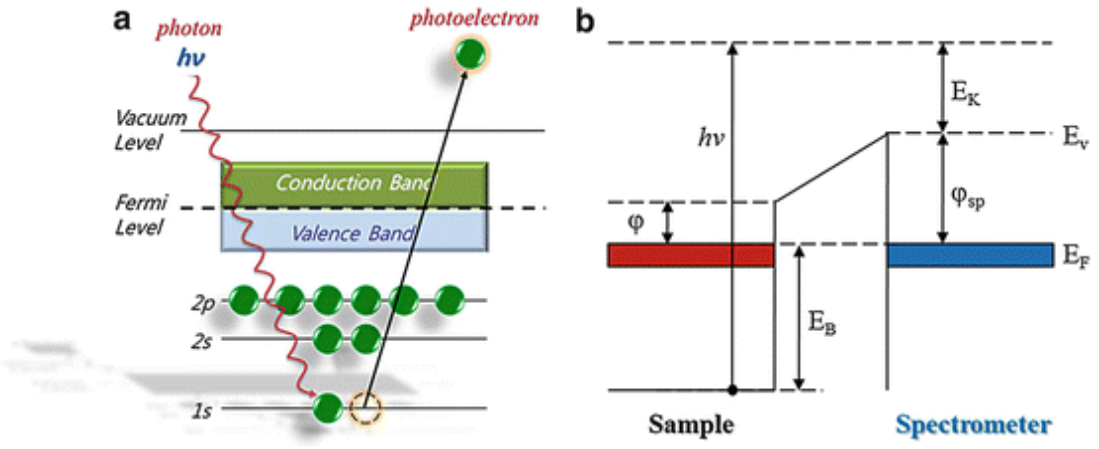

Figure 4. 6 (a) Schematic representation of the core-level photoelectron emission by the photoelectric effect in a metal. (b) Energy-level illustration of the sample and the spectrometer in a core-level photoemission experiment of a metallic sample [22].

Equation 4.4 describes the core electrons being ejected

$$KE = h\upsilon - E_b - \varphi, \quad (4.4),$$

and for an insulating material, the equation becomes:

$$E_b = h\upsilon - KE, \quad (4.5).$$

where KE is the kinetic energy of the electron, h is Planck's constant, υ is the frequency of the incident radiation, E_b is the binding energy and φ is the work function.

The exceptional features of XPS to determine the presence and atomic/ weight quantification of elements in a sample can be attributed to the monochromatic Al K_α X-ray source with excitation energy (hv=1486.6 eV) and base pressure of 1.2 x 10^{-9} Torr [23]. Subsequently, the understanding of the surface structure of the material is made easy, with the information on the state and environment of atoms obtained from the high-resolution scans of the peaks in the sample. Therefore, the purity of the sample can be determined from the XPS analysis. The identity of the functional groups can be established using XPS spectra, which ascertains functionalization.

In this work, XPS KRATOS-SUPRA spectrometer with monochromatic A1 K_{α}, radiation with excitation energy (hv=1486.6 eV), and base pressure of 1.2 x 10^{-9} Torr was utilized to establish the functionalization of the electrode materials.

4.8. Electrochemical Workstation

In an electrochemical cell, current and voltage are usually generated from chemical reactions by the input of the electrochemical signals. Three-electrode systems containing working electrodes (WE), reference electrodes (RE), and current electrodes (CE), are the commonly used electrochemical workstation. The WE are coupled with the prepared electrode and placed on its surface into the electrolyte where the reaction occurs. After a certain potential is applied to the WE, the transfer of electron occurs between the electrode and the electrolyte, and the generated current will pass through CE for balance. The RE serves as a reference when measuring WE potential, while no current passes through it (RE) [24]. A Metrohm Autolab workstation (PGSTAT302N) coupled with Nova 2.1 electrochemical software was employed to investigate the supercapacitive behavior of the electrode materials. The cyclic voltammetry (CV), and galvanostatic charge-discharge (GCD) were measured in the voltage range of 0 to 1 V and the electrochemical impedance spectroscopy (EIS) was also executed on the same workstation in the frequency range 10 mHz-100 kHz. The PGSTAT302N is an electronic tool developed to regulate the applied potential difference to an electrochemical cell between the working electrode (WE) and a reference electrode (RE). Noteworthily, there is a flow of current in WE, while there is no flow of current in RE. Generally, the potential difference between the WE and the RE was measured using a potentiostat, which applies the current via the counter electrode (CE) and measures the current as an iR voltage drop [25,26]. The PGSTAT302N provides cyclic

voltammetry, galvanostatic charge-discharge, and electrochemical impedance spectroscopy curves for the electrochemical evaluations of the electrodes.

References

[1] S. BRUNAUER, H.P. TELLER, E. EDWARD, Adsorption of Gases in Multimolecular Layers, J. Am. Chem. Soc. 60 (1938) 309–319. https://doi.org/10.1016/j.fuel.2016.10.086.

[2] J. Van Den Berg, R.W.J. Meester, Stability properties of a flow process in graphs, Random Struct. Algorithms. 2 (1991) 335–341. https://doi.org/10.1002/rsa.3240020308.

[3] K. Sing, The use of nitrogen adsorption for the characterisation of porous materials, Colloids Surfaces A Physicochem. Eng. Asp. 187–188 (2001) 3–9. https://doi.org/10.1016/S0927-7757(01)00612-4.

[4] J.P.D. Abbatt, Interactions of Atmospheric Trace Gases with Ice Surfaces: Adsorption and Reaction, Chem. Rev. 103 (2003) 4783–4800. https://doi.org/10.1021/cr0206418.

[5] M. Naderi, Surface Area: Brunauer-Emmett-Teller (BET), in: Prog. Filtr. Sep., 2015: pp. 585–608. https://doi.org/10.1016/B978-0-12-384746-1.00014-8.

[6] M. Suga, S. Asahina, Y. Sakuda, H. Kazumori, H. Nishiyama, T. Nokuo, V. Alfredsson, T. Kjellman, S.M. Stevens, H.S. Cho, M. Cho, L. Han, S. Che, M.W. Anderson, F. Schüth, H. Deng, O.M. Yaghi, Z. Liu, H.Y. Jeong, A. Stein, K. Sakamoto, R. Ryoo, O. Terasaki, Recent progress in scanning electron microscopy for the characterization of fine structural details of nano materials, Prog. Solid State Chem. 42 (2014) 1–21. https://doi.org/10.1016/j.progsolidstchem.2014.02.001.

[7] A. Grover, R. Sinha, D. Jyoti, C. Faggio, Imperative role of electron microscopy in toxicity assessment: A review, Microsc. Res. Tech. (2021) 1–14. https://doi.org/10.1002/jemt.24029.

[8] P.J. Goodhew, J. Humphreys, J. Humphreys, Electron Microscopy and Analysis, Third Edit, Taylor & Francis, London, 2000. https://doi.org/10.1201/9781482289343.

[9] Y. Zhu, H. Inada, K. Nakamura, J. Wall, Imaging single atoms using secondary electrons with an aberration-corrected electron microscope, Nat. Mater. 8 (2009) 808–812. https://doi.org/10.1038/nmat2532.

[10] K. Akhtar, S.A. Khan, S.B. Khan, A.M. Asiri, Scanning electron microscopy: Principle and applications in nanomaterials characterization, 2018. https://doi.org/10.1007/978-3-319-92955-2_4.

[11] R.H. ATALLA, U.P. AGARWAL, L.S. BOND, Raman Spectroscopy, in: S.Y. Lin, C.W. Dence (Eds.), Springer Ser. Wood Sci., Springer Berlin Heidelberg, 1992: pp. 162–176.

[12] J.A. Oke, FUNCTIONALIZED MULTIWALL CARBON NANOTUBES FOR ELECTRONIC AND MAGNETIC APPLICATIONS, University of South Africa, 2020.

[13] M. Knoll, E. Ruska, Das Elektronenmikroskop, Zeitschrift Für Phys. 78 (1932) 318–339. https://doi.org/https://doi.org/10.1007/BF01342199.

[14] L.E. Franken, K. Grünewald, E.J. Boekema, M.C.A. Stuart, A Technical Introduction to Transmission Electron Microscopy for Soft-Matter: Imaging, Possibilities, Choices, and Technical Developments, Small. 16 (2020). https://doi.org/10.1002/smll.201906198.

[15] D.B. Williams, C.B. Carter, Transmission Electron Microscopy, Springer US, Plenum, 1996.

[16] P.P.B. HIRSCH, A. HOWIE, R.B. NICHOLSON, D.. W.. PASHLEY, M.J. WHELAN, Electron microscopy of thin crystals, Butterworths, London, 1965.

[17] K. El Bourakadi, R. Bouhfid, A. el K. Qaiss, Characterization techniques for hybrid nanocomposites based on cellulose nanocrystals/nanofibrils and nanoparticles, in: Cellul. Nanocrystal/Nanoparticles Hybrid Nanocomposites, WoodHead Publishing, 2021: pp. 27–64.

[18] P.M. Chaikin, T.C. Lubensky, Principles of Condensed Matter Physics, Cambridge University Press, 2000.

[19] L.A.A. Rodriguez, Di.N. Travessa, Core/Shell Structure of TiO2-Coated MWCNTs for Thermal Protection for High-Temperature Processing of Metal Matrix Composites, Adv. Mater. Sci. Eng. 2018 (2018) 1–11. https://doi.org/10.1155/2018/7026141.

[20] C. Defosse, P.G. Rouxhet, Introduction to X-Ray Photoelectron Spectroscopy, in: J.W. Stucki, W.L. Banwart (Eds.), Adv. Chem. Methods Soil Clay Miner. Res., 63rd ed., Springer, Dordrecht, 1980: pp. 169–203. https://doi.org/10.1007/978-94-009-9094-4_3.

[21] F.A. Stevie, C.L. Donley, Introduction to x-ray photoelectron spectroscopy, J. Vac. Sci. Technol. A. 38 (2020) 063204. https://doi.org/10.1116/6.0000412.

[22] W.H. Doh, V. Papaefthimiou, S. Zafeiratos, Applications of Synchrotron-Based X-Ray Photoelectron Spectroscopy in the Characterization of Nanomaterials, in: C.S.S.R. Kumar (Ed.), Surf. Sci. Tools Nanomater. Charact., 40th ed., Springer Berlin Heidelberg, Berline, 2015: pp. 1–652. https://doi.org/10.1007/978-3-662-44551-8.

[23] G. Greczynski, L. Hultman, Self-consistent modelling of X-ray photoelectron spectra from air-exposed polycrystalline TiN thin films, Appl. Surf. Sci. 387 (2016) 294–300. https://doi.org/10.1016/j.apsusc.2016.06.012.

[24] C.G. Zoski, Handbook of Electrochemistry, Elsevier, 2006.

[25] A.J. Bard, L.R. Faulkner, Electrochemical Methods: Fundamentals and Applications, 2nd ed., Wiley, New York, 2000.

[26] D. Dobos, Electrochemical data : a handbook for electrochemists in industry and universities, Elsevier scientific publishing company, Amsterdam, 1975.

Chapter Five[41]

Non-Modulated Synthesis of Cobalt-Doped MoS_2 (Co-MoS_2) for Improved Supercapacitor Performance

This chapter has been published.

[1] **Bello, I. T.**, Otun, K. O., Gayi Nyongombe, Adedokun, O., Kabongo, G. L., and Dhlamini, M. S. (2022), Non-Modulated Synthesis of Cobalt-Doped MoS_2 for Improved Supercapacitor Performance. *International Journal of Energy Research*, Volume 46, No. 7, Page 8908-8918, https://doi.org/10.1002/er.7765

5.1. Introduction

Of recent, we have seen numerous changes in our society that have sparked an ever-increasing desire for environmentally friendly energy storage systems with increased performance. Regular sources of energy, such as (biomass, hydroelectric power, wind, and solar energy), are inconvenient to use as a primary energy source in practical applications due to their inconstancy [1,2]. Electrochemical capacitors, as one of the energy storage devices (i.e., fuel cells, batteries, and capacitors), have garnered tremendous attention because of the prominent roles they played in solving the energy crisis, global warming, and environmental pollution. The environmental friendliness, fast charge-discharge rates, high power densities, and exceptional cyclic stabilities properties of supercapacitor are promising features of the device over existing energy storage devices [3,4]. On the other hand, conventional batteries, exhibit slow discharge rates but can store a large quantity of charge (i.e., exhibit high energy density). The typical capacitor is noted for having a low energy density, although it has a high charge-discharge rate. Fuel cells are not economical due to the unceasing contribution of external energy for their operation. However, the shortfall on existing devices can be highly improved with the supercapacitors that possess high power density, instantaneous discharge capacity, and remarkable life-cycle. The only drawback affecting supercapacitors is their low energy densities. Interestingly, new electrodes and electrolytes have been developed by the scientific communities to enhance the supercapacitors' energy densities without adversely affecting the devices' high-power densities [4–6].

Electrochemical double-layer capacitors, pseudo-capacitors, and hybrid capacitors are the three types of supercapacitors categorized by their made-up materials. The electrochemical double-layer capacitors (EDLCs) consist of carbon-based material and store charges via an electric double layer phenomenon. While pseudo-capacitors, which are made of any conducting polymers, metal

nitrides, metal oxides, metal sulfides, among others, used reversible redox processes to store charge, and hybrid capacitors involve both EDLC and pseudo-capacitors materials [7–10]. Pseudo-capacitors have high capacitance with low stability compared to EDLCs that have low capacitance with high stability. As a result, composite materials are needed to achieve a better capacitive property while also improving stability. To overcome these limitations, two-dimensional (2D) materials can be explored as suitable replacements due to their different physicochemical properties. The Van der Waals force, improved surface area, and layered structure of two-dimensional (2D) nanosheets with few atomic thicknesses allow the interaction of ions from electrolytes with its rare flexibility and mechanical strength [11–13].

Nowadays, transition metal dichalcogenides (TMDs) with the prevalent structure of MX_2 (M = Mo, W, X = S, or Se) have been actively studied for the performance improvement of the supercapacitor's materials. TMDs are graphene analogs with varying oxidation states and large surface areas, enabling them to store energy in EDLCs and exhibit pseudo-capacitor behavior [13,14]. Because of their natural abundance, easily controllable morphologies, multiple valences, and acceptable bandgap widths, various transition metal sulfides, including that of copper sulfide, nickel sulfide, zinc sulfide, molybdenum sulfide, manganese sulfide, strontium sulfide, and vanadium sulfide, have stirred interest for supercapacitor applications. Among the transition metal sulfides, MoS_2 is a promising electrode material for supercapacitor applications, because of its fascinating sheet-like structure, which provides a huge surface area for double-layered charge storage and a greater intrinsic fast ionic conductivity [15–17]. MoS_2 is made up of covalently S-Mo-S atoms held together by weak van der Waals interactions and has a theoretically larger capacity than graphite. It comes in a variety of polytype formations, including 2H and 1T phases, as well as oxidation states ranging from +2 to +6. In addition, it has a higher in-plane ionic and

electrical conductivity than oxides [10,18]. Because of its unique morphology, outstanding mechanical, and electrical properties, MoS_2 has been investigated for different energy storage, optoelectronics, sensing, and photocatalysis applications due to its similar structure to graphene [19,20].

Molybdenum sulfide (MoS_2) is a member of TMDs families that are analogous to graphene with an akin lamellar structure and a weak Van der Waals force of attraction between S-Mo-S layers. MoS_2 materials have become a popular alternative for supercapacitors due to their graphene-like structure and intriguing electrical, mechanical, and optical properties [21]. The high theoretical capacitance (approx. 1504 Fg^{-1}) of MoS_2 has pinched the attention of the scientific world to extensively explore its promising properties for supercapacitor candidates [22]. Based on its theoretical capacitance values, the intensive investigation of several composites of MoS_2-based supercapacitors has been successfully reported for metal hydroxides, activated carbon, graphene, metal oxide, carbon nanotubes, polymers, and metal sulfides [23–29].

There are also a few metal-doped composites reported for MoS_2-based supercapacitors such as Nickel [30], Manganese [31], Cobalt [11]**,** and Platinum [32] for improving performance. In this work, we reported one-pot hydrothermally assisted non-modulated synthesis of Cobalt-doped MoS_2 for supercapacitor electrode materials. The structural elucidation of the as-prepared composites was done using XRD, Raman spectroscopy, SEM, TEM, and BET analyses. The cyclic voltammetry (CV), electrochemical impedance (EIS), and galvanostatic charge-discharge (GCD) measurements were used to investigate the capacitive properties of the electrode materials. Improved specific capacitance values of 164 Fg^{-1} and 146 Fg^{-1} were, respectively, reported for electrodes at 1A/g, as compared with recent reports on cobalt doped MoS_2 electrodes.

5.2. Methodology

5.2.1. Preparation of Non-modulated Co-doped MoS_2

In the preparation of Co-doped MoS_2, the source of molybdenum is ammonium molybdate, while thiourea serves as the sulfur source and the cobalt source was from cobalt nitrate. The doped MoS_2 was synthesized in a one-pot hydrothermally assisted method with different cobalt concentrations. 1.0 mmol and 30 mmol of molybdenum and sulfur salts were respectively dissolved in 30 mL of deionized water containing cobalt salt. The resultant solutions were vigorously stirred until a homogenous solution was formed. The solution was transferred to a 100 mL Teflon-lined Autoclave and heated at 220 $^{\circ}$C for 18 hours. After cooling to ambient temperature, the black precipitate was collected by centrifugation. The washing was done severally with deionized water followed by ethanol to remove any residual impurities and dried overnight at 80 $^{\circ}$C. The molar ratio of the dopant (cobalt) to molybdenum was 1:1 and 3:1, while the ratio of the sulfur was kept constant throughout the preparations. Lastly, the as-synthesized materials were denoted as CMS_1 and CMS_3 respectively.

5.2.2. Working Electrode Preparation

When making the electrodes, a commercially available 1 cm x 1 cm nickel foam was cleaned with 2.0 M HCl, deionized water, and ethanol through a sonication process for 15 min and dried in a vacuum. An active material (CMS_1 and CMS_3) was mixed with mesoporous carbon black, PVDF (in the ratio 80:10:10) with appropriate droppings of NMP and sonicated for 10 minutes to make a slurry. The slurry was dropped over the cleaned nickel foam and dried for 12 hours in a vacuum oven at 80 $^{\circ}$C. The mass of the active material deposited on the nickel foam after drying was approximately 1 to 2 mg.

5.2.3. Characterizations

A Rigaku Smartlab X-ray diffractometer (0.154 nm Cu Kα line) was successfully employed to study the crystal structures of the prepared materials. Field emission scanning electron microscopy (FE-SEM JSM-7800 F, JOEL Ltd) and transmission electron microscopy (TEM) were used to analyze the surface morphology and microstructure, respectively. HORIBA scientific XploRA was used to measure Raman spectra at 532 nm (2.411 eV) LASER light excitation energy. A surface area prosimetra (TriStar II 3020 version 2.00) was used to determine the Brunauer-Emmett-Teller (BET) surface area.

5.2.4. Electrochemical Measurements

A three-electrode configuration of Autolab PGSTAT302N electrochemical working station was employed to investigate the electrochemical performance of the electrode materials (CMS_1 and CMS_3) in an electrolyte medium of 1 M KOH. The three-electrode cells included the prepared working electrode on nickel foam, a counter electrode (Platinum wire), and a reference electrode (Ag/AgCl, 3 M KCl). The cyclic voltammetry (CV) loops were analyzed at a different scan rate, ranging from 5, 10, 20, 50, and 100 mVs^{-1} in a potential window between -0.1 to 0.4 V. At varying current densities of 1, 2, 3, 5, and 10 Ag^{-1}, galvanostatic charge-discharge (GCD) tests were taken. The electrochemical impedance spectroscopy (EIS) was also tested at an amplitude of 5 mV, between the frequency range of 100 kHz to 10 MHz, and the cyclic stability was tested at 1 Ag^{-1} with 0 to 0.5 V cut-off voltage. To calculate the performance parameters of the supercapacitor electrodes, equations 1, 2, and 3 were respectively used to determine the specific capacitances (C_{sp}) from GCD curves, energy (E), and power densities (P).

$$C_{sp} = \frac{\mathrm{I}\Delta\mathrm{t}}{\mathrm{m}\Delta V} \tag{5.1}$$

where I, is the current density, m, active mass, Δt, and ΔV are the average of charge-discharge time and voltage.

$$E = {}^{1}/_{2}\frac{Cs\Delta V^{2}}{3.6} \quad (5.2),$$

$$P = \frac{3600\times energy\ density}{\Delta t} \quad (5.3).$$

5.3. Results and Discussion

5.3.1. X-ray diffraction patterns

The X-ray diffraction (XRD) patterns of the Co-doped MoS_2 (CMS_1 and CMS_3) are shown in Figure 5.1, which reveals the structural and polycrystalline nature of the materials. The presence of laminar structures initiating from the intercalation guest ions and molecules was corroborated by the diffraction peaks corresponding to the plane (002) at 14 degrees. At the (002) and (001) corresponding planes, the peaks appeared to split into two individual peaks, one at a higher angle and the other at a lower angle [33–35]. The observed diffraction peaks at 2 thetas = 26^0 and 28.8^0 correspond to the reflection from (220) and (311) planes of face-centered cubic Co_9S_8, revealing the formation of the small amount of cobalt sulfide [36]. Also, the two theta diffraction peaks located at 33.14^0, $36.07^{0,}$ and 58.97^0 matched well with the planes of (100), (102), and (110), respectively, for hexagonal Co-MoS_2 with JCPDS card number: 37-1492. Besides, the weakening and broadening of some of the diffraction peaks with slight shifts affirmed the inclusion of cobalt in the electrode materials [37]. These further indicate the ideal nature of the samples, which is confirmed by the SEM images. In addition, some of the extra peaks pronounced in CMS_3 may depict the excessive presence of cobalt ions as their concentration increases, which might also affect the electrochemical performance of their respective electrodes.

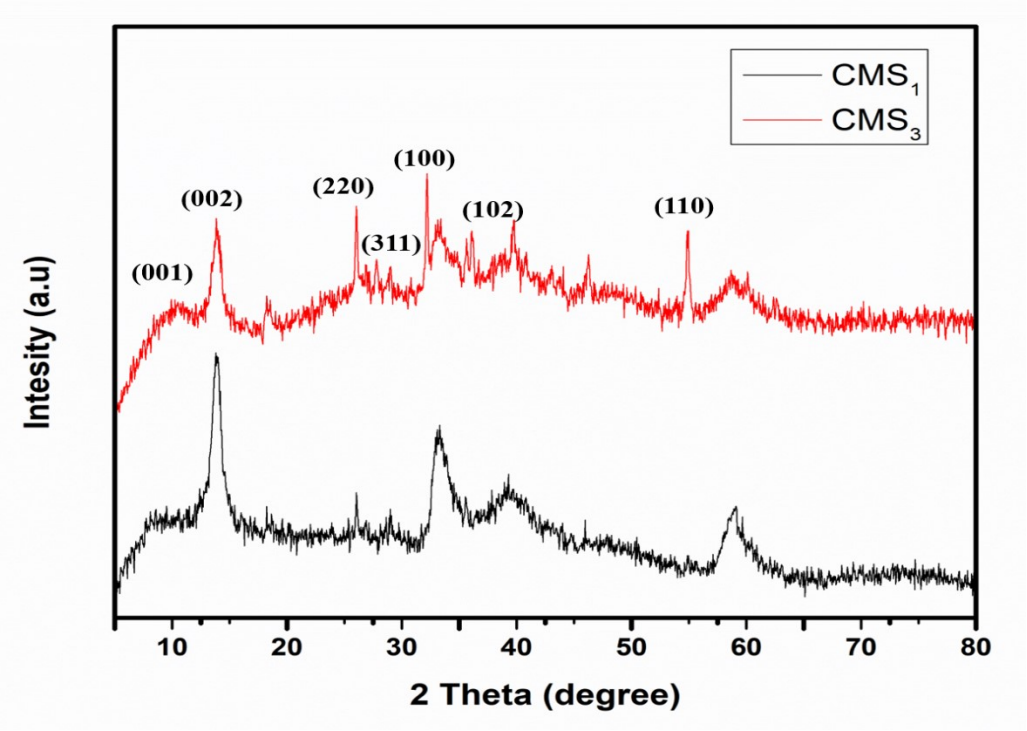

Figure 5. 1 X-ray diffraction (XRD) patterns of the Co-doped MoS_2.

5.3.2. Raman Spectroscopy Analysis

Raman spectroscopy technique was employed to study the doping effects and variations caused by the addition of cobalt to the pristine structure of MoS_2. The active peaks of MoS_2 from the Raman spectra are shown in Figure 5.2. The in-plane E^1_{2g} and A_{1g} out-plane vibrational modes of the MoS_2 are, respectively, corresponding to peaks located at 373.5 cm^{-1} and 400.8 cm^{-1}. Both the E^1_{2g} and A_{1g} vibrational modes are red-shifted compared to bulk MoS_2 (383 and 408 cm^{-1}), and a similar redshift has been reported in the presence of biaxial strain on free-standing MoS_2 sheets [38]. However, the observed shift and biaxial strain could be due to the presence of abundant dopants and defects. Furthermore, as seen by the integrated intensity ratio of E^1_{2g}/A_{1g} (approx. ~0.5) as expected for the Co-Mo-S- phase, Raman spectroscopy similarly shows the abundance of edge-terminated structures. This is because the A_{1g} (E^1_{2g}) mode is preferentially excited for the edge-

(terrace-) terminated layers, and the Co-doped MoS_2 reveals many active sites for enhancing its electrochemical performances [22,38,39].

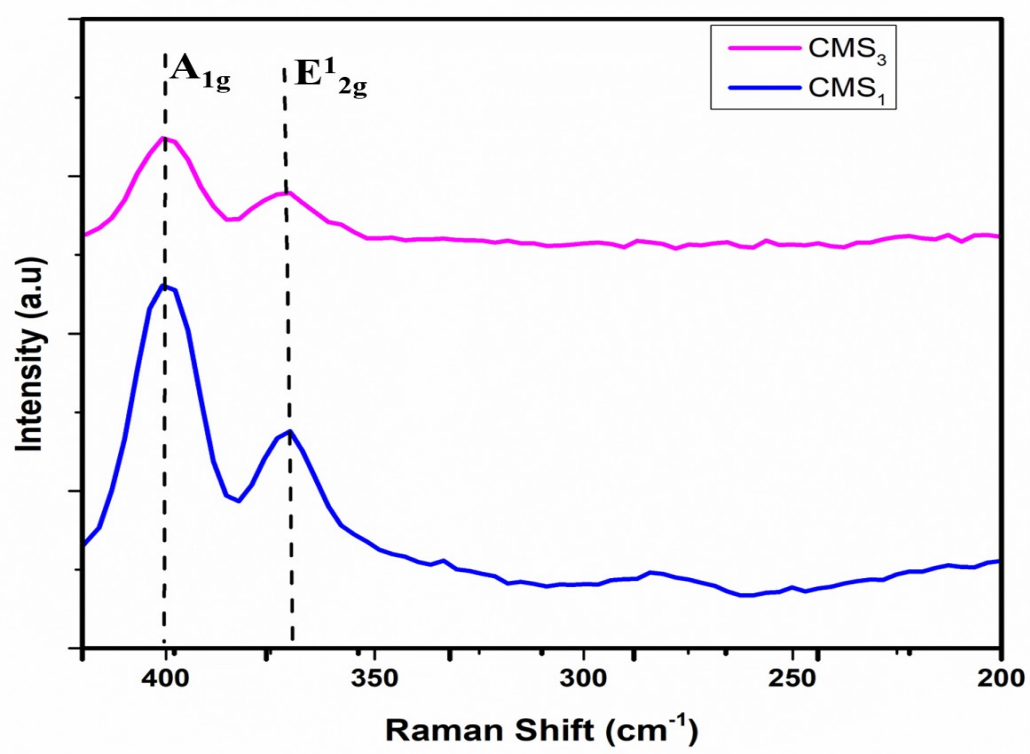

Figure 5. 2 Raman Spectra of the Co-doped MoS_2.

5.3.3. Scanning Electron Microscopy

The morphology and elemental composition of the electrode materials were studied using field emission scanning electron microscopy (FE-SEM). The SEM image (Figure 5.3a) revealed a flower-like morphology of MoS_2-based materials, which shows that more active sites can be anticipated. The flower-like architecture will effectively increase the pore surface area of the easier accessibility of electrolytic ions, resulting in improved electrochemical performance. The detailed elemental composition of the Co-doped MoS_2 electrode materials was shown in figure 5.3b, with the confirmations of the Co incorporated. The carbon peak can be traced to be originated from the carbon capping of the samples before starting SEM-EDS measurement to avoid charging of the

samples during the measurement. The molybdenum and sulfur are situated on the same peaks, due to the operating energy levels of both elements which were respectively around 2.29 and 2.30 KeV.

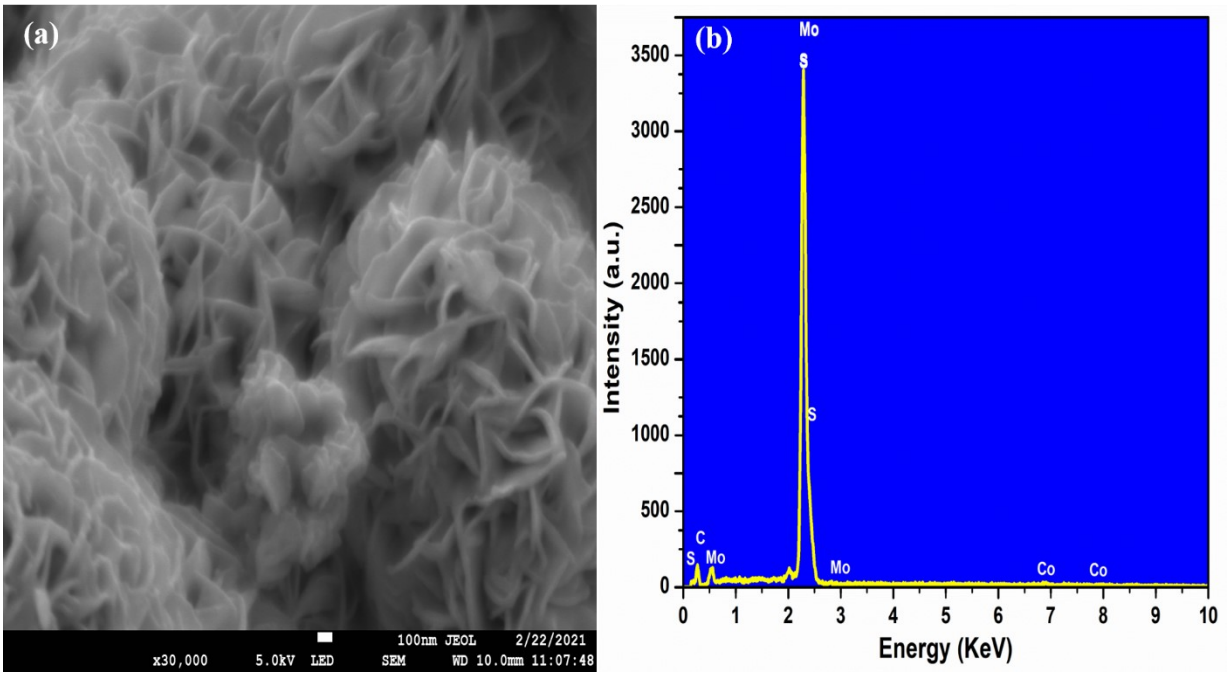

Figure 5. 3 (a) SEM image and (b) EDS Spectra of the as-synthesized electrode materials.

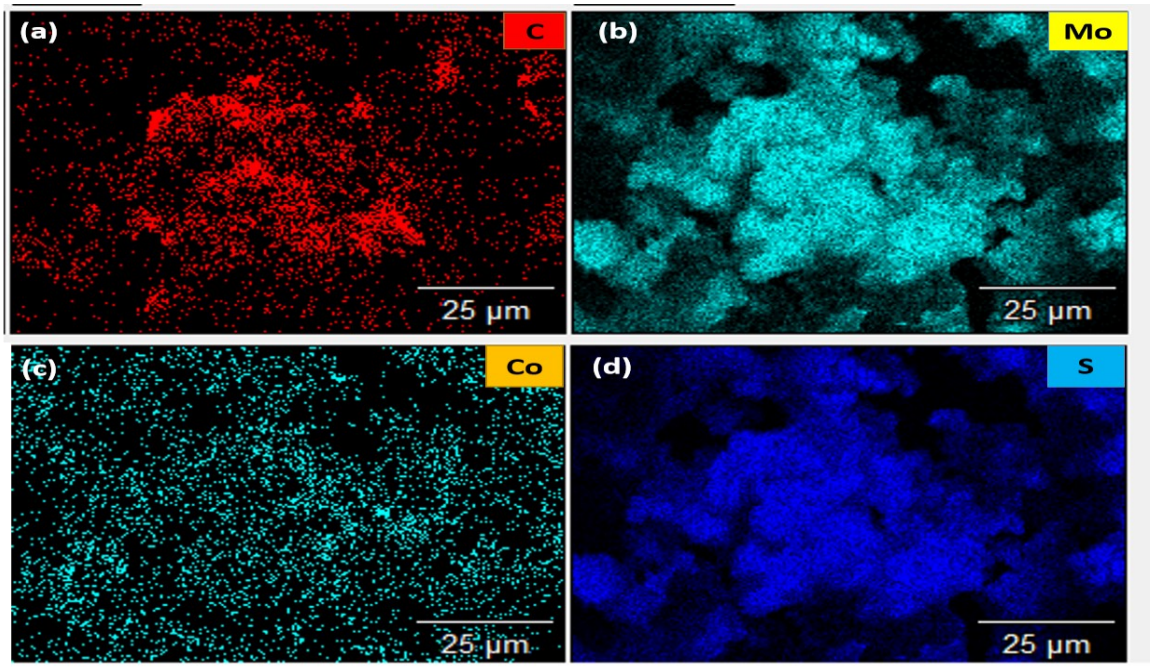

Figure 5. 4 (a-d): EDS-Mapping Images of the Co-doped MoS_2 electrode materials.

At a high magnification of 10 µm, the EDS mapping technique was used to analyze the elemental distribution of the electrode materials. As shown in figure 5.4a-d, the mapping studies of the electrode materials showed a uniform distribution of Mo, S, and the incorporated Co.

5.3.4. Transmission Electron Microscopy

Transmission electron microscopy is a technique for characterizing material to obtain structural dislocations, crystal structure, grain boundaries, as well as chemical analysis [40]. The microstructural studies from the TEM image Figure 5.5 show that the microstructure of electrode materials created by agglomerating nanosheets of various nanometer diameters has been validated. Because the S-S joins the lamellar structures through a feeble van der Waals interaction, the sheets are arranged into the structure as produced [41].

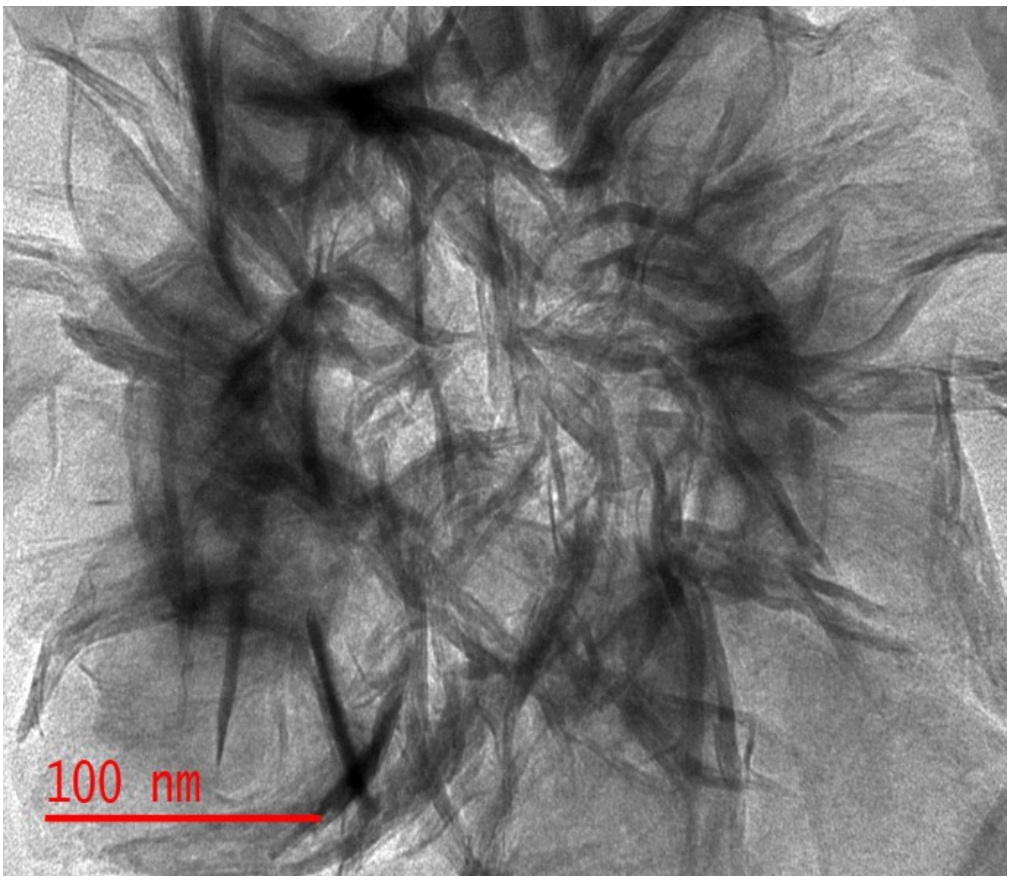

Figure 5. 5 TEM image of the Co-doped MoS_2 electrode materials.

5.3.5. BET Measurements

The electrode material's surface area has a substantial impact on a supercapacitor's electrochemical performance. Physical gas adsorption is the method of choice for investigating the porous properties of the electrode materials. The isotherm data obtained from these adsorptions employed to determine the surface area, pore-volume, and pore size distribution. [42]. Figures (5.6a and 5.6b) show the N_2 adsorption-desorption isotherms of CMS_1 and CMS_3 with inset of their pore size distributions, respectively. The calculated BET results from N_2 adsorption-desorption isotherms of CMS_1 and CMS_3 have the surface areas to be 18.0607 m^2/g and 14.5519 m^2/g respectively. BET surface areas calculated in this study are higher than the previously reported values for Co-MoS_2 (11.6082 m^2/g) [11], which can translate to an improvement in their supercapacitor performances. Monolayer gas adsorption inside the pores can be identified using the linear increase in adsorption at low pressure (P/Po = 0.00–0.10). After that, up to P/Po = 0.8, the curve reveals a near plateau zone, showing some nanopores alongside mesopores. A rapid and spiky increase in adsorption (P/Po = 0.8–1.0) indicates gas adsorption between the interlayers of the sample. [36]. As shown in the inset Figure (4a and 4b), the pore size distributions of the electrode materials were calculated by the Barret-Joyner-Halenda (BJH) from adsorption isotherms. The adsorption average pore width (4V/A by BET) for the electrode samples are 12.91897 nm and 14.80209 nm, respectively. The cumulative pore volume (BHJ adsorption) between 1.7000 nm and 300.0000 nm widths for the samples, were, respectively, found to be 0.065693 cm^3/g and 0.060905 cm^3/g. The presence of mesoporous structure was confirmed by type IV isotherms with a typical hysteresis loop in all electrode materials.

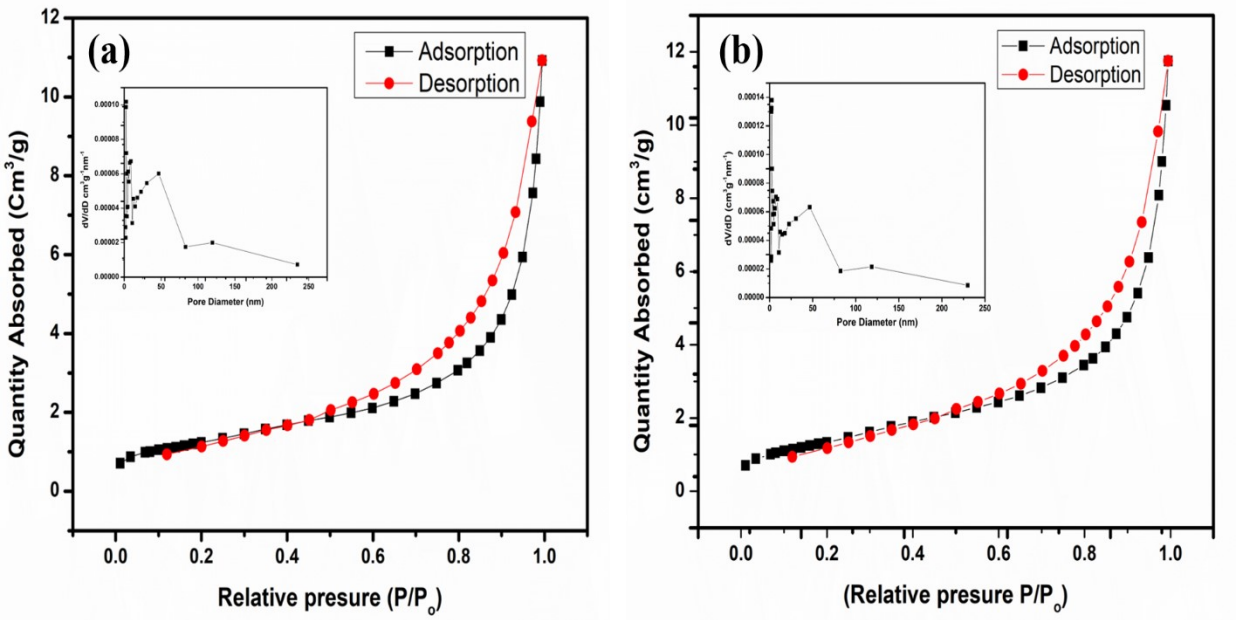

Figure 5. 6 N_2 adsorption-desorption isotherms of CMS_1 (a) and CMS_3 (b) with an inset of their pore size distributions.

5.3.6. Electrochemical Performance Analysis

The electrochemical performance of the electrode materials was investigated using cyclic voltammetry (CV), galvanostatic charge-discharge (GCD), and electrochemical impedance spectroscopy (EIS) (CMS_1 and CMS_3). The CV curves of the CMS electrodes at the scan sweep of 5, 10, 20, 50, and 100 mVs^{-1} are shown in Figure (5.7a and 5.7b), the electrodes loop from the CV showed rectangular shapes with typical redox peak from molybdenum ions ($Mo^{4+}/Mo^{(4-\Delta)+}$) and cobalt ions (Co^{2+}/Co^{3+}). At a high scan rate of 100 mVs^{-1}, the CV loops sustained their shapes, which show the perfect pseudocapacitive reaction of the electrode materials with low contact resistance. The weird-like CV curves as observed might be due to the oxygen trace in the cell because oxygen reduction is quasi-reversible on the CV. Although the electrodes containing Co_9S_8 were identified from the XRD patterns (Figure 5.1), their overall contributions to the electrochemical performance of the electrodes are negligible. The fast response of the electrodes

and fast charge-discharging properties was also observed, and a distinct change between the cathodic (reduction) peaks of the CV loops of the electrodes was obvious. The redox peaks are visible in the composite, confirming the pseudo-capacitance behavior. The Faradaic processes that occur at the electrode-electrolyte interface are responsible for the pseudocapacitive performance [43].

The GCD analysis of the electrode materials was conducted at different current densities of 1, 2, 3, 5, and 10 Ag^{-1} in 1M KOH electrolyte. Figures (5.7c and 5.7d) revealed the GCD curves of almost perfect triangular shapes, with a little drop of internal resistance at the start of discharge curves, which could be attributable to the active materials' contact resistance with highly conductive nickel foam surface. Also, the oxidation and reduction reaction at the electrode-electrolyte boundary of the electrode materials shows the pseudo-capacitance properties of the electrodes as observed from semi-symmetry curves of the GCD [44]. Both electrodes showed an excellent capacitance rate, with the specific capacities of 164, 154, 129, 104, and 61 Fg^{-1} obtained for the CMS_1 electrode at 1,2,3,5, and 10 Ag^{-1} current densities. Likewise, for the CMS_3 electrode the capacities of 146, 127, 115, 75, and 42 Fg^{-1} were, respectively, obtained at 1,2,3,5, and 10 Ag^{-1} current densities. The highest specific capacitance of 164 and 146 Fg^{-1} is correspondingly achieved for the two electrodes at 1 Ag^{-1} current density. The lengthier period of discharge was observed at 1 Ag^{-1}, which may be due to the large surface area of the electrodes. Moreover, as the current densities increase, there is a decrement in the discharge time, which is corresponding to the reported CV data. Equations (2) and (3) were used to compute the energy and power densities of the electrode materials, using the capacitance obtained from the GCD curves. The energy densities of 3.67 and 2.05 Wh/kg with power densities of 3279.97 and 2960.26 W/kg were calculated for both electrode materials, respectively. The comparative performance of this study

with the electrochemical performance of the reported works on cobalt and other metal-doped MoS_2-based supercapacitors is shown in Table 5.1.

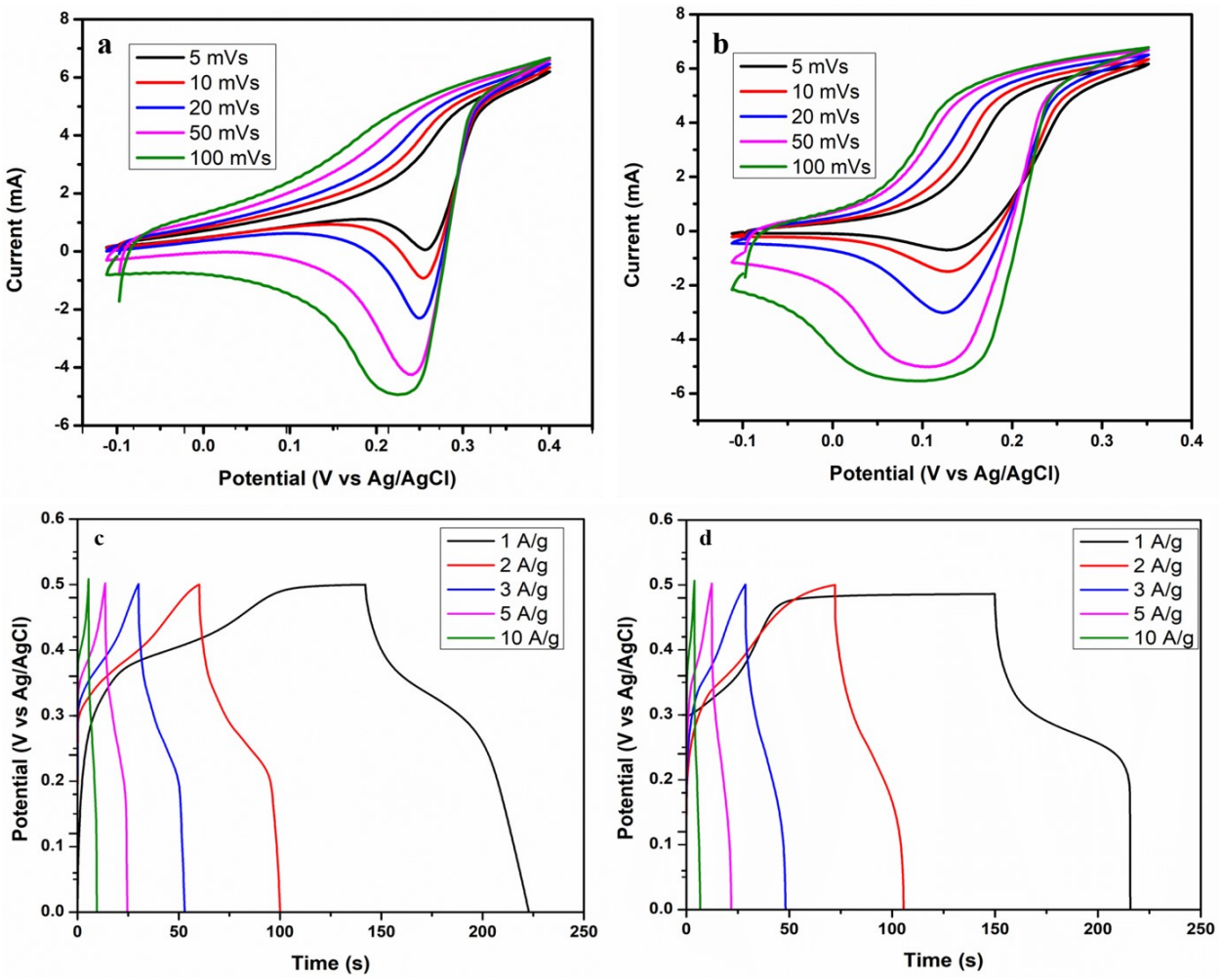

Figure 5. 7 (a-d): CV and GCD curves for both (CMS_1 and CMS_3) Electrodes.

To further confirm the pseudocapacitive behavior of the electrode materials as an ideal composite for supercapacitor applications, the anodic and cathodic peak current analysis was conducted as depicted in Figure 5.8 (a, b), which was linearly proportional to the square root of the scan rate [45]. The inset in Figure 5.8 (a, b), shows the intercept, slope, and R. square values of both the anodic and cathodic peaks. This confirmed the confined surface and diffusion control process of the electrode materials.

The improvement mechanism of the electrodes was further investigated using electrochemical impedance spectroscopy (EIS). The EIS study helps in the prediction of a theoretical circuit model for a better understanding of the electrode-electrolyte interface, conductivity calculation, and even electrolyte resistance. Over a frequency range of 100 kHz to 10 MHz, with an amplitude of 5 mV and a bias voltage of 0.23 V, EIS was also used to measure ion transfer and electrical conductivity of the electrodes. Figure 5.8 (c and d) depict the related Nyquist plots with their inset lower frequencies' plots. The x-intercept at the high-frequency area of the Nyquist plot gives equivalent series resistance (ESR), which includes three distinct resistances: (i) resistance of the electroactive material, (ii) resistance of the electrolyte, and (iii) contact resistance at the interface, which is estimated to be around 5.3 Ω. The diameter of the semicircle at a medium frequency can be used to calculate the charge transfer resistance (R_{ct}) resulting from the faradic redox process. The Warburg region, which is connected to the diffusion of redox species in the sample and mirrors the slope of the curve in the low-frequency zone, is the third region.

As shown in Figure 5.9a, the capacitances decrease slightly as the current density increases, which shows an outstanding ability of fast charge-discharge and the restriction of ions on the surface of the electrode materials could also be responsible. Moreover, the capacitance retention of 85.5% and 79% ratio were observed at 1 Ag^{-1} after 3000 cycles during the cyclic stability test of the CMS_1 and CMS_3 electrodes, respectively, as shown in Figure 5.9b. Co-MoS_2 is an efficient electrode material for supercapacitors due to its high capacitive performance and outstanding cycle stability.

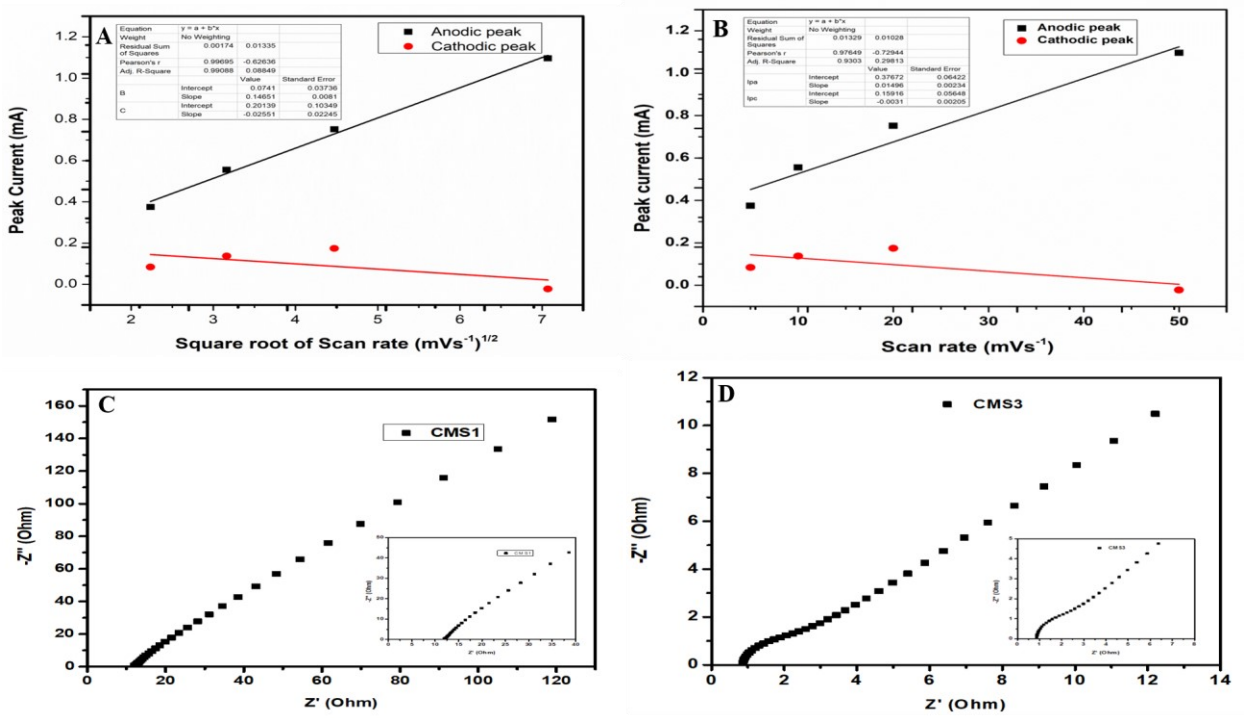

Figure 5.8 (a, b) Peak current against the square root of scan rate, and Peak current against the scan rate, and (c, d) EIS Nyquist plots (inset lower frequencies plots).

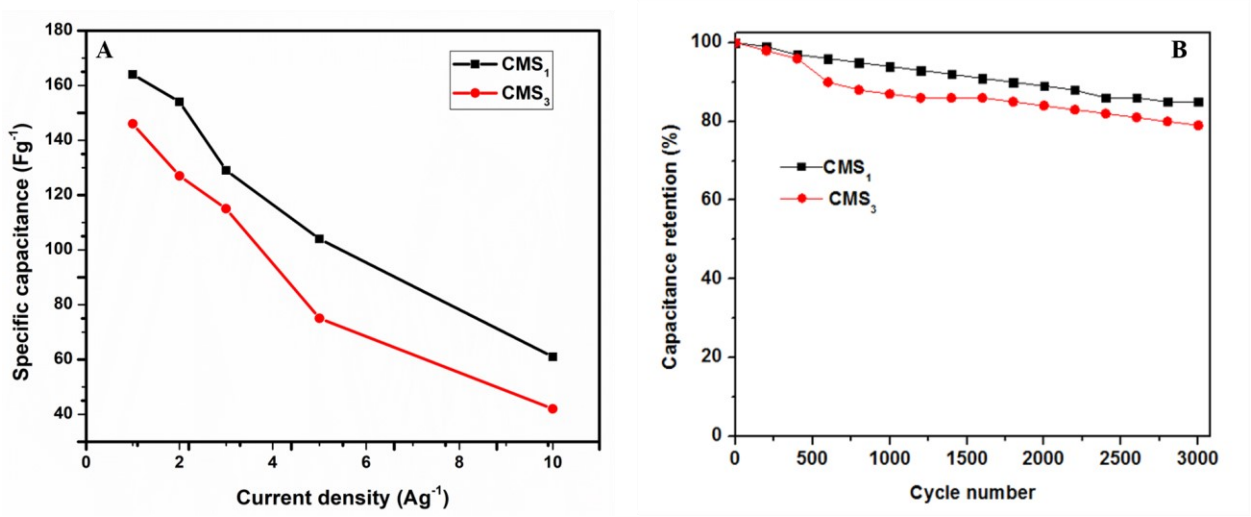

Figure 5.9 (a) Specific capacitance comparison with current density, and (b) Cyclic stability tests after 3000 cycles.

Table 5. 1 Comparison performance of metal-doped MoS_2-based supercapacitors.

Electrode substrates	**Electrolytes**	**Current density**	**Electrode configurations**	**Specific capacitance (Fg^{-1})**	**Ref.**
Mn-MoS_2 nanoflower	0.5 M Na_2SO_4	1 Ag^{-1}	2	88	[31]
Pt-MoS_2 nanosheets	1 M Na_2SO_4	1 Ag^{-1}	2	200.87	[32]
Cu-MoS_2 film	1 M Na_2SO_4	1 Ag^{-1}	3	502	[46]
Co-MoS_2 nanosheets	2 M KOH	1 Ag^{-1}	3	510	[33]
Ni-MoS_2 nanosheets	1 M Na_2SO_4	1 Ag^{-1}	3	286	[30]
Co-MoS_2 nanoflower	1 M KOH	1 Ag^{-1}	2	86	[11]
Co-MoS_2 nanoflower	1 M KOH	1 Ag^{-1}	3	164 (CMS_1) 146 (CMS_3)	This work

5.4. Conclusion

A one-pot hydrothermally assisted technique has been successfully employed to synthesize cobalt-doped MoS_2 nanoflowers. The structural, surface morphology and microstructural, and surface areas of the samples were established by XRD, Raman, SEM, TEM, and BET analyses. The BET analyses confirmed the presence of mesoporous structure with a typical hysteresis loop of type IV

isotherms in all electrode materials The fabrication of the supercapacitor electrode was successfully done by drop-casting the slurry prepared from the as-synthesized active materials, carbon black, and PVDF in NMP. The energy storage performances of the electrodes were electrochemically investigated using CV, GCD, and EIS measurements in a three-electrode configuration system. The Co-MoS_2 (CMS_1) electrode offered the highest specific capacitance value of 164 Fg^{-1} at 1 Ag^{-1} with cyclic stability of 85.5% after 3000 cycles. This study also confirmed that the oxygen reduction is quasi-reversible due to the observed weird-like CV curves. These results inferred that Co-doped MoS_2 can be making an outstanding electrode material for supercapacitor applications. This method can potentially be developed to improve the charge storage capabilities of other transition metal sulfides.

References

[1] L.L. Zhang, R. Zhou, X.S. Zhao, Graphene-based materials as supercapacitor electrodes, J. Mater. Chem. 20 (2010) 5983–5992. https://doi.org/10.1039/c000417k.

[2] N. Choudhary, C. Li, J. Moore, N. Nagaiah, L. Zhai, Y. Jung, J. Thomas, Asymmetric Supercapacitor Electrodes and Devices, Adv. Mater. 29 (2017). https://doi.org/10.1002/adma.201605336.

[3] Z. Chang, X. Ju, P. Guo, X. Zhu, C. Liao, Y. Zong, X. Li, X. Zheng, Enhanced performance of supercapacitor electrode materials based on hierarchical hollow flowerlike HRGOs/Ni-doped MoS_2 composite, J. Alloys Compd. 824 (2020) 153873. https://doi.org/10.1016/j.jallcom.2020.153873.

[4] H. Gupta, S. Chakrabarti, S. Mothkuri, B. Padya, T.N. Rao, P.K. Jain, High performance supercapacitor based on 2D-MoS_2 nanostructures, Mater. Today Proc. 26 (2018) 20–24. https://doi.org/10.1016/j.matpr.2019.04.198.

[5] I.T. Bello, O.A. Oladipo, O. Adedokun, M.S. Dhlamini, Recent advances on the preparation and electrochemical analysis of MoS_2-based materials for supercapacitor applications : A mini-review, Mater. Today Commun. 25 (2020) 101664. https://doi.org/10.1016/j.mtcomm.2020.101664.

[6] Z. Yu, L. Tetard, L. Zhai, J. Thomas, Supercapacitor electrode materials: Nanostructures from 0 to 3 dimensions, Energy Environ. Sci. 8 (2015) 702–730. https://doi.org/10.1039/c4ee03229b.

[7] Y. Wang, Y. Song, Y. Xia, Electrochemical capacitors: Mechanism, materials, systems, characterization and applications, Chem. Soc. Rev. 45 (2016) 5925–5950. https://doi.org/10.1039/c5cs00580a.

[8] J.C. Ellenbogen, Supercapacitors : A Brief Overview, (2006).

[9] Z. Niu, J. Chen, H.H. Hng, J. Ma, X. Chen, A leavening strategy to prepare reduced graphene oxide foams, Adv. Mater. 24 (2012) 4144–4150. https://doi.org/10.1002/adma.201200197.

[10] K.S. Kumar, N. Choudhary, Y. Jung, J. Thomas, Recent Advances in Two-Dimensional Nanomaterials for Supercapacitor Electrode Applications, ACS Energy Lett. 3 (2018) 482–495. https://doi.org/10.1021/acsenergylett.7b01169.

[11] R. Rohith, M. Manuraj, R.I. Jafri, R.B. Rakhi, Co-MoS_2 nanoflower coated carbon fabric as a flexible electrode for supercapacitor, Mater. Today Proc. (2021). https://doi.org/10.1016/j.matpr.2020.12.1054.

[12] Z. Yu, C. Li, D. Abbitt, J. Thomas, Flexible, sandwich-like Ag-nanowire/PEDOT:PSS-nanopillar/MnO2 high performance supercapacitors, J. Mater. Chem. A. 2 (2014) 10923–10929. https://doi.org/10.1039/c4ta01245c.

[13] Y. Yang, H. Fei, G. Ruan, C. Xiang, J.M. Tour, Edge-oriented MoS_2 nanoporous films as flexible electrodes for hydrogen evolution reactions and supercapacitor devices, Adv. Mater. 26 (2014) 8163–8168. https://doi.org/10.1002/adma.201402847.

[14] W. Choi, N. Choudhary, G.H. Han, J. Park, D. Akinwande, Y.H. Lee, Recent development of two-dimensional transition metal dichalcogenides and their applications, Mater. Today. 20 (2017) 116–130. https://doi.org/10.1016/j.mattod.2016.10.002.

[15] I.T. Bello, K.O. Otun, G. Nyongombe, O. Adedokun, G.L. Kabongo, M.S. Dhlamini, Synthesis , Characterization , and Supercapacitor Performance of a Mixed-Phase Mn-Doped MoS_2 Nanoflower, Nanomaterials. 12 (2022) 1–12.

[16] S. Zhai, Z. Fan, K. Jin, M. Zhou, H. Zhao, Y. Zhao, F. Ge, X. Li, Z. Cai, Synthesis of zinc

sulfide/copper sulfide/porous carbonized cotton nanocomposites for flexible supercapacitor and recyclable photocatalysis with high performance, J. Colloid Interface Sci. 575 (2020) 306–316. https://doi.org/10.1016/j.jcis.2020.04.073.

[17] M.F. Iqbal, A.K.M. Yousef, A. Hassan, S. Hussain, M.N. Ashiq, Mahmood-Ul-Hassan, A. Razaq, Significantly improved electrochemical characteristics of nickel sulfide nanoplates using graphene oxide thin film for supercapacitor applications, J. Energy Storage. 33 (2021) 102091. https://doi.org/10.1016/j.est.2020.102091.

[18] N.R. Chodankar, A.K. Nanjundan, D. Losic, D.P. Dubal, J.B. Baek, Graphene and molybdenum disulphide hybrids for energy applications: an update, Mater. Today Adv. 6 (2020) 100053. https://doi.org/10.1016/j.mtadv.2019.100053.

[19] S.Z. Hussain, M. Ihrar, S.B. Hussain, W.C. Oh, K. Ullah, A review on graphene based transition metal oxide composites and its application towards supercapacitor electrodes, SN Appl. Sci. 2 (2020) 1–23. https://doi.org/10.1007/s42452-020-2515-8.

[20] K. Ahmad, M.A. Shinde, H. Kim, Molybdenum disulfide/reduced graphene oxide: Progress in synthesis and electro-catalytic properties for electrochemical sensing and dye sensitized solar cells, Microchem. J. 169 (2021) 106583. https://doi.org/10.1016/j.microc.2021.106583.

[21] I.T. Bello, S.A. Adio, A.O. Oladipo, O. Adedokun, L.E. Mathevula, M.S. Dhlamini, Molybdenum sulfide-based supercapacitors: From synthetic, bibliometric, and qualitative perspectives, Int. J. Energy Res. (2021) 12665–12692. https://doi.org/10.1002/er.6690.

[22] D. Kong, H. Wang, J.J. Cha, M. Pasta, K.J. Koski, J. Yao, Y. Cui, Synthesis of MoS_2 and $MoSe_2$ films with vertically aligned layers, Nano Lett. 13 (2013) 1341–1347. https://doi.org/10.1021/nl400258t.

[23] F. Clerici, M. Fontana, S. Bianco, M. Serrapede, F. Perrucci, S. Ferrero, E. Tresso, A. Lamberti, In situ MoS_2 Decoration of Laser-Induced Graphene as Flexible Supercapacitor Electrodes, ACS Appl. Mater. Interfaces. 8 (2016) 10459–10465. https://doi.org/10.1021/acsami.6b00808.

[24] D.N. Sangeetha, M.S. Santosh, M. Selvakumar, Flower-like carbon doped MoS_2/Activated carbon composite electrode for superior performance of supercapacitors and hydrogen evolution reactions, J. Alloys Compd. 831 (2020) 154745. https://doi.org/10.1016/j.jallcom.2020.154745.

[25] Y. Ge, R. Jalili, C. Wang, T. Zheng, Y. Chao, G.G. Wallace, A robust free-standing MoS_2/poly(3,4-ethylenedioxythiophene):poly(styrenesulfonate) film for supercapacitor applications, Electrochim. Acta. 235 (2017) 348–355. https://doi.org/10.1016/j.electacta.2017.03.069.

[26] X. Liao, Y. Zhao, J. Wang, W. Yang, L. Xu, X. Tian, Y. Shuang, MoS_2/MnO_2 heterostructured nanodevices for electro-, Nano Res. 11 (2018) 4–7.

[27] F. Huang, R. Meng, Y. Sui, F. Wei, J. Qi, Q. Meng, Y. He, One-step hydrothermal synthesis of a CoS_2@MoS_2 nanocomposite for high-performance supercapacitors, J. Alloys Compd. 742 (2018) 844–851. https://doi.org/10.1016/j.jallcom.2018.01.324.

[28] Z. Li, Z. Qin, W. Zhang, Z. Li, Controlled synthesis of $Ni(OH)_2$/MoS_2 nanohybrids for high-performance supercapacitors, Mater. Chem. Phys. 209 (2018) 291–297. https://doi.org/10.1016/j.matchemphys.2017.12.072.

[29] P. Tiwari, J. Jaiswal, R. Chandra, Hierarchal growth of MoS_2@CNT heterostructure for all solid state symmetric supercapacitor: Insights into the surface science and storage mechanism, Electrochim. Acta. 324 (2019).

https://doi.org/10.1016/j.electacta.2019.134767.

[30] S. Palanisamy, P. Periasamy, K. Subramani, A.P. Shyma, R. Venkatachalam, Ultrathin sheet structure Ni-MoS_2 anode and MnO_2/water dispersion graphene cathode for modern asymmetrical coin cell supercapacitor, J. Alloys Compd. 731 (2018) 936–944. https://doi.org/10.1016/j.jallcom.2017.10.118.

[31] S.S. Singha, S. Rudra, S. Mondal, M. Pradhan, A.K. Nayak, B. Satpati, P. Pal, K. Das, A. Singha, Mn incorporated MoS_2 nanoflowers: A high performance electrode material for symmetric supercapacitor, Electrochim. Acta. 338 (2020). https://doi.org/10.1016/j.electacta.2020.135815.

[32] J. Shao, Y. Li, M. Zhong, Q. Wang, X. Luo, K. Li, W. Zhao, Enhanced-performance flexible supercapacitor based on Pt-doped MoS_2, Mater. Lett. 252 (2019) 173–177. https://doi.org/10.1016/j.matlet.2019.05.124.

[33] A. Sun, L. Xie, D. Wang, Z. Wu, Enhanced energy storage performance from Co-decorated MoS2 nanosheets as supercapacitor electrode materials, Ceram. Int. 44 (2018) 13434–13438. https://doi.org/10.1016/j.ceramint.2018.04.113.

[34] D. Wang, X. Zhang, S. Bao, Z. Zhang, H. Fei, Z. Wu, Phase engineering of a multiphasic 1T/2H MoS_2 catalyst for highly efficient hydrogen evolution, J. Mater. Chem. A. 5 (2017) 2681–2688. https://doi.org/10.1039/c6ta09409k.

[35] D. Wang, B. Su, Y. Jiang, L. Li, B.K. Ng, Z. Wu, F. Liu, Polytype 1T/2H MoS2 heterostructures for efficient photoelectrocatalytic hydrogen evolution, Chem. Eng. J. 330 (2017) 102–108. https://doi.org/10.1016/j.cej.2017.07.126.

[36] R.B. Rakhi, N.A. Alhebshi, D.H. Anjum, H.N. Alshareef, Nanostructured cobalt sulfide-on-fiber with tunable morphology as electrodes for asymmetric hybrid supercapacitors, J.

Mater. Chem. A. 2 (2014) 16190–16198. https://doi.org/10.1039/c4ta03341h.

[37] M. Manuraj, J. Chacko, K.N. Narayanan Unni, R.B. Rakhi, Heterostructured MoS_2-RuO_2 nanocomposite: A promising electrode material for supercapacitors, J. Alloys Compd. 836 (2020) 155420. https://doi.org/10.1016/j.jallcom.2020.155420.

[38] N. Scheuschner, O. Ochedowski, A.M. Kaulitz, R. Gillen, M. Schleberger, J. Maultzsch, Photoluminescence of freestanding single- and few-layer MoS_2, Phys. Rev. B - Condens. Matter Mater. Phys. 89 (2014) 2–7. https://doi.org/10.1103/PhysRevB.89.125406.

[39] J. Fan, J. Ekspong, A. Ashok, S. Koroidov, E. Gracia-Espino, Solid-state synthesis of few-layer cobalt-doped MoS_2 with CoMoS phase on nitrogen-doped graphene driven by microwave irradiation for hydrogen electrocatalysis, RSC Adv. 10 (2020) 34323–34332. https://doi.org/10.1039/d0ra05560c.

[40] D.B. Williams, C.B. Carter, Transmission Electron Microscopy, Springer US, Plenum, 1996.

[41] L. Yue, X. Wang, T. Sun, H. Liu, Q. Li, N. Wu, H. Guo, W. Yang, Ni-MOF coating MoS_2 structures by hydrothermal intercalation as high-performance electrodes for asymmetric supercapacitors, Chem. Eng. J. 375 (2019). https://doi.org/10.1016/j.cej.2019.121959.

[42] J.C. Groen, J. Pérez-Ramírez, Critical appraisal of mesopore characterization by adsorption analysis, Appl. Catal. A Gen. 268 (2004) 121–125. https://doi.org/10.1016/j.apcata.2004.03.031.

[43] L. Zhang, J. Wang, J. Zhu, X. Zhang, K. San Hui, K.N. Hui, 3D porous layered double hydroxides grown on graphene as advanced electrochemical pseudocapacitor materials, J. Mater. Chem. A. 1 (2013) 9046–9053. https://doi.org/10.1039/c3ta11755c.

[44] D.P. Dubal, V.J. Fulari, C.D. Lokhande, Effect of morphology on supercapacitive properties

of chemically grown β-$Ni(OH)_2$ thin films, Microporous Mesoporous Mater. 151 (2012) 511–516. https://doi.org/10.1016/j.micromeso.2011.08.034.

[45] Y. Gogotsi, R.M. Penner, Energy Storage in Nanomaterials - Capacitive, Pseudocapacitive, or Battery-like?, ACS Nano. 12 (2018) 2081–2083. https://doi.org/10.1021/acsnano.8b01914.

[46] B.D. Falola, L. Fan, T. Wiltowski, I.I. Suni, Electrodeposition of Cu-Doped MoS_2 for Charge Storage in Electrochemical Supercapacitors , J. Electrochem. Soc. 164 (2017) D674–D679. https://doi.org/10.1149/2.0421712jes.

Chapter Six[51]

Synthesis, Characterization, and Supercapacitor Performance of a mixed-phase Mn-doped MoS_2 Nanoflower

This section has been published.

[1] Bello, I. T., Otun, K. O., Gayi Nyongombe, Adedokun, O., Kabongo, G. L., and Dhlamini, M. S. (2022), Synthesis, Characterization, and Supercapacitor Performance of a mixed-phase Mn-doped MoS_2 Nanoflower. *Nanomaterials*, Volume 12 (2022), Page 1-12, https://doi.org/10.3390/nano12030490

6.1. Introduction

Electrochemical energy storage devices have currently attracted substantial consideration for harnessing their energy potentials across the scientific world. This is due to the ever-increasing demand for eco-friendly energy storage devices (fuel cells, battery, and supercapacitors) as the better replacement to the existing energy sources (fossil fuel) that are deteriorating climatic conditions around the world [1–3]. The seasonal recurrence of the conventional form of renewable energy resources like solar, hydel, wind, biomass, and tidal have made the storing mechanism of such energies become vigorous. Therefore, the fast depletion of these energy resources based on their availability has called for developing alternative sources of energy storage devices [4]. The desire to produce a storage device that has a fast charge-discharge ability, with stable cyclic performance, safe operation and cost-effectiveness led to the development of supercapacitors. Supercapacitors are high-power energy storage devices that possess better capacitance output than conventional capacitors [5]. In the field of energy harvesting devices, the supercapacitor is one of the most researched topics. High energy/power density, fast charge/discharge capability, and excellent cycling stability are some of the distinguishing characteristics of supercapacitors that make them an appealing candidate [5–9]. Based on the storage mechanisms, supercapacitors are classified into electrochemical double-layer capacitors (EDLC) and Pseudo-capacitor. EDLC stores charge via the accumulation of electrolyte ions at the interface of electrode-electrolyte. At the electrode/electrolyte interface, no charge is transferred, which can store charges by non-faradaic reactions. The second category is pseudo-capacitors, which uses the redox reaction system to store charge between electrode-electrolyte. The faradaic reactions are used to transfer charges for energy storage applications [10–12].

Recently, carbon-based materials such as activated carbon, carbon black, graphene, carbon nanotubes, and their derivatives are commonly used as active materials in designing EDLC devices because of their good conductivity and excellent stability [4,11]. However, graphene's strong hydrophobicity, poor dispersity, and aggregation property prevent it from being used as an efficient supercapacitor electrode material [13–15]. Various transition metal sulfides such as copper sulfide, Nickel Sulfide, Zinc sulfide, Molybdenum sulfide, manganese sulfide, strontium sulfide, vanadium sulfide have attracted wide attention for supercapacitors applications, due to their natural abundance, easily controlled morphologies, multiple valences, and appropriate bandgap widths. Among them, MoS_2 is a potential electrode material for supercapacitor applications due to its intriguing sheet-like structure, which offers a large surface area for double-layered charge storage and higher intrinsic fast ionic conductivity [4,16–18]. The analogous structure of molybdenum sulfide (MoS_2) with that of graphene has made it considered for various energy storage, optoelectronics, sensing, and photocatalysis applications owing to their unique morphology, excellent mechanical, and electrical properties [12,19–22]. MoS_2 comprises covalently bonded S-Mo-S atoms, which are held together by weak van der Waals forces with higher capacity (theoretical) than graphite [23,24]. It has different polytype structures of 2H and 1T phases, coupled with variable oxidation states of +2 and +6. It also possesses higher in-plane ionic and electrical conductivity than oxide [25,26]. Through the faradaic charge transfer mechanism, MoS_2 can store charge in both inter and intralayer. As a result, MoS_2 and its composite become viable materials for high-performance pseudo-capacitor electrodes [9,12]. Considerable attention has been paid to MoS_2 to improve its charge storage performance and to circumvent the interlayer self-aggregation because of the S-M-S interlayer van der Waals force. Therefore, the adjustment of its

structural design and microscopic morphology and its composite optimizations is highly needed to improve their super-capacitive behavior.

Several findings have been reported on the successfully prepared composite materials with activated carbon [27,28], metal oxides [29,30], graphene [31–33], metal hydroxide [34,35], conducting polymers [36–38], carbon nanotube [8], and metal sulfides [39,40]. However, there are few reported works on the metal-doped composites of MoS_2-based supercapacitors. Nickel-doped MoS_2 nanosheets were reported by Palanisamy and his colleagues for the fabrication of asymmetric supercapacitor with the specific capacitance of 286 Fg^{-1} at 1 Ag^{-1} using three electrode systems in 1 M Na_2SO_4 [41]. Falola et al., 2017, reported a specific capacitance of 502 Fg^{-1} at 1Ag^{-1} using three-electrode configurations in 1 M Na_2SO_4, from the copper doped MoS_2 film [42]. Two system electrode configurations were also employed to study the electrochemical performance of platinum doped MoS_2 nanosheets by Shao and co-workers [43]. The specific capacitance of 200.87 Fg^{-1} at 1 Ag^{-1} in 1 M concentration of Na_2SO_4 electrolyte was obtained. Recently, Singha et al., 2020, obtained a specific capacitance of 88 Fg^{-1} at 1 Ag^{-1} in 2 M KOH using two-electrode configuration systems with Manganese doped MoS_2 nanoflower as an active material [44]. More recently, cobalt doped MoS_2 nanosheets and nanoflowers were, respectively, reported by Sun et al., 2018, and Rohit et al., 2021. The specific capacitance of 510 Fg^{-1} at 1 Ag^{-1} in 2 M KOH for Co-MoS_2 nanosheets using three configuration systems was reported [45]. Likewise, two system configurations were used to study the capacitive behavior of Co-MoS_2 nanoflowers with a specific capacitance of 86 Fg^{-1} at 1 Ag^{-1} in 1 M KOH electrolytes [46]. However, several types of binders were included as part of the active materials for all aforementioned successful reports for the metal-doped MoS_2-based supercapacitors. The binder is an inactive element that restricts capacitance by contributing its weight to the total mass of the active material. As a result, there is a need to

leverage various synthesis approaches that lead to the production of binder-free electrodes cost-effectively.

In this work, we reported binder-free mixed-phase manganese doped MoS_2 (Mn-doped MoS_2) electrodes for electrochemical performance behavior. The synthesis, and characterizations were reported in detail in the subsequent sections, and the electrochemical measurements were employed to investigate the capacitive behavior of the electrode materials. The specific capacitance of 70.37 Fg^{-1} at 1 Ag^{-1} in 1 M KOH using three configuration electrode systems is reported. This suggests a potential material for a binder-free electrode material for metal-doped MoS_2-based supercapacitors.

6.2. Methodology

6.2.1. Synthesis of Manganese doped MoS_2 (Mn-MoS_2) Nanoflowers

Manganese doped MoS_2 was synthesized through facile hydrothermally assisted techniques. 2.5 g of ammonium molybdate and 4.5 g of thiourea were, respectively, dissolved in 60 mL of deionized water with vigorous stirring at room temperature. After 30 minutes of continuous stirring, 0.7 g of manganese (II) acetate tetrahydrate was added to make a composite solution. The resulting solution was aggressively agitated until it became homogeneous. The solution was transferred to a 100 mL Teflon-lined Autoclave and heated at 220 °C for 18 hours [47]. After cooling to ambient temperature, the black precipitate was collected by centrifugation. To eliminate any remaining impurities, the washing was repeated many times with deionized water and ethanol, then dried in a vacuum oven at 80 °C for 12 hours. The obtained sample of manganese doped MoS_2 was denoted as (MMS).

6.2.2. Preparation of Working Electrodes

A commercially available 1 cm × 3 cm nickel foam was cleaned using 2.0 M HCl, deionized water, and ethanol in a sonication procedure for 15 minutes before being vacuum dried. To make a slurry, an active substance of Mn-doped MoS_2 (MMS) was mixed with carbon black (in the ratio 80:20), and appropriate NMP drops and sonicated for 10 minutes. The slurry was drop cast over cleaned nickel foam and dried for 12 hours in a vacuum oven at 80 degrees Celsius. After drying, the active material on the nickel foam was approximately weighed to be 2 mg.

6.2.3. Characterizations

A Rigaku Smartlab X-ray diffractometer (0.154 nm Cu Kα line), field emission scanning electron microscopy (FE-SEM JSM-7800 F, JOEL Ltd), and HORIBA scientific XploRA with LASER light excitation energy (2.411 eV) at 532 nm, were respectively employed to study the crystal structures, morphological and Raman spectroscopic properties of the electrode material. A surface area prosimetra (TriStar II 3020 version 2.00) was used to determine the Brunauer-Emmett-Teller (BET) surface area.

6.2.4. Electrochemical Measurements

A three-electrode configuration system of Autolab PGSTAT302N electrochemical working station was employed to study the electrochemical performance of Mn-doped MoS_2 in 1 M KOH electrolyte. The three-electrode cells include a reference electrode (Ag/AgCl, 3 M KCl), a counter electrode (Platinum wire), and the working electrode (nickel foam). The cyclic voltammetry (CV) curves were measured in a potential window between -0.4 and 0.4 V at a different scan rate, ranging from 5, 10, 20, 50, and 100 mVs^{-1}. The galvanostatic charge-discharge (GCD) measurements were recorded at different current densities of 1, 2, 3, 5, and 10 Ag^{-1}, respectively.

The electrochemical impedance spectroscopy (EIS) was also tested at an amplitude of 5 mV, between the frequency range of 100 kHz to 10 MHz.

6.3. Results and Discussion

6.3.1. Morphology and Elemental Composition Analysis

The morphology and elemental composition of the electrode material were studied using field emission scanning electron microscopy with an EDS analysis system attachment (FE-SEM JSM-7800 F, JOEL Ltd). The as-synthesized materials showed a hierarchical 3D-structure flower-like morphology. The flower-like morphology of the material is highly porous, as shown in Figure 6.1a. The porosity of the material might be due to the weak Van der Waals force of attraction between flexible MoS_2 layers [48,49]. The porosity of the material contributed highly to the performance of the electrochemical behavior. Figure 6.1b, shows the elemental composition of the prepared sample, which shows the presence of the incorporated Mn. The carbon and oxygen originated from carbon capping of the sample and the oxygen peak can be traced to the oxygen from the methods of preparation, which includes water.

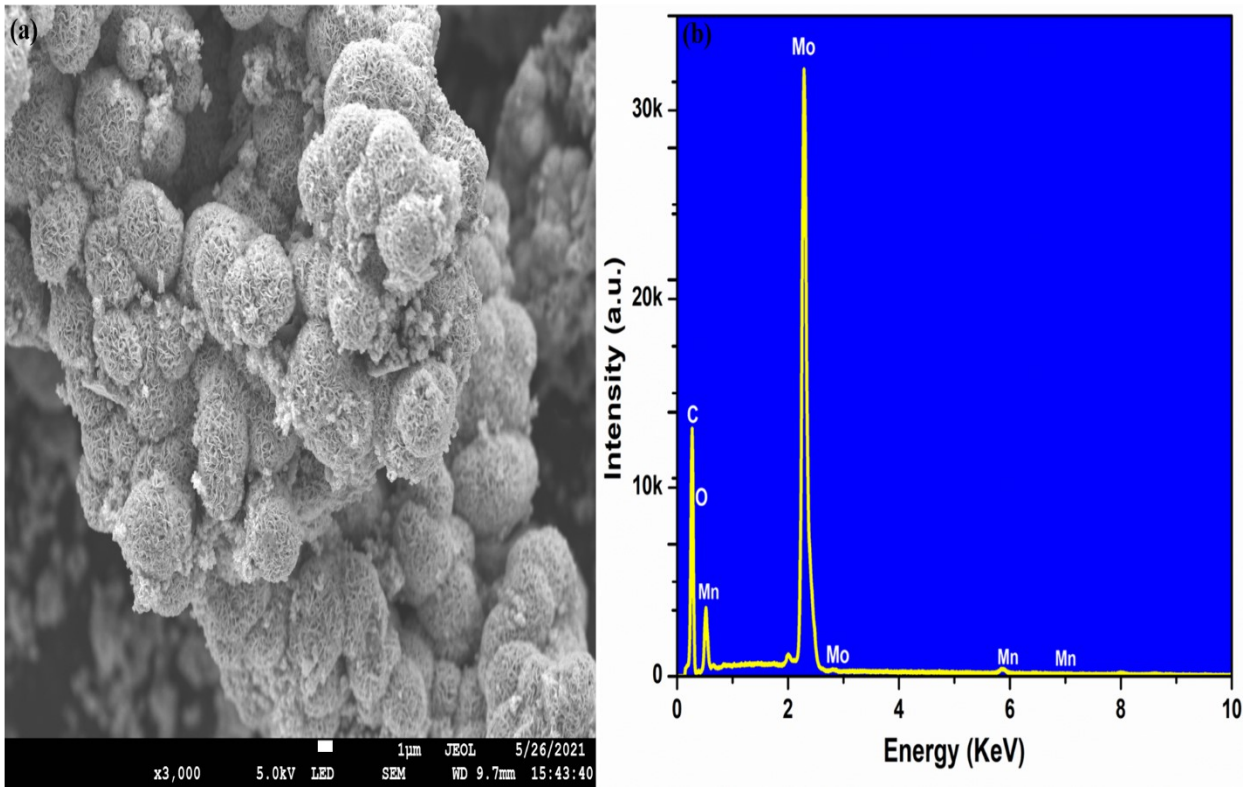

Figure 6. 1 (a, b): SEM and EDS spectra of the Mn-doped MoS_2 electrode material.

The molybdenum and sulfur peaks were overlapping as both elements are operating at the same energy level of 2.29 and 2.30 KeV, respectively. Meanwhile, the appearance of the sulfur element in the mapping images shows its presence in the sample but was overlapped on the EDS peaks due to the proximity of molybdenum and sulfur energy levels.

The elemental distribution of the sample was performed using EDS elemental mapping analysis recorded at a higher magnification of 10 μm. The studies also showed a uniform distribution of the Mo, S, and incorporated Mn, as shown in the mapping analysis of the sample in figure 6.2(a-f). Table 6.1 shows a fundamental composition of the sample.

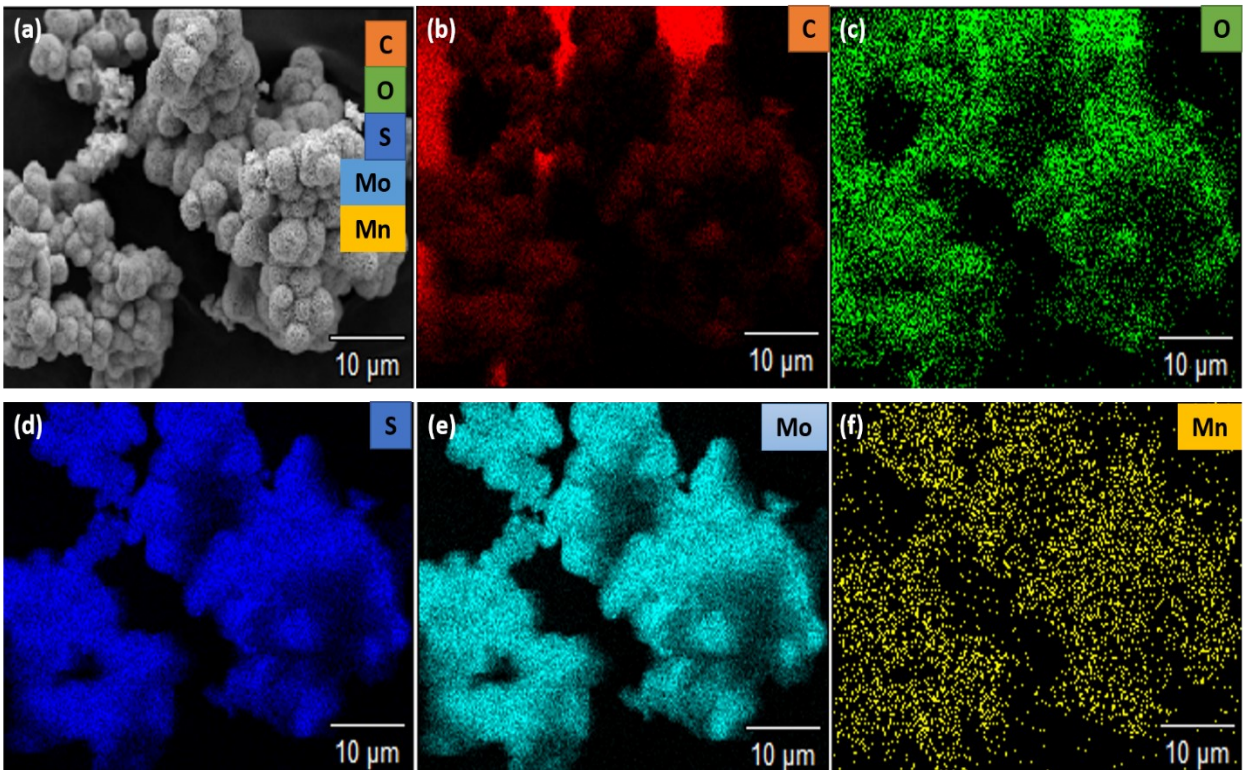

Figure 6. 2 (a-f): Elemental mapping of the Mn-doped MoS_2 electrode material.

Table 6. 1 Quantitative composition of the elements present in the Mn-doped MoS_2.

Element Line	*Weight %*	*Norm. Wt.%*	*Atom %*	*Formula*	*Compnd %*	*Norm. Compnd%*
C K	26.7	26.7	57.3	C	26.7	26.7
O K	16.5	16.5	26.4	O	16.5	16.5
Mn K	5.4	5.4	2.5	Mn	5.4	5.4
Mo L	51.4	51.4	13.8	Mo	51.4	51.4
Total	100.0	100.0	100.0		100.0	100.0

6.3.2. Raman Spectroscopy Studies

The crystal structure of the sample was investigated by Raman spectroscopy analysis. Figure 6.3 shows the pattern of the Raman measurement of the Mn-doped MoS_2. The characteristic peaks at 289, 381, 411, and 454 cm^{-1} correspond to the in-plan and out-plane vibrations of E_{1g}, E^1_{2g}, A_{1g}, and A_{2u} modes of 2H-phase MoS_2, respectively. The extra peak of 1T-phase MoS_2 is located at 341 cm^{-1}, indicating that the as-prepared material is of mixed phases [50]. Also, an additional peak emerges at 481 cm^{-1}, which may belong to local vibrational modes of Mn^{2+} dopants [51]. This strongly suggests the successful preparation of the Mn-doped MoS_2 nanoflower for electrode material usage.

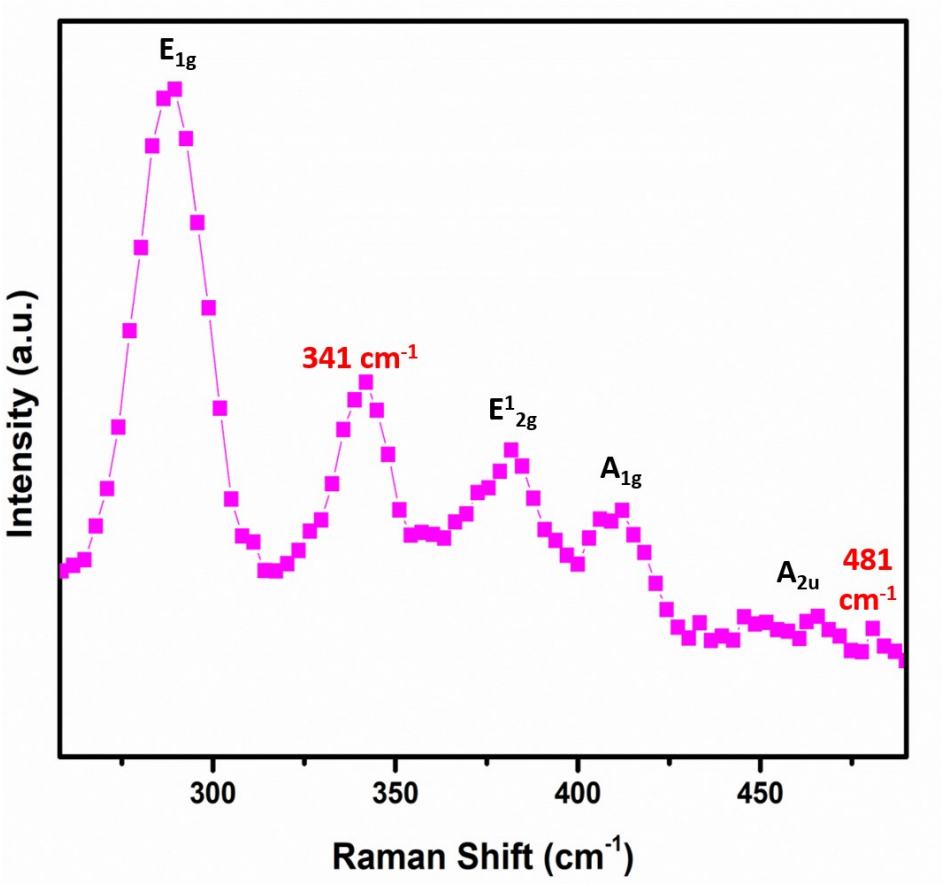

Figure 6. 3 Raman patterns of the Mn-doped MoS_2 electrode material.

6.3.3. X-ray diffraction Measurements

Figure 6.4 depicts the patterns from the XRD measurement results. The corresponding planes (002), (101), (103), (105), and (110) of the 2H-phase MoS_2 were associated with the diffraction peaks at about 14.11, 33.31, 39.25, 49.52, and 58.98 degrees (JCPDS No. 37-14920) [49,52]. The high-intensity peak of the (002) plane indicates a well-stacked layer structure along the c-axis. The diffraction peaks represented by the (#) located at angle 23.01, 30.68, 36.83, and 53.58 degrees corresponding to the Mn_2O_3 planes of (211), (222), (400), and (440) orientations (JSPDS No. 41-1442) [53].

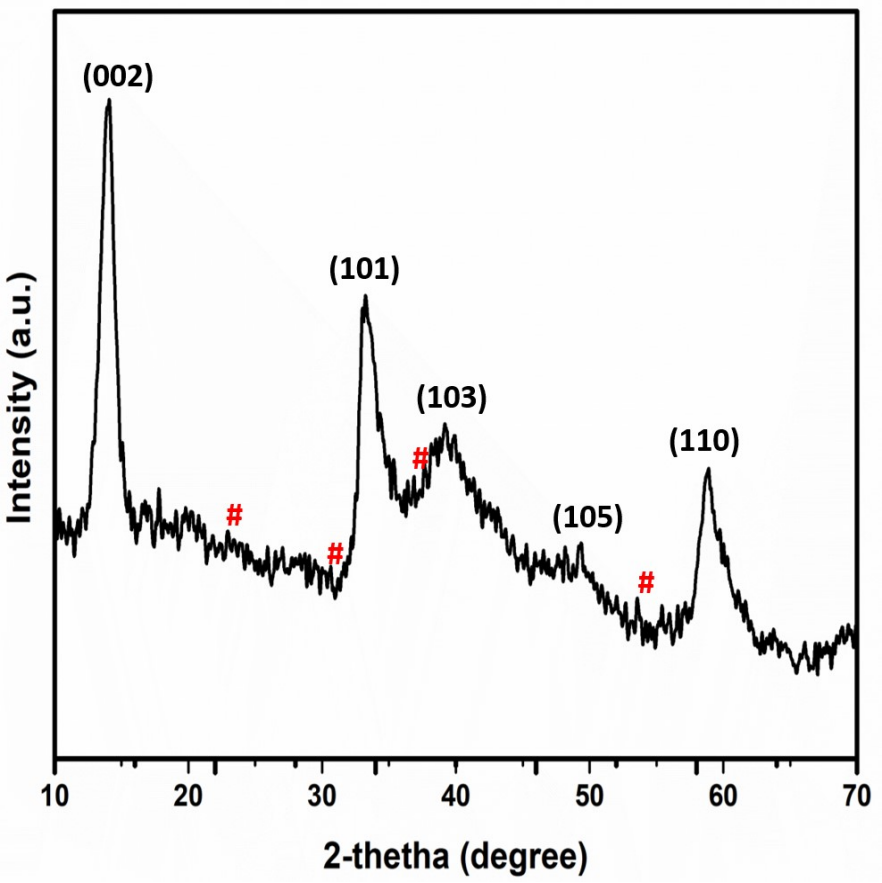

Figure 6. 4 XRD patterns of the Mn-doped MoS_2 electrode material. The (#) corresponds to Mn_2O_3 planes of the XRD patterns.

6.3.4. N_2 Adsorption-desorption Studies

The electrochemical performance of a supercapacitor is greatly influenced by the surface area of the electrode material. Physical gas adsorption is the preferred approach for evaluating the porous characteristics of electrode materials. The isotherm obtained from these adsorption data is used to calculate the surface area, pore volume, and pore size distribution [54]. Figure 6.5 shows the N_2 adsorption-desorption isotherms of Mn-doped MoS_2 with an inset of its pore size distributions. The calculated BET results from N_2 adsorption-desorption isotherms of Mn-doped MoS_2 have a surface area of 46.0628 m^2/g. BET surface area calculated in this study was higher than the previously reported values for bare MoS_2 (23.9 m^2/g) [55], which can translate to an improvement in its supercapacitor performances. The linear increase in adsorption at low pressure (P/Po = 0.00–0.10) can be used to identify monolayer gas adsorption inside the pores. After that, up to P/Po = 0.8, the curve reveals a near plateau zone, showing the presence of some nanopores alongside mesopores. The adsorption of the gas between the interlayers of the sample is indicated by a rapid and spiky increase in the adsorption (P/Po = 0.8–1.0) [56]. As shown in the inset figure 4a, the pore size distributions of the electrode material were calculated by the Barret-Joyner-Halenda (BJH) from adsorption isotherms. The adsorption average pore width (4V/A by BET) for the electrode sample is 11.26607 nm. The cumulative pore volume (BJH adsorption and desorption) between 1.7000 nm and 300.0000 nm widths for the sample, were, respectively, found to be 0.141921 cm^3/g and 0.140928 cm^3/g. Type IV isotherms with a characteristic hysteresis loop indicated the mesoporous structure in the electrode material.

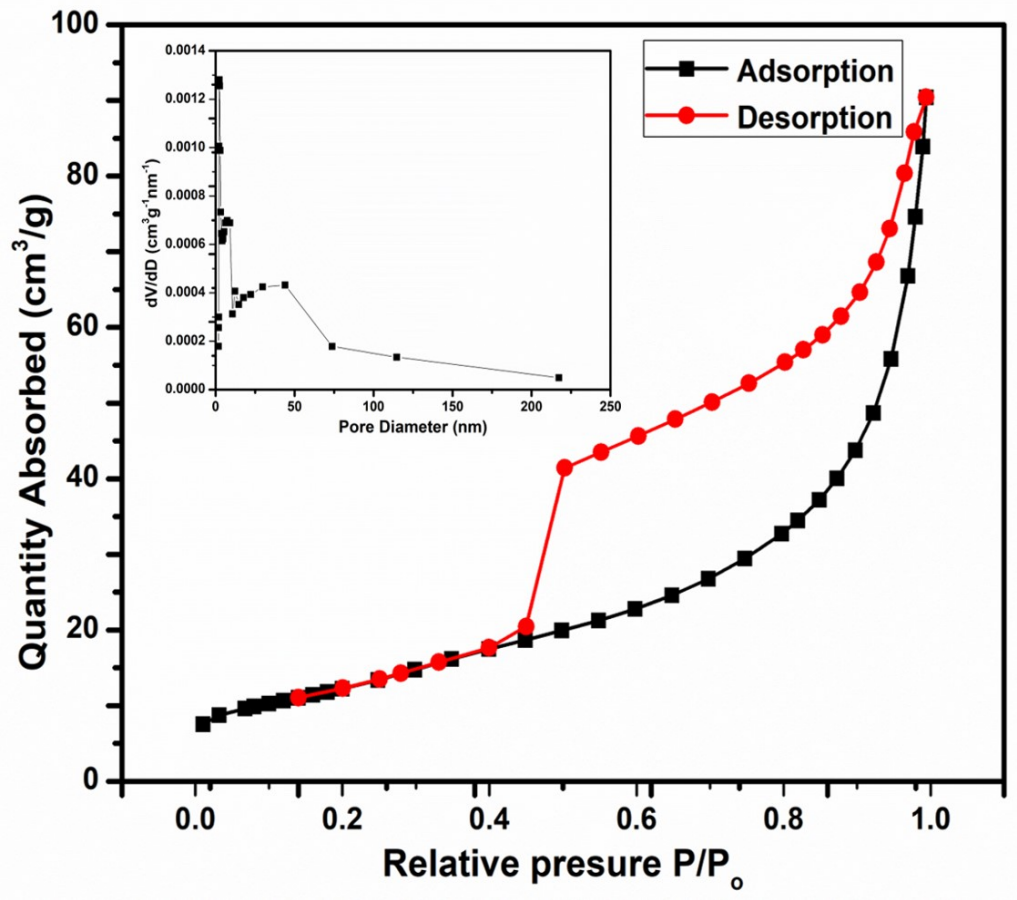

Figure 6. 5 N_2 adsorption-desorption isotherms of Mn-doped MoS_2 with an inset of its pore size distributions.

6.3.5. Electrochemical Performance Analysis

6.3.5.1. Electrochemical Impedance Spectroscopy studies

Electrochemical impedance spectroscopy (EIS) was used to evaluate the electrodes' improved mechanism. The EIS research aids in the development of a theoretical circuit model for a better understanding of the electrode-electrolyte interface, conductivity calculations, and even electrolyte resistance [45,46]. Figure 6.6 depicts the related Nyquist plots with their inset lower frequency plot and the equivalent circuits. Over a frequency range of 100 kHz to 10 MHz, with an amplitude of 5 mV and a bias voltage of 0.23 V, EIS was used to measure ion transport and electrical

conductivity of the electrodes. The x-intercept at the high-frequency area of the Nyquist plot gives equivalent series resistance (ESR), which includes three distinct resistances: (i) resistance of the electroactive material, (ii) resistance of the electrolyte, and (iii) contact resistance at the interface, which is estimated to be around 5.3 Ω. The charge transfer resistance (R_{ct}) resulting from the faradic redox process can be calculated using the diameter of the semicircle at a medium frequency. The third region is the Warburg region, which is linked to redox species diffusion in the sample and mimics the slope of the curve in the low-frequency zone.

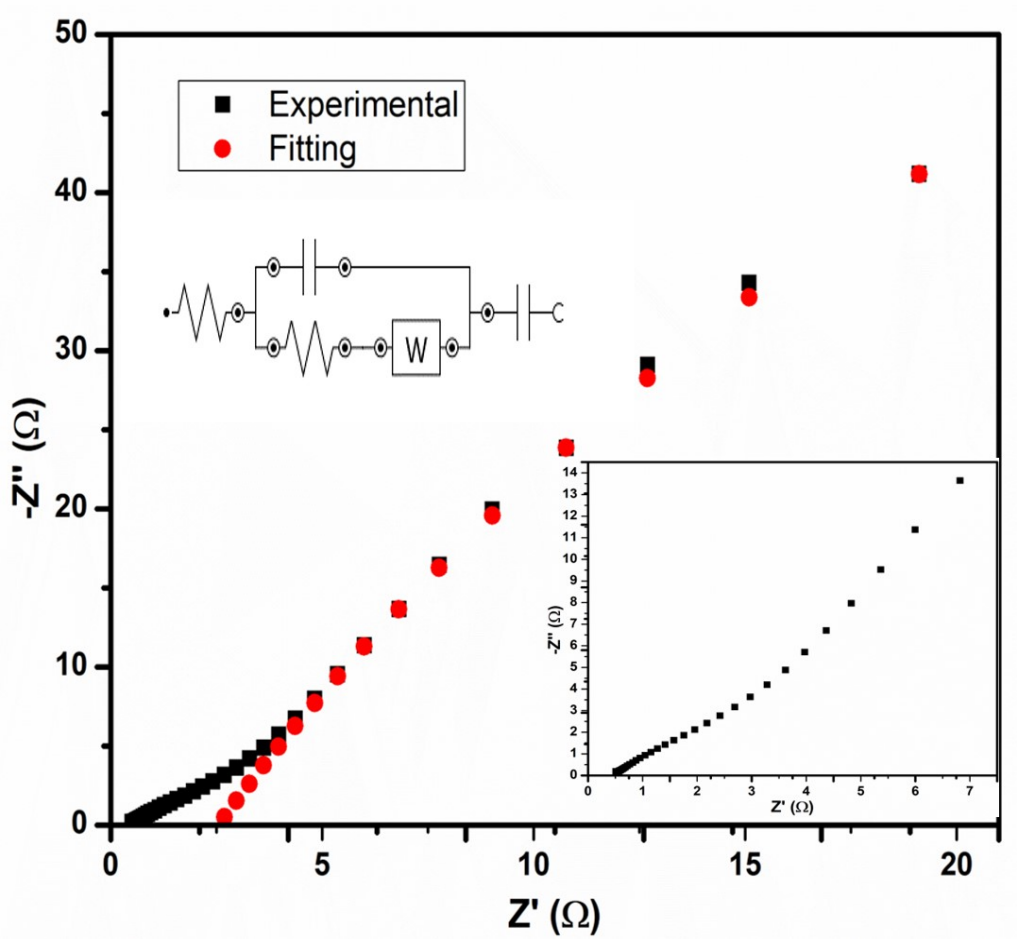

Figure 6. 6 Nyquist plots (inset lower frequency and equivalent circuit).

6.3.5.2. Cyclic Voltammetry (CV)

The CV tests of Mn-doped MoS_2 electrode were studied within the potential window of -0.4 V to 0.5 V with a scan rate between 5 mVs^{-1} to 100 mVs^{-1} (5, 10, 20, 50, and 100 mVs^{-1}). As shown in figure 6.7, the CV loops show a typical quasi-rectangular shape with the presence of a redox peak between 0.2 V and 0.4 V in the forward and reverse scan, which may be due to the different state valences ($Mo^{4+}/Mo^{(4-\Delta)+}$) from the molybdenum ions. This represents the ideal pseudocapacitive behavior of the Mn-doped MoS_2 electrodes, with low contact resistance. The CV loops increase as the scan rate increased, with their curves remaining constant at the highest scan rate of 100 mVs^{-1}. The current drawn increases with the voltage as the scan rate increase, increasing the loop area. The electrodes' fast response and charge-discharging capabilities were also noticed, as well as a clear distinction between the cathodic (reduction) peaks of the electrodes' CV loops. The pseudo-capacitance behavior is confirmed by the presence of redox peaks in the composite. The pseudocapacitive performance is due to the Faradaic reactions that occur at the electrode-electrolyte interface [57].

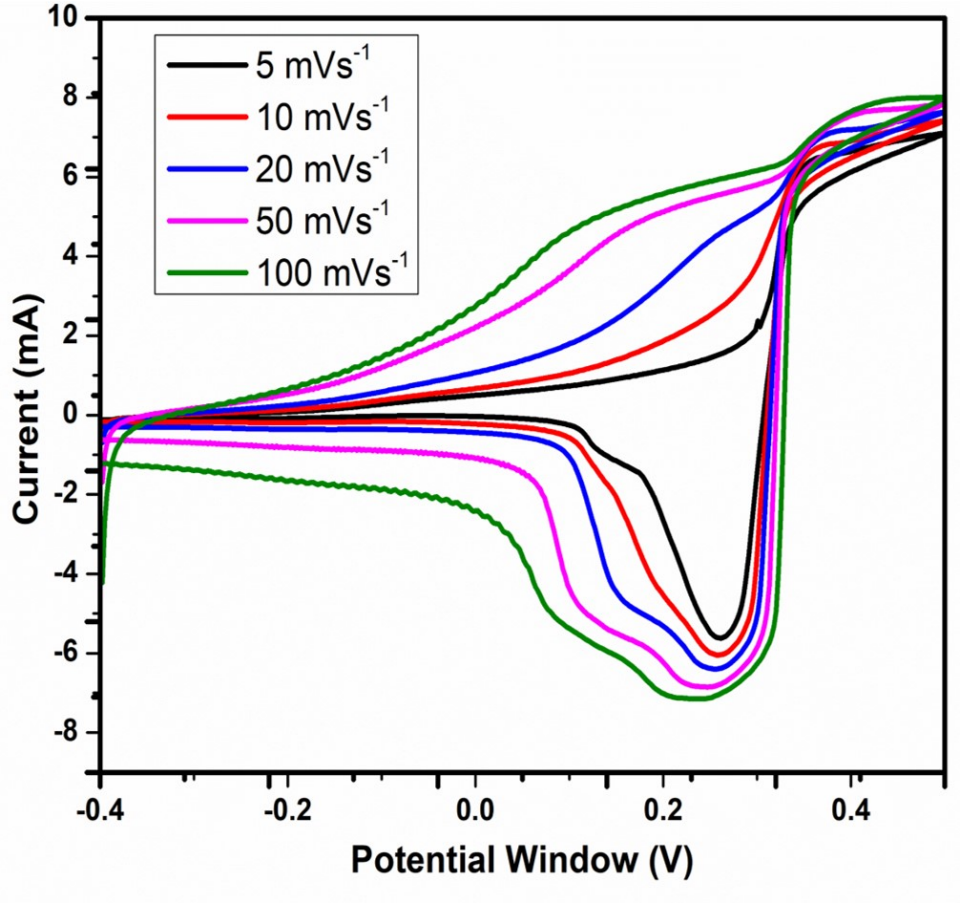

Figure 6. 7 CV Curves of the Mn-doped MoS_2 electrode.

6.3.5.3.Galvanostatic charge-discharge (GCD) Analysis

The GCD plots of the Mn-doped MoS_2 electrode material were shown in figure 6.8. The GCD studies of the electrode material were conducted at different current densities of 1, 2, 3, 5, and 10 Ag^{-1}. The GCD curves have nearly perfect triangular forms, with a small reduction in internal resistance at the onset of discharge curves, which could be due to the active materials' contact resistance with the highly conductive nickel foam surface. Also, as seen in semi-symmetry curves of the GCD, the oxidation and reduction processes at the electrode-electrolyte border of the electrode materials indicate the pseudo-capacitance behavior of the electrodes [58]. The specific capacitances were calculated from the GCD curves using $C_{sp} = \frac{\mathrm{I}\Delta\mathrm{t}}{\mathrm{m}\Delta V}$ to determine the

performance parameters of the supercapacitor electrode. The Mn-doped MoS_2 electrode showed the specific capacitances of 70.37, 58.89, 57.69, 44.11, and 29.90 Fg^{-1} at the current densities of 1, 2, 3, 5, and 10 Ag^{-1}, respectively. The highest specific capacitance of the electrode observed was 70.37 Fg^{-1} at 1 Ag^{-1} current density.

The highest specific energy and power densities obtained were calculated using both $E = {}^{1}/_{2}\frac{Cs\Delta V^2}{3.6}$ and $P = \frac{3600\times E}{\Delta t}$ equations to have 3.14 Wh/kg and 4346.35 W/kg, respectively. At the current density of 1 Ag^{-1}, the lengthier period of the discharge was observed, which may be due to the electrode's surface area. Furthermore, when the current densities increase, the discharge time decreases, which corresponds to the stated CV data. The charge storage in the material occurred because of either a surface-limited non-faradaic reaction (i.e., adsorption) or the intercalation of electrolyte ions into the material's interlayer spacing [59]. The performance parameters of the galvanostatic charge-discharge curve were presented in Table 6.2. As shown in Table 6.2, the energy density decreases as the current density increases, due to their proportionality to the specific capacitance. Also, while the contact between the electrolyte and electrode is limited, power density increases with scan rate because it offers less resistance at higher scan rates.

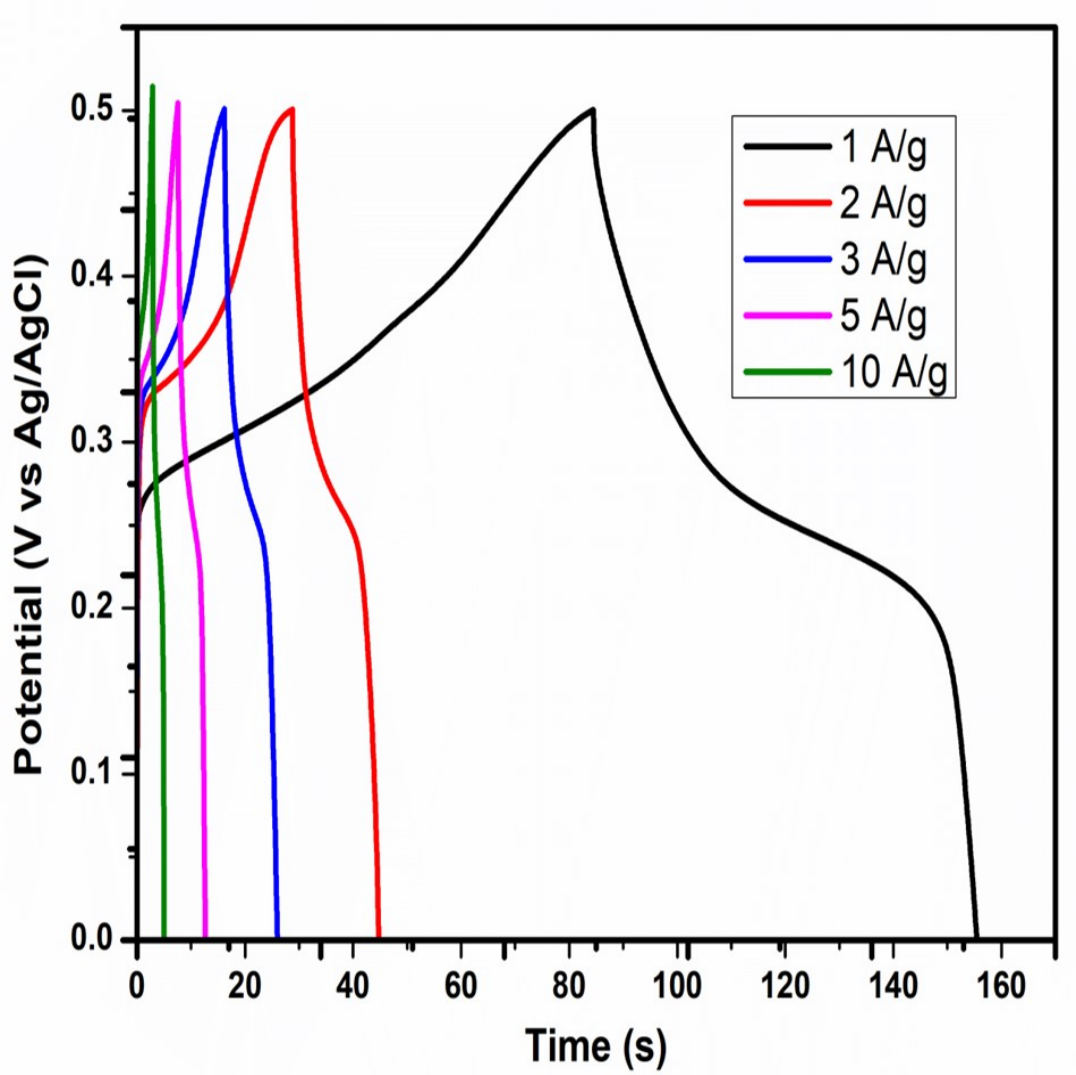

Figure 6. 8 GCD curves of the Mn-doped MoS_2 Electrode Material.

6.3.5.4.Anodic and Cathodic Peak Current Measurement

The anodic and cathodic peak current measurement, as shown in Figure 6.9a, was directly proportional to the square root of the scan rate, to further corroborate the electrode materials' pseudocapacitive behavior as an appropriate composite for supercapacitor applications [60]. The intercept, slope, and R square values of both the anodic and cathodic peaks are shown in the inset of Figure 6.9a. The capacitances dramatically decrease as the current density increases, as shown

in Figure 6.9b, indicating an exceptional ability for fast charge-discharge, and the restriction of ions on the electrode materials' surfaces could be responsible.

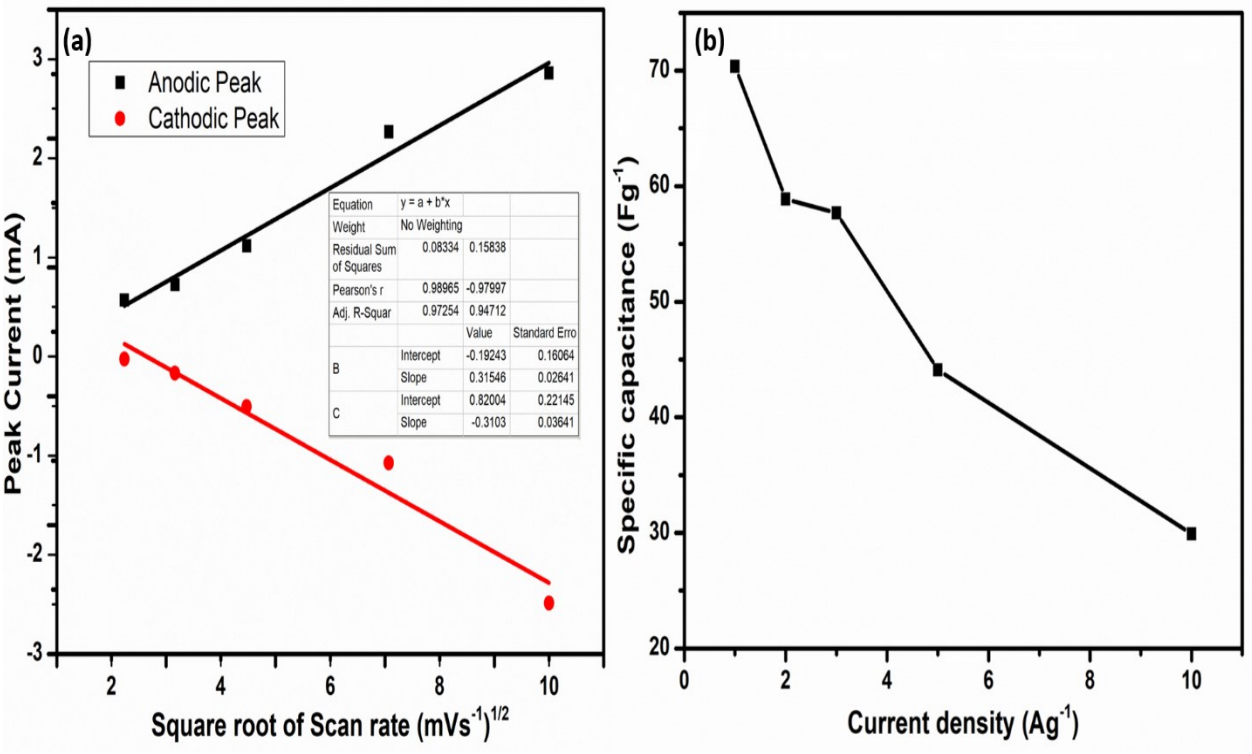

Figure 6. 9 (a) Peak current against the square root of scan rate, and (b) Specific capacitance comparison with current density.

Table 6. 2 Performance Parameters of the Galvanostatic Charge-Discharge.

Current Density (A/g)	**Specific Capacitance (F/g)**	**Energy Density (Wh/kg)**	**Power Density (W/kg)**
1	70.37	2.07	257.14
2	58.89	2.29	529.69
3	57.69	2.31	805.85
5	44.11	2.58	1454.52
10	29.90	3.14	4346.35

6.4. Conclusion

A mixed-phase Mn-doped MoS_2 nanoflower was synthesized by a one-pot facile hydrothermal technique. The elucidation of the as-synthesized material was done by XRD, RAMAN, SEM-EDS, BET methods. The presence of a mixed-phase in the as-synthesized electrode material was established from the XRD and RAMAN spectrum results. The nanoflower morphology of the Mn-doped MoS_2 was also established from the SEM-EDS images and the surface of areas with the presence of mesoporous structure was likewise revealed from the BET techniques. The supercapacitor performance of the fabricated supercapacitor electrode was electrochemically investigated using cyclic voltammetry, galvanostatic charge-discharge, and electrochemical impedance spectroscopy measurements in a three-electrodes cells system. The Mn-doped MoS_2 nanoflower exhibit a specific capacitance of 70. 37 Fg^{-1} at a current density of 1 Ag^{-1}, with corresponding energy and power densities of 3.14 $Whkg^{-1}$ and 4346.35 Wkg^{-1} respectively. The electrode's performance shows that a mixed-phase Mn-doped MoS_2 can be an outstanding material for the metal-doped MoS_2 supercapacitive electrodes. Smart device fabrication and further optimization of the electrode performance such as the characterization of the electrodes before and after cycles were recommended for future work for a better understanding of the electrode-electrolyte interface of the materials.

References

[1] S. Mothkuri, S. Chakrabarti, H. Gupta, B. Padya, T.N. Rao, P.K. Jain, Synthesis of MnO_2 nano-flakes for high performance supercapacitor application, Mater. Today Proc. 26 (2018) 142–147. https://doi.org/10.1016/j.matpr.2019.03.236.

[2] R. Aihemaitituoheti, N.A. Alhebshi, T. Abudula, Effects of Precursors and Carbon Nanotubes on Electrochemical Properties of Electrospun Nickel Oxide Nanofibers-Based Supercapacitors, Molecules. 26 (2021) 5656. https://doi.org/10.3390/molecules26185656.

[3] M. Winter, R.J. Brodd, What are batteries, fuel cells, and supercapacitors?, Chem. Rev. 104 (2004) 4245–4269. https://doi.org/10.1021/cr020730k.

[4] I.T. Bello, O.A. Oladipo, O. Adedokun, M.S. Dhlamini, Recent advances on the preparation and electrochemical analysis of MoS_2-based materials for supercapacitor applications : A mini-review, Mater. Today Commun. 25 (2020) 101664. https://doi.org/10.1016/j.mtcomm.2020.101664.

[5] I.T. Bello, S.A. Adio, A.O. Oladipo, O. Adedokun, L.E. Mathevula, M.S. Dhlamini, Molybdenum sulfide-based supercapacitors: From synthetic, bibliometric, and qualitative perspectives, Int. J. Energy Res. (2021) 12665–12692. https://doi.org/10.1002/er.6690.

[6] X. Chia, A.Y.S. Eng, A. Ambrosi, S.M. Tan, M. Pumera, Electrochemistry of Nanostructured Layered Transition-Metal Dichalcogenides, Chem. Rev. 115 (2015) 11941–11966. https://doi.org/10.1021/acs.chemrev.5b00287.

[7] B. Xie, Y. Chen, M. Yu, T. Sun, L. Lu, T. Xie, Y. Zhang, Y. Wu, Hydrothermal synthesis of layered molybdenum sulfide/N-doped graphene hybrid with enhanced supercapacitor performance, Carbon N. Y. (2016). https://doi.org/10.1016/j.carbon.2015.11.077.

[8] K.J. Huang, L. Wang, J.Z. Zhang, L.L. Wang, Y.P. Mo, One-step preparation of layered

molybdenum disulfide/multi-walled carbon nanotube composites for enhanced performance supercapacitor, Energy. 67 (2014) 234–240. https://doi.org/10.1016/j.energy.2013.12.051.

[9] X. Geng, Y. Zhang, Y. Han, J. Li, L. Yang, M. Benamara, L. Chen, H. Zhu, Two-Dimensional Water-Coupled Metallic MoS_2 with Nanochannels for Ultrafast Supercapacitors, Nano Lett. 17 (2017) 1825–1832. https://doi.org/10.1021/acs.nanolett.6b05134.

[10] P.Y. Chan, S.R. Majid, Metal oxide-based electrode materials for supercapacitor applications, in: Adv. Mater. Their Appl. - Micro to Nano Scale, 2012: pp. 13–30. http://www.onecentralpress.com/wp-content/uploads/2017/08/Chapter-2-AMA-11.pdf.

[11] C. Liu, Z. Yu, D. Neff, A. Zhamu, B.Z. Jang, Graphene-based supercapacitor with an ultrahigh energy density, Nano Lett. 10 (2010) 4863–4868. https://doi.org/10.1021/nl102661q.

[12] J.M. Soon, K.P. Loh, Electrochemical double-layer capacitance of MoS_2 nanowall films, Electrochem. Solid-State Lett. 10 (2007) 250–254. https://doi.org/10.1149/1.2778851.

[13] B. Xu, S. Yue, Z. Sui, X. Zhang, S. Hou, G. Cao, Y. Yang, What is the choice for supercapacitors: Graphene or graphene oxide?, Energy Environ. Sci. 4 (2011) 2826–2830. https://doi.org/10.1039/c1ee01198g.

[14] X. Zhang, Z. Sui, B. Xu, S. Yue, Y. Luo, W. Zhan, B. Liu, Mechanically strong and highly conductive graphene aerogel and its use as electrodes for electrochemical power sources, J. Mater. Chem. 21 (2011) 6494–6497. https://doi.org/10.1039/c1jm10239g.

[15] Y. Wang, Z. Shi, Y. Huang, Y. Ma, C. Wang, M. Chen, Y. Chen, Supercapacitor devices based on graphene materials, J. Phys. Chem. C. 113 (2009) 13103–13107.

https://doi.org/10.1021/jp902214f.

[16] S. Zhai, Z. Fan, K. Jin, M. Zhou, H. Zhao, Y. Zhao, F. Ge, X. Li, Z. Cai, Synthesis of zinc sulfide/copper sulfide/porous carbonized cotton nanocomposites for flexible supercapacitor and recyclable photocatalysis with high performance, J. Colloid Interface Sci. 575 (2020) 306–316. https://doi.org/10.1016/j.jcis.2020.04.073.

[17] M.F. Iqbal, A.K.M. Yousef, A. Hassan, S. Hussain, M.N. Ashiq, Mahmood-Ul-Hassan, A. Razaq, Significantly improved electrochemical characteristics of nickel sulfide nanoplates using graphene oxide thin film for supercapacitor applications, J. Energy Storage. 33 (2021) 102091. https://doi.org/10.1016/j.est.2020.102091.

[18] L. Zheng, F. Teng, X. Ye, H. Zheng, X. Fang, Photo/Electrochemical Applications of Metal Sulfide/TiO2 Heterostructures, Adv. Energy Mater. 10 (2020) 1–32. https://doi.org/10.1002/aenm.201902355.

[19] D. Merki, X. Hu, Recent developments of molybdenum and tungsten sulfides as hydrogen evolution catalysts, Energy Environ. Sci. 4 (2011) 3878–3888. https://doi.org/10.1039/c1ee01970h.

[20] K. Chang, W. Chen, In situ synthesis of MoS_2/graphene nanosheet composites with extraordinarily high electrochemical performance for lithium ion batteries, Chem. Commun. 47 (2011) 4252–4254. https://doi.org/10.1039/c1cc10631g.

[21] Y. Li, H. Wang, L. Xie, Y. Liang, G. Hong, H. Dai, MoS_2 nanoparticles grown on graphene: An advanced catalyst for the hydrogen evolution reaction, J. Am. Chem. Soc. 133 (2011) 7296–7299. https://doi.org/10.1021/ja201269b.

[22] Z. Yin, H. Li, H. Li, L. Jiang, Y. Shi, Y. Sun, G. Lu, Q. Zhang, X. Chen, H. Zhang, Single-layer MoS_2 phototransistors, ACS Nano. 6 (2012) 74–80.

https://doi.org/10.1021/nn2024557.

[23] C. Sha, B. Lu, H. Mao, J. Cheng, X. Pan, J. Lu, Z. Ye, 3D ternary nanocomposites of molybdenum disulfide/polyaniline/reduced graphene oxide aerogel for high performance supercapacitors, Carbon N. Y. 99 (2016) 26–34. https://doi.org/10.1016/j.carbon.2015.11.066.

[24] J. Xiao, D. Choi, L. Cosimbescu, P. Koech, J. Liu, J.P. Lemmon, Exfoliated MoS_2 nanocomposite as an anode material for lithium ion batteries, Chem. Mater. 22 (2010) 4522–4524. https://doi.org/10.1021/cm101254j.

[25] K.S. Kumar, N. Choudhary, Y. Jung, J. Thomas, Recent Advances in Two-Dimensional Nanomaterials for Supercapacitor Electrode Applications, ACS Energy Lett. 3 (2018) 482–495. https://doi.org/10.1021/acsenergylett.7b01169.

[26] N. Zheng, X. Bu, P. Feng, Synthetic design of crystalline inorganic chalcogenides exhibiting fast-ion conductivity, Nature. 426 (2003) 428–432. https://doi.org/10.1038/nature02159.

[27] D.N. Sangeetha, M. Selvakumar, Active-defective activated carbon/MoS_2 composites for supercapacitor and hydrogen evolution reactions, Appl. Surf. Sci. 453 (2018) 132–140. https://doi.org/10.1016/j.apsusc.2018.05.033.

[28] D.N. Sangeetha, M.S. Santosh, M. Selvakumar, Flower-like carbon doped MoS_2/Activated carbon composite electrode for superior performance of supercapacitors and hydrogen evolution reactions, J. Alloys Compd. 831 (2020) 154745. https://doi.org/10.1016/j.jallcom.2020.154745.

[29] X. Liao, Y. Zhao, J. Wang, W. Yang, L. Xu, X. Tian, Y. Shuang, MoS_2/MnO_2 heterostructured nanodevices for electro-, Nano Res. 11 (2018) 4–7.

[30] F.N.I. Sari, J.M. Ting, MoS_2/MoOx-Nanostructure-Decorated Activated Carbon Cloth for Enhanced Supercapacitor Performance, ChemSusChem. 11 (2018) 897–906. https://doi.org/10.1002/cssc.201702295.

[31] M.A. Bissett, I.A. Kinloch, R.A.W. Dryfe, Characterization of MoS_2-Graphene Composites for High-Performance Coin Cell Supercapacitors, ACS Appl. Mater. Interfaces. (2015). https://doi.org/10.1021/acsami.5b04672.

[32] F. Clerici, M. Fontana, S. Bianco, M. Serrapede, F. Perrucci, S. Ferrero, E. Tresso, A. Lamberti, In situ MoS_2 Decoration of Laser-Induced Graphene as Flexible Supercapacitor Electrodes, ACS Appl. Mater. Interfaces. 8 (2016) 10459–10465. https://doi.org/10.1021/acsami.6b00808.

[33] E.G. Da Silveira Firmiano, A.C. Rabelo, C.J. Dalmaschio, A.N. Pinheiro, E.C. Pereira, W.H. Schreiner, E.R. Leite, Supercapacitor electrodes obtained by directly bonding 2D MoS2 on reduced graphene oxide, Adv. Energy Mater. 4 (2014) 1–8. https://doi.org/10.1002/aenm.201301380.

[34] Z. Li, Z. Qin, W. Zhang, Z. Li, Controlled synthesis of $Ni(OH)_2$/MoS_2 nanohybrids for high-performance supercapacitors, Mater. Chem. Phys. 209 (2018) 291–297. https://doi.org/10.1016/j.matchemphys.2017.12.072.

[35] C. Hao, F. Wen, J. Xiang, L. Wang, H. Hou, Z. Su, W. Hu, Z. Liu, Controlled incorporation of Ni(OH)2 nanoplates into flowerlike MoS_2 nanosheets for flexible all-solid-state supercapacitors (Advanced Functional Materials (2014) 24 (6700-6707)), Adv. Funct. Mater. 24 (2014) 6740. https://doi.org/10.1002/adfm.201401268.

[36] H. Tang, J. Wang, H. Yin, H. Zhao, D. Wang, Z. Tang, Growth of polypyrrole ultrathin films on MoS_2 monolayers as high-performance supercapacitor electrodes, Adv. Mater. 27

(2015) 1117–1123. https://doi.org/10.1002/adma.201404622.

[37] L. Ren, G. Zhang, Z. Yan, L. Kang, H. Xu, F. Shi, Z. Lei, Z.H. Liu, Three-Dimensional Tubular MoS_2/PANI Hybrid Electrode for High Rate Performance Supercapacitor, ACS Appl. Mater. Interfaces. 7 (2015) 28294–28302. https://doi.org/10.1021/acsami.5b08474.

[38] Y. Ge, R. Jalili, C. Wang, T. Zheng, Y. Chao, G.G. Wallace, A robust free-standing MoS_2/poly(3,4-ethylenedioxythiophene):poly(styrenesulfonate) film for supercapacitor applications, Electrochim. Acta. 235 (2017) 348–355. https://doi.org/10.1016/j.electacta.2017.03.069.

[39] W. Luo, G. Zhang, Y. Cui, Y. Sun, Q. Qin, J. Zhang, W. Zheng, One-step extended strategy for the ionic liquid-assisted synthesis of Ni_3S_4-MoS_2 heterojunction electrodes for supercapacitors, J. Mater. Chem. A. 5 (2017) 11278–11285. https://doi.org/10.1039/c7ta02268a.

[40] F. Huang, R. Meng, Y. Sui, F. Wei, J. Qi, Q. Meng, Y. He, One-step hydrothermal synthesis of a CoS_2@MoS_2 nanocomposite for high-performance supercapacitors, J. Alloys Compd. 742 (2018) 844–851. https://doi.org/10.1016/j.jallcom.2018.01.324.

[41] S. Palanisamy, P. Periasamy, K. Subramani, A.P. Shyma, R. Venkatachalam, Ultrathin sheet structure Ni-MoS_2 anode and MnO_2/water dispersion graphene cathode for modern asymmetrical coin cell supercapacitor, J. Alloys Compd. 731 (2018) 936–944. https://doi.org/10.1016/j.jallcom.2017.10.118.

[42] B.D. Falola, L. Fan, T. Wiltowski, I.I. Suni, Electrodeposition of Cu-Doped MoS_2 for Charge Storage in Electrochemical Supercapacitors , J. Electrochem. Soc. 164 (2017) D674–D679. https://doi.org/10.1149/2.0421712jes.

[43] J. Shao, Y. Li, M. Zhong, Q. Wang, X. Luo, K. Li, W. Zhao, Enhanced-performance flexible

supercapacitor based on Pt-doped MoS_2, Mater. Lett. 252 (2019) 173–177. https://doi.org/10.1016/j.matlet.2019.05.124.

[44] S.S. Singha, S. Rudra, S. Mondal, M. Pradhan, A.K. Nayak, B. Satpati, P. Pal, K. Das, A. Singha, Mn incorporated MoS_2 nanoflowers: A high performance electrode material for symmetric supercapacitor, Electrochim. Acta. 338 (2020). https://doi.org/10.1016/j.electacta.2020.135815.

[45] A. Sun, L. Xie, D. Wang, Z. Wu, Enhanced energy storage performance from Co-decorated MoS_2 nanosheets as supercapacitor electrode materials, Ceram. Int. 44 (2018) 13434–13438. https://doi.org/10.1016/j.ceramint.2018.04.113.

[46] R. Rohith, M. Manuraj, R.I. Jafri, R.B. Rakhi, Co-MoS_2 nanoflower coated carbon fabric as a flexible electrode for supercapacitor, Mater. Today Proc. (2021). https://doi.org/10.1016/j.matpr.2020.12.1054.

[47] Q. Xiong, X. Zhang, H. Wang, G. Liu, G. Wang, H. Zhang, H. Zhao, One-step synthesis of cobalt-doped MoS_2 nanosheets as bifunctional electrocatalysts for overall water splitting under both acidic and alkaline conditions, Chem. Commun. 54 (2018) 3859–3862. https://doi.org/10.1039/c8cc00766g.

[48] A. Kushima, X. Qian, P. Zhao, S. Zhang, J. Li, Ripplocations in van der Waals layers, Nano Lett. 15 (2015) 1302–1308. https://doi.org/10.1021/nl5045082.

[49] S.S. Singha, S. Mondal, T.S. Bhattacharya, L. Das, K. Sen, B. Satpati, K. Das, A. Singha, Au nanoparticles functionalized 3D-MoS_2 nanoflower: An efficient SERS matrix for biomolecule sensing, Biosens. Bioelectron. 119 (2018) 10–17. https://doi.org/10.1016/j.bios.2018.07.061.

[50] L. Cai, J. He, Q. Liu, T. Yao, L. Chen, W. Yan, F. Hu, Y. Jiang, Y. Zhao, T. Hu, Z. Sun, S.

Wei, Vacancy-induced ferromagnetism of MoS_2 nanosheets, J. Am. Chem. Soc. 137 (2015) 2622–2627. https://doi.org/10.1021/ja5120908.

[51] J. Wang, F. Sun, S. Yang, Y. Li, C. Zhao, M. Xu, Y. Zhang, H. Zeng, Robust ferromagnetism in Mn-doped MoS_2 nanostructures, Appl. Phys. Lett. 109 (2016) 1–6. https://doi.org/10.1063/1.4961883.

[52] K.D. Rasamani, F. Alimohammadi, Y. Sun, Interlayer-expanded MoS_2, Mater. Today. 20 (2017) 83–91. https://doi.org/10.1016/j.mattod.2016.10.004.

[53] G. Zheng, W. Zhang, R. Shen, J. Ye, Z. Qin, Y. Chao, Three-dimensionally Ordered Macroporous Structure Enabled Nanothermite Membrane of Mn_2O_3/Al, Sci. Rep. 6 (2016) 2–11. https://doi.org/10.1038/srep22588.

[54] J.C. Groen, J. Pérez-Ramírez, Critical appraisal of mesopore characterization by adsorption analysis, Appl. Catal. A Gen. 268 (2004) 121–125. https://doi.org/10.1016/j.apcata.2004.03.031.

[55] Y. Zhang, Z. Yin, C. Dai, X. Zhou, W. Chen, Interfacial thermodynamics and kinetics of sorption of diclofenac on prepared high performance flower-like MoS_2, J. Colloid Interface Sci. 481 (2016) 210–219. https://doi.org/10.1016/j.jcis.2016.07.046.

[56] R.B. Rakhi, N.A. Alhebshi, D.H. Anjum, H.N. Alshareef, Nanostructured cobalt sulfide-on-fiber with tunable morphology as electrodes for asymmetric hybrid supercapacitors, J. Mater. Chem. A. 2 (2014) 16190–16198. https://doi.org/10.1039/c4ta03341h.

[57] L. Zhang, J. Wang, J. Zhu, X. Zhang, K. San Hui, K.N. Hui, 3D porous layered double hydroxides grown on graphene as advanced electrochemical pseudocapacitor materials, J. Mater. Chem. A. 1 (2013) 9046–9053. https://doi.org/10.1039/c3ta11755c.

[58] D.P. Dubal, V.J. Fulari, C.D. Lokhande, Effect of morphology on supercapacitive properties

of chemically grown β-$Ni(OH)_2$ thin films, Microporous Mesoporous Mater. 151 (2012) 511–516. https://doi.org/10.1016/j.micromeso.2011.08.034.

[59] N. Li, X. Zhu, C. Zhang, L. Lai, R. Jiang, J. Zhu, Controllable synthesis of different microstructured MnO_2 by a facile hydrothermal method for supercapacitors, J. Alloys Compd. 692 (2017) 26–33. https://doi.org/10.1016/j.jallcom.2016.08.321.

[60] Y. Gogotsi, R.M. Penner, Energy Storage in Nanomaterials - Capacitive, Pseudocapacitive, or Battery-like?, ACS Nano. 12 (2018) 2081–2083. https://doi.org/10.1021/acsnano.8b01914.

Chapter Seven

General Conclusion and Recommendations for Future Work

This chapter summarizes the main results obtained from the entire period of experimental findings. The main achievements from the study such as the published work and the recommendations for future works were highlighted in this section.

7.1. Conclusion

In this study, we investigated the improvement of transition metal-based superconductor materials for improved performance in an energy storage application. The hydrothermal method was employed as the synthesis technique in the work to prepare the electrode materials samples. The methods of the preparation were the best among the reviewed techniques harnessed during this study due to their simplicity, cost-effectiveness, and ability to obtain 2D-or-3D nanomaterials as their final products. Hydrothermal methods have been regarded as the most attractive way of synthesizing MoS_2 nanosheets because of their simplicity and wide range of applicability with relatively high electrochemical performance. The hydrothermal method was adopted in the synthesis of the electrode materials used in this study due to its general acceptability.

The bibliometric analysis of the evolution of literary works related to its supercapacitor devices since the usage of MoS_2 as the active materials in energy storage (Supercapacitor) was evaluated. The bibliometric studies will guide researchers to explore the previously prioritized areas and encourage future collaborations. The bibliometric analysis of the studied materials gives us perspectives on the strengths and weaknesses of the materials, which enable us to identify the area of focus and the targeted publication outlets.

The elucidation of the prepared samples in terms of their morphology and elemental compositions, structural and microstructural properties, and surface area of the electrode materials was carried out by the characterization techniques listed in the previous chapter four. The objectives set from the onset of the experimental phase were to optimize the effect of the single

metal-based composite of the TMDs nanomaterials. The choice of MoS_2 among the TMDs families was dues to its wider spread applicability, which has been highlighted in chapter three of this report. The major objectives presently studied for metal-composites in this work are Cobalt and Manganese doped electrodes for their electrochemical properties.

The electrochemical behaviors of both metal-based composites of MoS_2 electrodes were fascinating and improved values of the specific capacitances of the fabricated electrodes. The results from Co-doped MoS_2 electrodes inferred that they can be an outstanding electrode material for supercapacitor applications. This study also confirmed that the oxygen reduction is quasi-reversible due to the observed weird-like CV curves. This method can potentially be developed to improve the charge storage capabilities of other transition metal sulfides. Likewise, the results of Mn-doped MoS_2 composites showed mixed-phase Mn-doped MoS_2 nanoflowers with mesoporous structures from their surface areas. The electrode's performance shows that a mixed-phase Mn-doped MoS_2 can be an excellent material for the metal-doped MoS_2 supercapacitive electrodes.

Finally, during the investigation, we observed that the optoelectronic properties of Co-doped MoS_2 nanocomposites can be altered by the concentration of cobalt and be a formidable candidate for photoconductivity.

7.2. Future Work and Recommendations

Notwithstanding the improved synthetic samples obtained and the excellent supercapacitive behavior reported, the purity of the prepared metal composites of MoS_2 must be improved. Furthermore, more functionalization of transition metals with MoS_2 and other TMDs families for enhancement of energy storage applications.

The following studies could be considered for future works:

- Smart device fabrication and further optimization of the electrode performance such as the characterization of the electrodes before and after cycles were recommended for future work for a better understanding of the electrode-electrolyte interface of the materials.
- The realization of advanced storage capacity from flexible and wearable supercapacitors should be achievable soon with the current pace at which the study of MoS_2-based supercapacitors is growing.
- In-depth kinetic analysis for a better understanding of the electrode materials should be done.
- Upscaling fabrication of energy storage devices using Plasma Enhanced Chemical Vapor Deposition *(*PECVD*)* techniques is required.
- Further studies on the photoconductivity application of Co-doped MoS_2.
- Further optimization study such as the effect of the temperature and time on the structural and morphological properties of the materials must be investigated for the future works.

Appendix

Published Papers